UNIVERSITÄT ZU LÜBECK

Aus dem Institut für systemische Entzündungsforschung
der Universität zu Lübeck

Direktor: Prof. Dr. Jörg Köhl

Regulation of IgE and IgG antibodies in the context of murine food allergies

Inauguraldissertation

Zur Erlangung der Doktorwürde (Dr. med.)
Der Universität zu Lübeck
-Aus der Sektion Medizin-

Vorgelegt von
SARAH-MARIA FREYE
Aus Görlitz

Lübeck 2025

1. Berichterstatter*in: Prof. Dr. rer. nat. Rudolf Manz
Ko-Betreuer*in: Prof. Fred Finkelman, MD
2. Berichterstatter*in: Prof. Dr. med. Christoph Thorns
Tag der mündlichen Prüfung: 24.03.2026
Zum Druck genehmigt. Lübeck, den 25.03.2026
-Promotionskommission der Sektion Medizin-

Table of Contents

Table of Figures

1. Abbreviations

Ag Antigen

AID Activation-induced cytidine deaminase

AUC Area under the curve

BAFF B cell activating factor

BCR B cell receptor

BSA Bovine serum albumin

CDR Complementary determining region

CFSE Carboxyfluorescein succinimidyl ester

C_H region heavy chain constant region

CLR C-type lectin receptor

CSR Class switch recombination

DSB DNA-double-strand-break

DZ Dark zone

ELISA Enzyme-linked Immunosorbent Assay

ER Endoplasmic reticulum

ERK Ras-extracellular-signal-regulated kinase

Fab region Fragment antigen-binding region

FACS Fluorescence-activated cell-sorting

Fc region Fragment crystallizable region

FcR Fc receptor

FDC follicular dendritic cell

FSC Forward scatter

FVD Fixable Viability Dye

GC Germinal Center

H chain Heavy chain (of Ig)

Ig Immunoglobulin

iGB cells Induced germinal center-phenotype B cells

IgE Immunoglobulin E

IgG1 Immunoglobulin G1

IgH Heavy (H) chain of an immunoglobulin

IgL Light (L) chain of an immunoglobulin

IgV region Variable region of the Immunoglobulin

IL Interleukin

IMGT database ImMunoGeneTics database

IP_3 Inositol-1, 4,5-triposphate

IQR Interquartile range

ITAM Immunoreceptor tyrosine-based activation motif

L chain Light chain

LPS Lipopolysaccharide

LZ Light zone

MAD Median absolute deviation

MBC Memory B cell

MFI Mean Fluorescence Intensity

MHC-II Major histocompatibility complex II

mIgG1 Membrane immunoglobulin G1

mLN Mesenteric lymph node

N. brasiliensis Nippostrongylus brasiliensis

2-NBDG 2-[N-(7-nitrobenz-2-oxa-1,3-diazol-4-yl) amino]-2-deoxy-D-glucose

NFAT Nuclear factor of activated T cells

NFκB Nuclear factor κB

NGS Next-generation sequencing

NIAID National Institute of Allergy and Infectious Diseases

OVA Ovalbumin

PC Plasma cell

PCR Polymerase chain reaction

pMHCII Peptide major histocompatibility complex II

qRT-PCR Quantitative reverse transcriptase PCR

RLU Relative light units

RT Room temperature

S region Switch region

SD Standard deviation

SE Standard error

SEM Standard error of the mean

SHM Somatic hypermutation

sIgE Specific IgE

SLIT Sublingual immunotherapy

SSC Side scatter

STAT Signal transducer and activator of transcription

Tfh cells T follicular helper cells

Th2 cells T-helper type 2 cells

TNP- antibodies Trinitrophenyl-antibody

2. Introduction

2.1 Clinical background: food allergy

2.1.1 Definitions

The guidelines of an NIAID (National Institute of Allergy and Infectious Diseases) sponsored expert panel define food allergy as an adverse health reaction caused by a specific immune response repetitively after the exposure to a certain food. Food allergies can be distinguished in IgE- mediated, non- IgE- mediated and mixed food allergies (Boyce et al., 2010). Non-IgE mediated food allergies describe a heterogenous group of separate clinical entities which affect different organs including the gastrointestinal tract (for example food-protein induced enterocolitis) or the skin (for example dermatitis herpetiformis) (Nowak-Węgrzyn et al., 2015) and occur in a more delayed onset. In contrast, IgE-mediated food allergies are associated with its rapid onset in the scope of a type I hypersensitivity reaction (Anvari et al., 2019).

Type I hypersensitivity reactions are defined as immediate IgE-mediated reactions occurring within one hour after allergen exposure. The interaction of allergen specific IgE on the FcεRI receptors on mast cells and basophils stimulates the cells to release mediators, for instance histamine and leukotrienes, upon successive exposure to the provoking allergen. This degranulation results in vasodilation, manifesting clinically as hypotension, angioedema, wheezing or anaphylaxis, among others (Ashraf Uzzaman, 2012; Maker et al., 2019; Mike Kulis, Benjamin L. Wright, 2015).

A prerequisite for an IgE-mediated food allergy is the sensitization of the patient (Boyce et al., 2010). A sensitized patient has a detectable level of food-specific IgE which might transform into a clinical food allergy (Anvari et al., 2019).

The mechanisms of an allergic reaction in a sensitized individual after an initial immune response include the presentation of allergen fragments to T-helper type 2 (Th2) cells and its activation, leading to a release of Th2 cytokines such as IL-4 and IL-13, amplifying the IgE response (Stone et al., 2010). This type 2 immune response conducted by different T helper cell subsets is the answer of the adaptive immune system against allergens and larger parasites, for example helminths (Haase & Voehringer, 2021).

These terms are important for the understanding of this thesis which explores mechanisms of the type 2 immune response on a cellular level, inspired by results of a murine food allergy model.

2.1.2 Epidemiology

Food allergy is reviewed as a common disease which affects up to one-tenth of the population. The prevalence grew during the last two or three decades, especially in

industrialized regions and more often in children than adults. Tree nuts, peanut, shellfish, fish, milk, egg, soy, wheat and seeds are typical foods which induce adverse reactions (Sicherer & Sampson, 2018).

It is difficult to state a concrete prevalence of food allergy because the number of patients detected depends on various factors such as study populations, geographic regions, ages and methodologies. The latter include the self-selection-bias of parents' or self-reports of allergies and current trends which raise the awareness of food allergy (Sicherer & Sampson, 2014; Warren et al., 2020).

Concrete prevalences of food allergies have been determined by oral food challenges for a group of 2848 12 months-old infants in Australia, showing a prevalence of 3,0% of peanut allergy, 8,9% of raw egg allergy and 0,8% of sesame allergy (Osborne et al., 2011). These infants of the population-based cohort study were tested again at the age of four years. At this time point, the prevalence of food allergy decreased to 1,9% for peanut allergy, 1,2% for egg allergy and to 0,4% for sesame allergy (Peters et al., 2017).

To illustrate the complexity of the interpretation of the prevalence of food allergy, the Isle of Wight Birth cohort study (n=1456) collected data of the cohort at the ages of 1, 2, 4, 10 and 18 years, demonstrating that the prevalence of food allergy partially resolved from early childhood to the age of 10 years from approximately 5% to 2%, and rising again at the age of 18 years to 4%. Food allergy was measured by the presentation of typical symptoms and a skin prick test (Venkataramana et al., 2018).

2.1.3 Symptoms and diagnosis

Clinical symptoms of IgE-mediated food allergies range in their severity from mild to life-threatening anaphylaxis. Examples of gastrointestinal symptoms are oral tingling, swelling, nausea, abdominal pain and vomiting. Skin manifestations include flushing, angioedema, pruritus and urticaria. Respiratory symptoms consist of wheezing and airway inflammation. Systemic reactions are hypotension, hypothermia, and life-threatening anaphylaxis (Yu et al., 2017).

A multi-step diagnostic approach, which is initiated if suspected symptoms of food allergy have been demonstrated, has been recently reviewed by Peters and colleagues: they suggest starting with a traditional skin prick test or measuring the titer of specific IgE (sIgE). In the case of an equivocal result, they suggest performing allergen component-resolved diagnostics or cellular tests like basophil or mast cell activation tests. Only if this approach leads again to an equivocal result, they recommend performing an oral food challenge (Peters et al., 2021). Oral food challenges provide a definitive diagnostic approach, but they are resource intensive and can cause anaphylactic reactions. New

diagnostic methods like basophil activation tests are limited to research settings (Yu et al., 2017).

2.1.4 Treatment and economic burden

The most important preventive treatment for patients suffering from a diagnosed food allergy is the avoidance of allergy-provoking food. As a first-line treatment, food-induced anaphylaxis requires immediate and rapid treatment with intramuscular epinephrine. Adjunctive treatments like bronchodilator medications and antihistamines can be applied. Glucocorticoids play a subordinate role due to their slow action (Boyce et al., 2010; Ring et al., 2021).

Studies from the Consortium for Food Allergy Research comparing oral, sublingual and epicutaneous immunotherapy conclude that they provide a safe desensitization in most of the subjects in comparison to placebo, but the establishment of a sustained unresponsiveness was rare (Sampson et al., 2019).

This lack of an effective long-term curative treatment creates an economic burden for the patients and their stakeholders, considering for instance the high cost-per-use of adrenaline autoinjectors (Fong et al., 2022) or the increase in hospitalization rates (Warren et al., 2020): hospitalization rates in England and Wales doubled between 1992 and 2012 due to food-allergy-induced anaphylaxis (Turner et al., 2015).

Consequently, an advanced knowledge of immunological mechanisms, which can either prevent or cure food allergies, is necessary to improve the treatment and reduce the economic burden of food allergies in the long-term.

2.2 Immunological background

2.2.1 B cell responses to food allergens

The pathogenesis of IgE-mediated food allergy in human beings is complex. Food allergens are typically proteins and atypically carbohydrates like galactose-α-1,3-galactose in mammalian meat allergy (Chandrasekhar et al., 2020; Macdougall et al., 2022). B cells encounter food allergens in the stomach and the duodenum, resulting in a local class switch recombination from naïve B cells, IgG or IgA switched B cells to IgE switched B cells, followed by the plasma cell differentiation and IgE production (Satitsuksanoa et al., 2021).

Furthermore, B cells encounter food allergen proteins in secondary and tertiary lymphoid tissues. These allergens are absorbed by dendritic cells. The dendritic cells present allergen-specific peptides to naïve T cells via major histocompatibility complex II (MHC II) molecules after migration to the draining lymph node. Naïve T cells develop into Th2 and

T follicular helper (Tfh) cells that generate Th2 cytokines including IL-4, IL-5 and IL-13. The interaction between Tfh cells and naïve B cells promotes a direct and sequential class switch recombination to IgE (Satitsuksanoa et al., 2021). Moreover, Tfh cells are crucial for the generation of germinal centers (Chandrasekhar et al., 2020) within secondary lymphoid tissues where B cells can differentiate to high-affinity IgE producing plasma cells or memory B cells (MBCs) (Udoye et al., 2023).

The MBC compartment comprises mostly non-IgE-expressing cells which restock the IgE+ plasma cell compartment upon antigen re-encounter (Jiménez-Saiz et al., 2018) because the half-life of murine allergen-specific IgE+ plasma cells is merely 60 days (Jiménez-Saiz et al., 2017) (figure 1). This re-activation of quiescent MBCs occurs in a T-cell-help dependent or independent manner. In the former case, T cell help involves surface markers such as CD40L or the Inducible T-cell costimulator (ICOS), which interact with the B cell. In the latter case, a T-cell independent reactivation is established by toll-like-receptor (TLR) ligands of virus particles. Consequences of the MBC reactivation are a reentry in the germinal center reaction (see chapter 2.2.4) or the differentiation into plasma cells (Moriyama et al., 2020).

Plasma cells (PCs) are the terminal state of B cell differentiation. Short-lived PCs, produced in the extrafollicular pathway, hence outside the germinal center, protect initially and rapidly against pathogens. In contrast, long-lived PCs are produced inside the germinal center, which is defined as follicular pathway, protecting against pathogens in the long-term (W. Ise & Kurosaki, 2020).

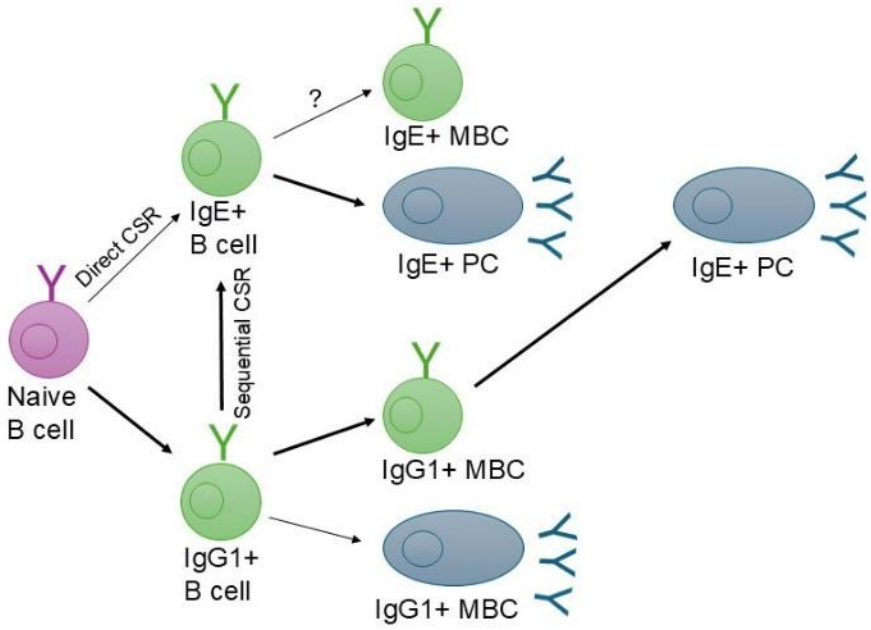

Figure 1: Visualization of B cell responses to food allergens and the production of IgE.
Upon primary exposure to a food allergen, naïve B cells can switch directly to IgE, expressing this antibody on their surface as B cell receptor. Alternatively, B cells switch via an intermediate IgG1 B cell state to IgE which is called sequential class switch recombination (CSR). IgE+ B cells are prone to develop into IgE+ plasma

cells (PC), a memory-phenotype is possible, its longevity is not identified. Upon re-exposure with the same food allergen, IgG1+ memory B cells (MBCs) can restock the transient IgE+ PC compartment. Modified after: Journal of Allergy and Clinical Immunology 2018, 142(5), 1441–1443. doi: https://doi.org/10.1016/j.jaci.2018.08.

2.2.2 Immunoglobulins

Immunoglobulins (Igs) or antibodies are the secreted version of the B cell receptor, consisting of several polypeptide chains: the heavy (H) and light (L) chains (Murphy & Weaver, 2018a). The human L chain contains one constant and one variable region, while the human H chain covers a variable region and several constant regions. The number of constant regions depends on the immunoglobulin isotype. An antibody can be divided after pepsin digestion into 2 Fab residues, the $F(ab')_2$ fragments (named in relation to “Ag binding”), and into the Fc fragment (named after “crystalline”). To begin with the Fab residues, they include the variable and constant domain of H and L chain, binding to the antigen via complementary determining regions (CDRs). CDRs are unique to each B cell clone. In contrast, the Fc fragments contain the other constant regions of the H chain (see figure 2) (James, 2022; Mix et al., 2006).

According to their Fc fragment, human Igs can be divided into five isotype classes: IgM, IgD, IgG, IgE and IgA. The IgG isotype is structured in four subclasses. Thereof, the human subclass IgG4 corresponds to the murine subclass IgG1, under the terms of their function (Mix et al., 2006).

Most effector functions of antibodies are executed if the Fc fragment binds to the Fc receptor (FcR) or C-type lectin receptors (CLRs) on the cell surface of different immune cells, like the Fc fragment of IgE on the FcεRI on mast cells. Despite this interaction with the high-affinity FcR, IgE can also bind to the CLR FcεRII (CD23) (Lu et al., 2018; Pincetic et al., 2014). This low-affinity receptor can be expressed on B cells, T cells, monocytes, eosinophils or intestinal epithelial cells, among others (Engeroff & Vogel, 2021; Murphy & Weaver, 2018c; Acharya et al., 2010). Examples of IgE-mediated effector functions are the degranulation of mast cells and basophils as well as the release of Th2 cytokines and vasoactive mediators (Lu et al., 2018).

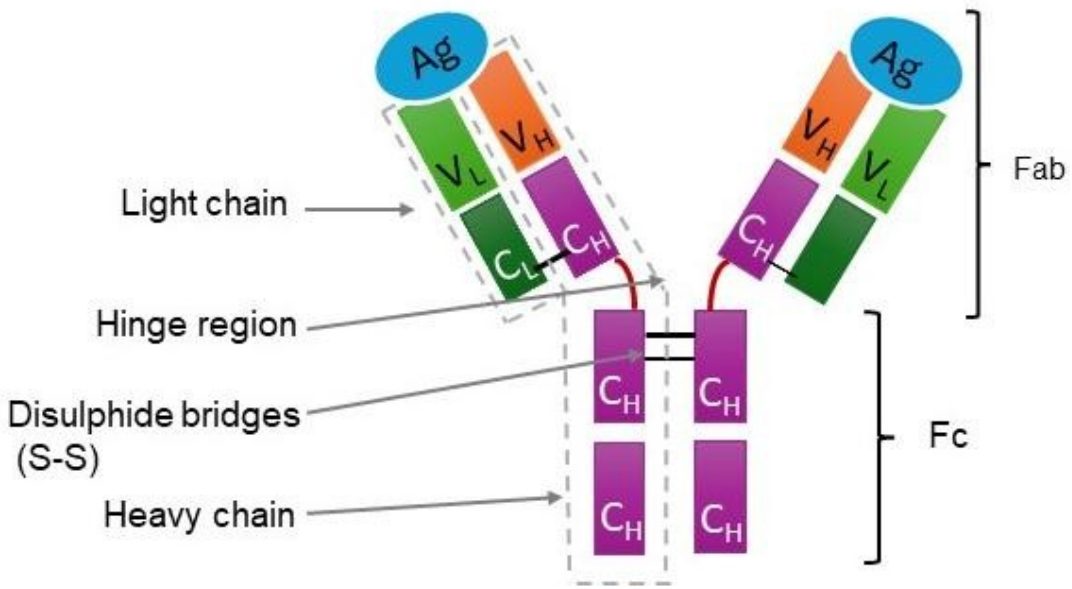

Figure 2: Visualization of the structure of IgG.
Immunoglobulin G covers four polypeptide chains: two heavy (H) and two light (L) chains, connected by disulfide bridges. The human L chain contains one constant (C) and one variable (V) region. The human H chain of IgG covers 3 constant regions and one variable region. An antibody can be divided after pepsin digestion into 2 Fab residues (named in relation to “antigen binding”) and into a Fc fragment (named after “crystalline”). Fab residues bind to the antigen (Ag) via complementary determining regions (CDRs). Modified after: Antibody Technology Journal. 2016; 6:17-32. doi: 10.2147/anti.s64762

The high diversity among immunoglobulins is formed antigen (Ag)-independently by means of combinatorial V-D-J joining, junctional diversity and different combinations of L and H chains during the B cell maturation in the bone marrow. In addition, it is formed Ag-dependently by somatic hypermutations and isotype class switching in peripheral lymphatic tissues.

To begin with the explanation of these mechanisms, combinatorial V-D-J joining describes the rearrangement of different gene segments. The gene segments coding the heavy chain are located on chromosome 14. Analyzing this chromosome on a germ-line level, the V region of the Ig H chain comprises the gene segments V_H (named after “variable”), D (named after “diversity”) and J_H (named after “joining”) (Mix et al., 2006).

Secondly, junctional diversity is the result of imprecise joining of coding sequences leading to several combinations of productive rearrangements, especially in CDR3 regions. It covers also the loss of cells by apoptosis in case of unproductive rearrangements, when the reading frame of the gene segments is interrupted (Murphy & Weaver, 2018b).

To continue with somatic hypermutations, these are mutations in the CDRs of the IgV regions occurring after Ag stimulation in the dark zone of germinal centers. The more often the antibody response is stimulated, the greater the chance of forming high-affinity antibodies. However, in the absence of selection, antibodies with lower affinity or with the

same affinity as well as dysfunctional antibodies can be produced (Huang, 2020b; Mix et al., 2006).

2.2.3 B cell receptors

B cell receptors (BCRs) contain two identical Ig heavy (IgH) and light (IgL) chains which have a unique variable region for antigen recognition. Membrane BCRs build a complex with CD79, enabling them to initiate various downstream signaling cascades.

Due to this structure, the BCR can cover variable functions: it is important for host defense after bacterial or viral infections due to the recognition of extracellular antigens. BCRs can activate clonal deletion among other mechanisms to remove autoreactive B cells. Another function is to acquire T cell help for further B cell differentiation (Tanaka & Baba, 2020).

Upon antigen encounter, the BCR-CD79 complex can be either phosphorylated and activated, contributing to the signaling cascade, or internalized, contributing to the antigen presentation via MHC-II (Hou et al., 2006).

A part of the CD79 molecule is the immunoreceptor tyrosine-based activation motif (ITAM) which is connected to SRC kinases. These kinases phosphorylate the tyrosine residues of the ITAMs, activating further signaling molecules, resulting in the generation of a signalosome, a signaling complex. Consequently, several downstream signaling cascades are initiated including Ras-extracellular-signal-regulated kinase (ERK), nuclear factor of activated T cells (NFAT) and nuclear factor κB (NFκB) cascades. The co-receptor CD19 needs to be phosphorylated to activate the PI3K-AKT-pathway (Tanaka & Baba, 2020). Each pathway involves complex downstream effects. For instance, the PI3K-AKT-pathway activates the transcription factor Blimp 1 which regulates B cell differentiation and inhibits the expression of the enzyme activation-induced cytidine deaminase. This enzyme is crucial for class switch recombination and somatic hypermutation (Z. Chen & Wang, 2019).

Downstream events of the PLCγ2-Calcium-NFAT pathway after BCR stimulation include a calcium response, named store-operated calcium entry (Tanaka & Baba, 2020). The intracellular calcium concentration rises in a biphasic manner due to the calcium release from the endoplasmic reticulum (ER) and the calcium inflow across the plasma membrane. In detail, the ligation of the inositol-1, 4,5-triposphate (IP_3) on the IP_3 receptor in the ER membrane induces a rapid and transient calcium release from the ER into the cytoplasm. This increase in calcium concentration is prolonged by opening the calcium channels in the plasma membrane, allowing extracellular calcium to enter the cell (Putney & Bird, 1993). The calcium response after BCR stimulation was investigated in this thesis (see chapter 4.2.1).

The exact mechanisms of BCR activation are hard to describe and still controversial. Several models are proposed to explain B cell activation, among them the cross-linking model, the conformation-induced oligomerization model, the dissociation-activation model and the conformational change model. The cross-linking model represents the view that different BCR monomers cross-link upon interaction with multivalent antigens, while monovalent antigens do not lead to BCR activation (Feng et al., 2020). In comparison, the dissociation-activation model describes the auto-inhibitory oligomeric structure of the BCR. BCR engagement dissociates the oligomers and activates the B cell (J. Yang & Reth, 2010). Anti-Ig Fab fragments or monovalent antigens which bind directly to the antigen binding site can open these BCR oligomers, triggering a calcium response and reducing the proximity between BCR monomers (Volkmann et al., 2016).

2.2.4 Germinal centers

Transient microstructures are generated inside follicles of secondary lymphoid tissues as a reaction to immunization or pathogens. These microstructures are germinal centers (GC) which consist of a light zone (LZ) and a dark zone (DZ) (Huang, 2020a). LZ and DZ are named after their histological appearance when stained. The LZ is lighter as it contains more stromal cells, for example dendritic cells, and less cell nuclei than the DZ. The two zones have different functions: clonal expansion of B cells and affinity maturation (Victora & Nussenzweig, 2022).

To start with the DZ, it is the compartment of clonal expansion and hypermutation to produce antibody mutants with different affinities to the antigen. By contrast, in the LZ, B cells with higher affinity to the antigen are multiplied and differentiated into PCs or MBCs, using the stimulation of Tfh cells and follicular dendritic cells (FDCs), among others. Additionally, LZ B cells were associated with class switch recombination (CSR) (Huang, 2020a), but recent publications state that CSR occurs prior to GC formation (James, 2022; Victora & Nussenzweig, 2022; Roco et al., 2019).

The differentiation of GC B cells depends on their affinity to the antigen: high-affinity B cells are prone to the PC fate, while low-affinity B cells are associated with the MBC fate (Suan et al., 2017). Possible reasons for the PC differentiation of high-affinity B cells could be either cell-intrinsic pathways induced by BCR signaling or their advanced antigen capture and ability to receive T cell help by increased expression of peptide major histocompatibility complex II (pMHCII) (James, 2022; Victora & Nussenzweig, 2012). Higher pMHCII expression on GC B cells is associated with longer and dynamic T-B contacts as well as a larger contact size (Shulman et al., 2014).

Amplified size and duration of the interaction between T cells and high-affinity B cells promote the calcium signaling inside the Tfh cells. Consequently, the calcium-dependent

cytokines IL-21 and IL-4 are generated (Shulman et al., 2014). IL-21 enhances GC B cell proliferation and the production of long-lived PCs. Furthermore, IL-21 can support GC maintenance and differentiation of plasmablasts together with IL-4. Besides, Tfh cells in the LZ express CD40L, interacting via cell-cell contacts with CD40 on GC B cells. CD40L is a family member of the tumor necrosis factor and strengthens B cell proliferation. The Tfh response is regulated by its affinity towards the antigen and by the amount of the antigen. Low levels of antigen lead to the upregulation of the transcription factor Foxp3, lowering the expression of CD40L and IL-21 (Victora & Nussenzweig, 2022).

Another cell population, the FDCs, contributes to the selection of GC B cells depending on their affinity. For this purpose, FDCs retain the antigen in the form of an immune complex, which consists of antigen, antibody and complement. In detail, FDCs express the complement receptor C3 for antigen retention as well as the Fc receptor FcγRIIb (Victora & Nussenzweig, 2022).

There are several models referring to different findings and components of B cell selection and affinity maturation in the GC (Victora & Nussenzweig, 2012, 2022). Figure 3 depicts a model of these processes focusing on the B cell fate and its interaction with other cells, summarizing the findings which are necessary for the understanding of this thesis.

Of note, B cell differentiation to MBCs and PCs is not restricted to the GC reaction (W. Ise & Kurosaki, 2020; Moriyama et al., 2020): Analyzing the murine MBC compartment, on the one hand, somatically mutated, high-affinity antibodies arising from a T cell-dependent GC reaction could be found. On the other hand, unmutated low-affinity antibodies arising from a T cell-dependent, but GC independent pathway could be detected (Kaji et al., 2012). This is in line with a study of Taylor and colleagues, showing that CD38+GL7+ MBC precursors can directly develop into mostly IgM+ MBCs without GC reaction or they can differentiate inside the GC to MBCs expressing switched Ig isotypes (Taylor et al., 2012).

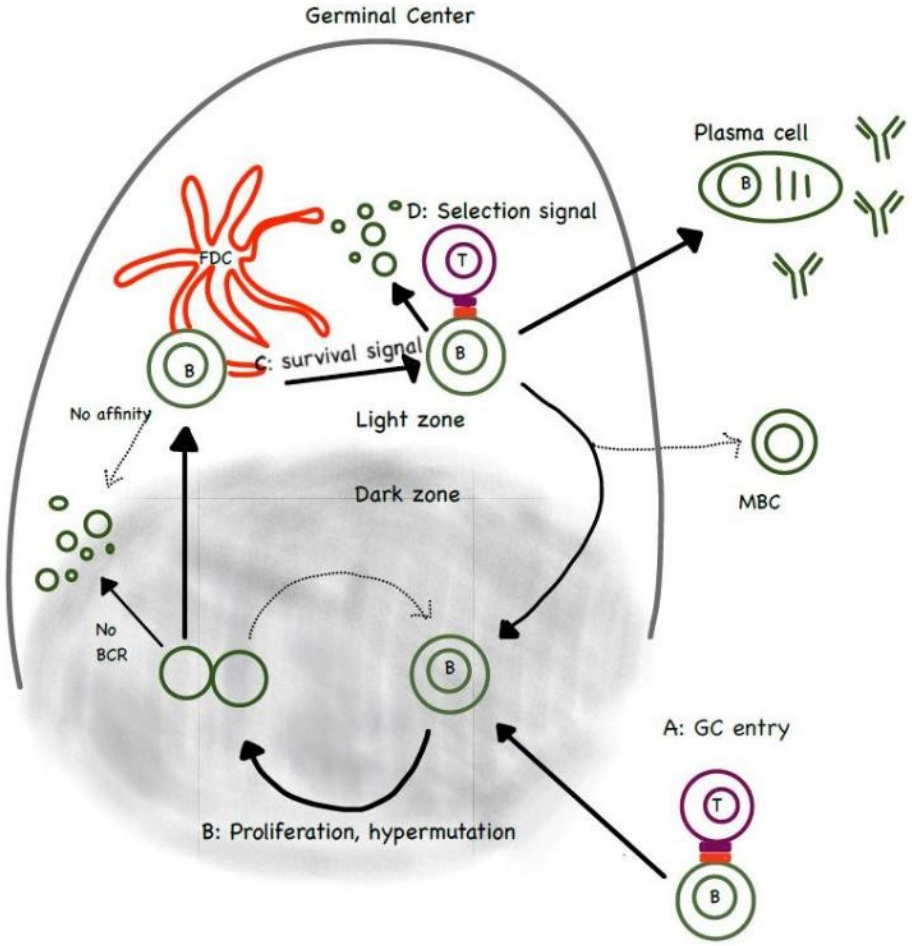

Figure 3: Visualization of B cell selection and affinity maturation inside the germinal center (GC). A: B cells contest for a restricted amount of T cells at the T:B border; B cells with the highest affinity can participate in the GC reaction. B: In the dark zone (DZ), GC B cells proliferate and undergo somatic hypermutation. If the result of mutation is a loss of the BCR, the B cells die. After several cycles of mutations and divisions, B cells migrate from the DZ to the light zone (LZ). C: Follicular dendritic cells (FDCs) retain the antigen, allowing interaction with the LZ B cell. B cells expressing low or no affinity for the presented antigen can die due to the missing BCR signal. D: B cells present the antigen to a restricted amount of T helper cells. High-affinity B cells express more peptide MHC on their surface, thus high-affinity B cells are more likely than low-affinity B cells to interact with T cells. A successful T cell- B cell-interaction results in 3 possible B cell fates: (1) re-entry into the DZ, (2) plasma cell fate outside the GC, (3) memory B cell fate (MBC) outside the GC. Modified after: Annu. Rev. Immunol. 2012. 30:429–57; doi: 10.1146/annurev-immunol-020711-075032

2.2.5 Class switch recombination

Class switching or class switch recombination is a strongly regulated and irreversible process (James, 2022) leading to the differentiation of IgM and IgD co-expressing B cells into B cells and plasma cells which express a single Ig subtype (Mix et al., 2006).

It includes a deletional recombination between two distinct switch regions (S regions). Each S region is associated with a specific heavy chain constant (C_H) region. S regions are located upstream of all C_H genes, except for Cδ. After immunization or infection, B cells alter their surface expression from IgM and/or IgD to IgG, IgE or IgA by substituting the μ and δ C_H regions with γ, ε or α C_H regions. An important enzyme for this process is the activation-induced cytidine deaminase (AID). AID deaminates the cytosine within the S region to uracil, thereby creating locations for DNA-double-strand-breaks (DSBs) in the

donor Sμ and acceptor S region. These DSBs are connected with each other by non-homologous end-joining, excising the switch circle from the gene. In the end, the heavy chain gene that encodes the new Ig isotype of the B cell is produced (figure 4) (Schrader, 2014).

In the context of my thesis, the analysis of the excised C_H regions in the switch circles was used to detect which CSR occurred in my experimental model.

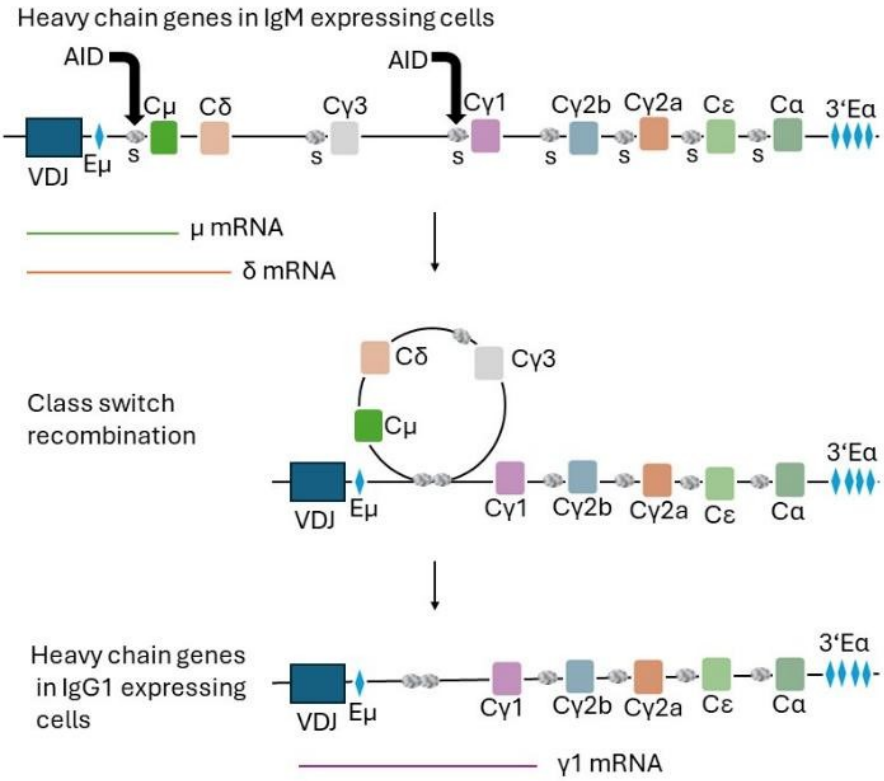

Figure 4: Visualization of murine IgH genes in naïve mature B cells expressing IgM and IgD, and class switch recombination to IgG1.
Class switch recombination (CSR) to IgG1 requires deamination of the switch regions Sμ and Sγ1 by activation-induced cytidine deaminase (AID), inducing DNA double-strand-breaks (DSB). Non-homologous end-joining of the DSBs create the γ1 mRNA, while the constant heavy chain regions for IgM, IgD and IgG3 are excised, forming a switch circle. Eμ and 3′Eα are major enhancers, regulating the expression of Ig H genes and the CSR. Modified after: J Immunol. 2014;193(11):5370-5378. doi:10.4049/jimmunol.1401849

Early type 2 immune responses include the direct switch from IgM to IgE outside the GC. The short-lived plasma cells generate low-affinity, rarely somatically hypermutated IgE antibodies which cannot cause allergic reactions. Conversely, later type 2 immune responses involve the GC-dependent sequential switch and differentiation from IgG1+ memory B cells to high-affinity IgE-secreting plasma cells. High-affinity IgE antibodies imply an anaphylactic potential (Haase & Voehringer, 2021). This summary is in line with experiments stating that in mice sensitized to peanut long-lived allergen-specific IgG1+ memory B cells can reconstitute the IgE+ PC compartment, depending on IL-4 secreting CD4+ T-cells and allergen re-exposure (Jiménez-Saiz et al., 2017).

However, it can be discussed whether the CSR takes place in GCs, as it has been shown that CSR of B cells was conducted prior to the differentiation into GC B cells and somatic hypermutation (Roco et al., 2019).

Signal transducer and activator of transcription (STAT) proteins are crucial for the Th2 immune response and the understanding of the regulation of the CSR. They are activated in the cytoplasm by Janus Kinases upon cytokine signaling. Two of the seven known STAT family members are important for the generation of IgE and IgG1 (Haase & Voehringer, 2021; Tolomeo & Cascio, 2024):

IL-4, secreted by Tfh inside the GC and by Th2 and preTfh cells outside the GC, binds to the IL-4 receptor and activates the transcription factor STAT6. Hence, the expression of the germline transcripts of IgG1 as well as IgE is promoted (Haase & Voehringer, 2021). Apart from this, STAT 6 can be activated by IL-13 interacting with the IL-13 receptor, promoting the transcription of the switch region S_ε of the IgE subclass and thus IgE switching. Furthermore, IL4 and CD40L promote the expression of AID, contributing to somatic hypermutation and class-switch (Stone et al., 2010). In contrast, IL-21 is the major Inhibitor of the class switch to IgE through an IL-21-R mediated STAT3-signal in human and murine B cells. IL-21 in combination with low doses of IL-4 promotes the CSR to IgG1+ (Z. Yang et al., 2020).

2.2.6 IgE and IgG antibodies as biomarkers for food allergies

Several studies analyzed the levels of IgE and IgG as well as their ratio depending on the symptoms of food allergy.

Firstly, an English study performed with 228 children tested for peanut allergy demonstrated 1.6-fold higher IgG4 levels in patients sensitized but tolerant to peanut (PS) in comparison to peanut allergic patients (PA). The ratio of peanut specific IgG4 to IgE was 8 times higher in PS compared to PA patients. In PS children, peanut-induced basophil and mast cell activation was inhibited. The activation could be partially restored after IgG4 depletion, suggesting the influence of different Ig isotypes as blocking antibodies (Santos et al., 2015).

This suggestion is in line with data from a mouse model showing that i.v. injection of IgG1 anti-trinitrophenyl (TNP)-antibodies in contrast to IgE-TNP antibodies in BALB/c mice, inoculated with ovalbumin/alum, could protect them from diarrhea and shock after oral TNP-BSA (bovine serum albumin) challenge. Kucuk and colleagues concluded an IgG-mediated inhibition of IgE-mediated allergic disease, resulting from interception of the absorbed antigen by IgG before it can bind to mast cell-associated IgE (Kucuk et al., 2012).

Along with the protective effect of IgG, its implication in the diagnostic of food allergy has been investigated. Datema and colleagues analyzed the sera of 137 peanut allergic patients and 25 tolerant patients for reactivities of different immunoglobulins against peanut extract and peanut allergens Ara h 1, 2, 3, 8, 9. In this way, they could demonstrate that IgE against Ara h 2 was the best biomarker to predict peanut challenge outcomes and the severity of symptoms. IgG and IgG4 antibodies ratios over IgE did not improve the prediction. Nonetheless, these ratios were higher in tolerant patients or patients presenting mild symptoms compared to patients suffering from a severe food allergy (Datema et al., 2019).

Beside peanut allergy, allergen-specific IgE to IgG4 ratios are a confirmed predictive parameter for egg allergy or tolerance, too (Okamoto et al., 2012; Vazquez-Ortiz et al., 2014).

Together, these studies indicate that not only individual immunoglobulins, but also the ratio of IgE and IgG4 in humans, or respectively IgE and IgG1 in mice, have an impact on the development of food allergies. Consequently, it is of great interest to understand which factors influence their ratio, contributing to a more allergy-releasing or more allergy-protective immune response.

2.3 Experimental background

2.3.1 Research question

Experiments of our research group explored the IgE response in a murine food allergy model, analyzing the antigen-binding complementary region 3 (CDR3) repertoires of IgE and IgG1. A clone was defined as BCRs containing the same VDJ rearrangement. The VDJ genes of IgE and IgG1 were divided into shared and unique clones. To begin with the shared clones, they covered identical VDJ rearrangement for IgE and IgG1. In contrast, unique clones encompassed only IgE clonotypes. In between the shared clones, there are IgE clones which contain mainly IgG1 copies, while other IgE clones comprise more IgE than IgG1 copies. Thus, IgE can be distinguished in IgE (IgE_E) or IgG1 (IgE_G) biased clones, demonstrating that the IgE to IgG1 formation is regulated at the level of individual B cell clones (Udoye et al., 2022).

To elaborate further on the role of individual B cell clones on the formation of IgE versus IgG1, this thesis aims to investigate the influence of B cell receptor signaling strength on class switch to IgE and IgG1 in a murine cell culture model.

The specific research questions are:

1. What is the impact of BCR signaling strength on the class switch to IgE and IgG1 in murine B cell cultures?

2. What is the impact of differential IL-4 levels and differential glucose levels on the ratio of IgE/IgG1 in murine B cell cultures?

2.3.2 Study design

Firstly, a model was established to reproduce different levels of BCR signaling strength using anti-Ig $F(ab')_2$ fragments.

To examine the influence of BCR signaling strength on the formation of IgE and IgG1, an innovative in vitro B cell culture system was adopted from Hanuida and Kitamura (Haniuda & Kitamura, 2019). This method was established by Nojima and colleagues who wanted to mimic a T cell-dependent GC reaction and induce extensive B cell proliferation. They characterized the B cells cultured in their in vitro system by flow cytometry, showing their GC-phenotype and defining them as induced germinal center-phenotype B cells (iGB cells) (Nojima et al., 2011). In addition, T cell help is imitated by co-culturing B cells with the feeder cell line 40 LB, which are BALB/c3T3 fibroblasts transfected with CD40L and BAFF, the B-cell activating factor (Haniuda & Kitamura, 2019; Nojima et al., 2011).

Within the scope of my experiments, B cells were isolated from the spleen of BALB/c mice and cultured in this novel in vitro system. The cells were stimulated with the cytokine IL-4 and different concentrations of anti-Ig $F(ab')_2$ fragments. After 4 days of cell culture, the cells were harvested and analyzed by flow cytometry for their expression of IgE and IgG1. Alternatively, the secretion of IgE and IgG1 was measured by an Enzyme-linked Immunosorbent Assay (ELISA).

My experiments were conducted with anti-Ig $F(ab')_2$ fragments instead of complete Igs to specifically assess the BCR signal, avoiding non-specific binding from Fc interactions. In detail, the interaction of FcγRIIb receptors on B cells with the Fc fragment of complete Igs would inhibit the BCR signaling pathway by closing the plasma membrane calcium channel (Diegel et al., 1994).

The described in vitro model was the basis for further experiments, including the analysis of the frequency of apoptotic cells by flow cytometry. Different types of cell death are linked to different morphological changes of the cells. Apoptosis is characterized by shrinkage, blebbing of the plasma membrane and the generation of apoptotic bodies, while necrosis is characterized by dilation of cellular organelles and swelling of the cell (Banfalvi, 2017; Worsley et al., 2022).

These morphological changes are detectable by flow cytometry. Annexin V, a phospholipid binding protein, binds to phosphatidyl serine which translocates during early apoptosis from the intracellular side of the plasma membrane to the extracellular side

(Banfalvi, 2017), enabling the detection of apoptotic cells as annexin V positive. The decrease in cell volume and size of apoptotic cells was detected by forward scatter (FSC) gating (Worsley et al., 2022), with late apoptotic cells having a more decreased FSC than early apoptotic cells.

Moreover, the kind of class switch occurring in this cell culture system was evaluated by a semiquantitative analysis of switch circles, which are excised during the CSR to IgG1 as well as during the direct and indirect switch to IgE.

In summary, this thesis answers my research questions by means of several in vitro experiments conducted with murine splenic B cells (figure 5).

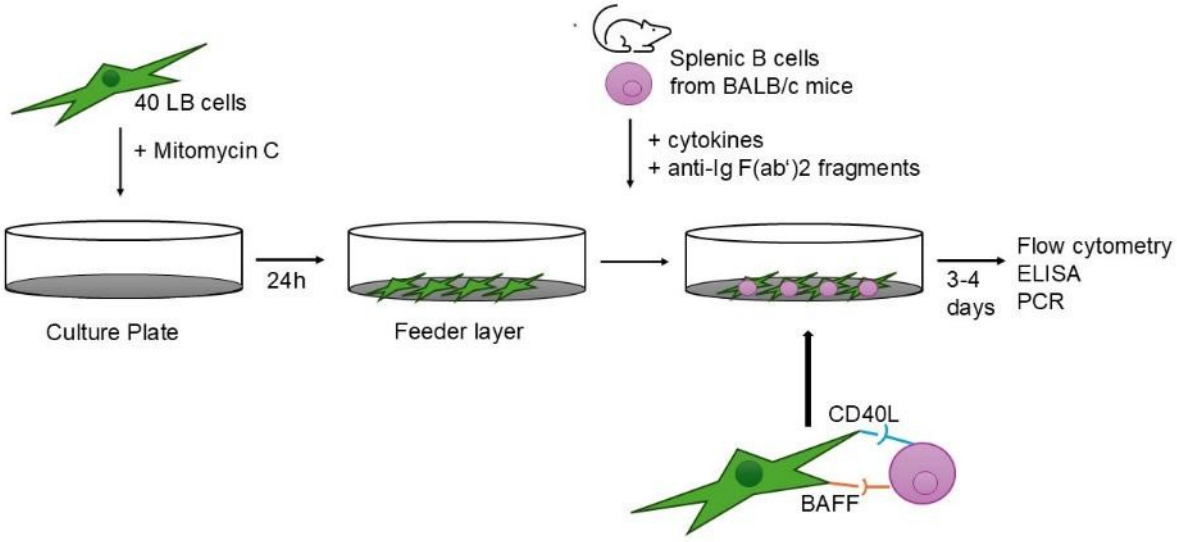

Figure 5: Visualization of the study design with the Induced Germinal Center B Cell Culture System. First, the feeder cell line 40 LB, BALB/c3T3 fibroblasts transfected with CD40L and BAFF (B cell activation factor), was treated with Mitomycin C to stop proliferation and seeded into the well plate. The adherent fibroblasts could attach to the plate. After one day, B cells are isolated from the spleen of naïve BALB/c mice and co-cultured with the 40 LB cells. Depending on the experiment, the culture was supplemented with cytokines and/or anti-Ig F(ab')$_2$ fragments. Depending on the method of the experiment, the cells were harvested after 3 or 4 days for further analysis via flow cytometry, ELISA, or semiquantitative PCR. Modified after: Bio-protocol. 2019;9(4):1-10. doi: 10.21769/BioProtoc.316

3. Methods and materials

3.1 Animals

Spleens were taken from female BALB/cAnNCrl mice at the age of 2-3 months according to the animal experiment approval 122-39_2016-06-17_Manz, "Töten zur Organentnahme". These animals were acquired from Charles River Laboratories (Sulzfeld, Germany) and sacrificed by trained members of the AG Manz.

3.2 Materials

3.2.1 Consumable materials

materials	source	catalog number
Cellstar 6 Well Cell Culture Plate, sterile, with lid	Greiner bio-one	657 160
Cellstar 48 Well Cell Culture Plate, sterile, with lid	Greiner bio-one	677 180
Cell strainer 70 µm Nylon	Th. Geyer	352 350
ELISA plate 96-well plate, white, flat bottom	Costar	3922
ELISA plate sealers	R&D Systems GmbH	DY992
Facs Tubes 5ml polysterene- Round-Bottom- Tubes (12x 75 mm)	Becton, Dickinson and Company	551579
Cellstar Tubes 50 ml	Greiner bio-one	227 261
Cellstar Tubes 15 ml	Greiner bio-one	188 271
Biosphare Filter tips (0.1-10 µL, 2- 100 µL, 100- 1000 µL)	Sarstedt AG & Co.	70.1130.210; 70.760.212; 70.762.211
NitraTex Medical Examination Gloves	Ansell	700112
Cellstar cell culture dishes, PS, 100 x 20 mn with vents	Greiner bio-one	664 160
Serological pipettes: 2 ml; 5 ml; 10 ml; 25 ml	Sarstedt AG & Co.	86.1252.001; 86.1253.001; 86.1254.001; 86.1685.001
Syringe 10 ml BD Discardit II	Becton, Dickinson and Company	309110
Safe Seal tube 1,5 ml, green	Sarstedt AG & Co.	72.798.005
Safe Seal tube 2,0 ml, blue	Sarstedt AG & Co.	72.695.005
Microtube 0,5 ml	Sarstedt AG & Co.	72.695.005
Cell scraper S	Sarstedt AG & Co.	83.3950
0.2 ml PCR Tubes with Flat Caps, high profile, clear	Bio-Rad	TFI0201
Versicap Mat, Ultra Clear Cap Strips	Thermo Fisher Scientific	AB1820

0.2 ml 8-Tube PCR Strips without Caps, low profile, clear	Bio-Rad	TLS0801
QIAshredder spin column	Quiagen	79654
PCR tubes 0,2 ml without cap, 8-stripes, transparent	Nerbe Plus	04-032-0500
Cap for PCR tubes 0,1 & 0,2ml, flat, 8-stripes, transparent	Nerbe Plus	04-043-0500
Microscope Slides, Menzel Gläser	Thermo Scientific	AAAA000001##12E
Amicon Ultra-4, PLGC Ultracel-PL Membran, 10 kDa	Merck Millipore	UFC801024
Cell culture flask, 50ml, 25cm^2	Greiner bio-one	690160

3.2.2 Chemicals and kits

chemicals	source	catalog number
Potassium chloride	Merck Biosciences GmbH	529552
Sodium chloride	Merck Biosciences GmbH	567440
Sodium phosphate dibasic dihydrate	Sigma-Aldrich	30435
potassium dihydrogen orthophosphate	Merck Biosciences GmbH	1048771000
Annexin V binding buffer	BioLegend	422201
EasySep™ Mouse Pan-B Cell Isolation Kit	Stem Cell	19854
MACS BSA Stock Solution	Miltenyi Biotec	P10-023100
Dimethyl sulfoxide (DMSO) (HYBRI-MAX)	Sigma-Aldrich	D2650
Ethylenediaminetetraacetic acid (EDTA)	Sigma-Aldrich	E5134
Isopropanol 70% Biocide	Th. Geyer	1150.5000
Tween 20	Sigma-Aldrich	P7949
Super Block Dry Blend Blocking Buffer	Thermo Fisher Scientific	37545
Tris base (Trizma base)	Sigma-Aldrich	93362
Super Signal ELISA Femto Maximum Sensitivity Substrate: H_2O_2 (Kit Peroxide), Enhancer (Kit)	Thermo Scientific	37074
Streptavidin-HRP	Becton, Dickinson and Company	554066
TaqMan™ Gene Expression Master Mix	Thermo Fisher Scientific	4369016
RNAse Away	Molecular Bio Products	7002
RNeasy Mini Kit (50)	Qiagen	74104 and 217004
PrimeScript RT Reagent Kit with gDNA Eraser (Perfect Real Time)	takarabio	RR047A

96–100% ethanol -EMPROVE ® exp Ethanol	Merck	100983
Trypan Blue Solution 0,4%	Thermo Fisher Scientific	15250-061
Gel Red ®Nucleic Acid Stain	Biotium	41003
Ultra Pure Agarose	Invitrogen	16500-500
Gene Ruler, DNA Ladder Mix	Thermo Scientific	SM0333
Acetic acid	Carl Roth	3738.4

3.2.3 Buffers and solutions

solution	composition
Tris-buffered saline, 10x	1 L Nanopure H_2O 15.125 g Tris Base 43.8 g NaCl pH 7.2
Super Signal ELISA Substrate	18 mL 1X Tris Saline pH 7.2 1mL H_2O_2 (Kit Peroxide) 1mL Enhancer (Kit)
Super block solution	Super Block Dry Powder 200 mL Nanopure H_2O
Blocking buffer	5 ml Super block solution; 45 ml WB
ELISA washing buffer (WB)	900 mL Nanopure H_2O 100 ml Tris Saline pH 7.2 500 µL Tween 20 (equals 0.05%)
10X PBS	8 g NaCl 0.2 g KCl 1.44 g Na_2HPO_4 0.24 g KH_2PO_4 pH 7,4 1 L Nanopure H_2O
PBS/BSA 0.5%	100 ml 10X PBS 900 ml Nanopure water 50 ml MACS BSA stock solution
MACS buffer	1 L PBS/BSA (0.5%) + 2 mM EDTA
FcyR-Block	2 mg/ml anti FcyR2b antibody - 2.4G2 clone 1:300 in PBS/BSA
50X TAE	242 g Tris base 100 ml EDTA 57,2 ml acetic acid 1 l Nanopure water

3.2.4 Cell culture

component	source	catalog number
ß-Mercaptoethanol (ß-Me)	Sigma-Aldrich	M3148
Penicillin streptomycin (P/S)	Thermo Fisher Scientific	15140-122
Fetal bovine serum (FBS)	Thermo Fisher Scientific	10270-106
Dulbecco's Modified Eagle Medium (DMEM), GlutaMAX™ Supplement +glucose + pyruvate 10% FBS and 1% P/S	Gibco, Thermo Fisher Scientific	31966-021
Roswell Park Memorial Institute 1640 (RPMI 1640) 10% FBS, 1% P/S, 50 µM ß-Me	Gibco, Thermo Fisher Scientific	61870-010
Dulbecco's phosphate-buffered saline (DPBS)	Gibco, Thermo Fisher Scientific	14190-094
Glucose solution	Gibco, Thermo Fisher Scientific	A2494001
AffiniPure F(ab')$_2$ Fragment Goat Anti-Mouse IgM, polyclonal	Dianova	115-006-075
Goat Anti-Mouse Ig kappa chain Antibody, F(ab′)2; polyclonal	Sigma-Aldrich	AQ500
Mitomycin C solved in Nanopure water	Sigma-Aldrich	M0503
LY294002 solved in DMSO	Merck Chemicals GmbH	440202-5MG

3.2.5 Cytokines, enzymes

component	source	catalog number
Recombinant Mouse IL-4 (carrier-free)	BioLegend	574302
DNase I unsterile	Sigma-Aldrich	10104159001

3.2.6 Antibodies and fluorescent dyes

antibody or dye	conjugate	clone	con-centration	dilution	source	catalog number
Fixable Viability Dye	eFlour780			1:1.600	eBioscience	65-0865-14
Mouse IgE, κ Isotype (Standard)	Purified		0.5 mg/ml		BD biosciences	553481
Rat Anti-Mouse IgE	Purified	R35-72	0.5 mg/ml	1: 400	BD biosciences	553413
Rat Anti-Mouse IgE	Biotin	R35-118	0.5 mg/ml	1:2500	BD biosciences	553419

anti-mouse IgG1 (Standard)	Purified		0.5 mg/ml		BioLegend	406601
Goat anti-mouse IgG1	unlabeled		1,0 mg/ml	1: 400	SouthernBiotech	1070-01
Goat Anti-Mouse IgG1	Biotin		0,5 mg/ml	1:2500	SouthernBiotech	1070-08
Annexin V	Pacific Blue			1:25	BioLegend	640917
2-NBDG			In PBS: 10 mM		Thermo Fisher Scientific	N13195
Cal-520 AM			2mM/ml		AAT Bioquest	21130
Anti-mouse IgG1	PE-Cy7	RMG1-1	0,2 mg/mL	1:400	BioLegend	406613
Anti-mouse IgE	PE	RME-1	0,2mg/ml	1:700	BioLegend	406907
Anti-mouse IgM	PerCP/Cy5.5	RMM-1	0,2 mg/ml	1:20	BioLegend	406511
Anti-mouse CD138	APC	281-2	0,2mg/ml	1:40	BioLegend	142506
Anti-mouse IgD	FITC	11-26c.2a	0,5mg/ml	1:200	BioLegend	405703
Anti-mouse IgD	Pacific blue	11-26c.2a	0,5mg/ml	1:50	BioLegend	405712
Anti-mouse CD19	BV785	6D5	0,2mg/ml	1:400	BioLegend	115543
Isotype control IgE	PE	eBRG1	0,2mg/ml	1:700	eBiosciences	12-4301-82
Anti-mouse CD8b.2	PE-Cy7	53-5.8	0,2 mg/mL	1:400	BioLegend	140415
Isotype control IgD	FITC	RTK2758	0,5mg/ml	1:200	BioLegend	400506
Isotype control IgM	PerCP/Cy5.5	RTK2758	0,2mg/ml	1:20	BioLegend	400545
Isotype control CD19	BV785	RTK2758	0,2 mg/ml	1:400	eBioscience	17-4321-41
Isotype control CD138	APC	eBR2a	0,2 mg/ml	1:40	BioLegend	400532

3.2.7 Primers

All purchased from Thermo Fisher Scientific

primer	Assay Name	Assay ID	Probe	Forward primer	Revers primer	Dye Label/ concentration
1	IGM-IGE-SWITCH	APM3XC	5'-ATAGACAGATGGGGGTGTCG-3'	5'-CTGGCCAGCCACTCACTTAT-3'	5'-AGGTGAAGGAAATGGTGCTC-3'	FAM-MGB / 20 X
2	IGM - IGG1-SWITCH	APNKXG9	5'-GGCTCCATAGTTCCATT-3'	5'-TCGAGAAGCCTGAGGAATGT-3'	5'-AGGTGAAGGAAATGGTGCTC-3'	FAM-MGB / 20X
3	IGG1 - IGE-SWITCH	APPRR26	5'-AGTCACTGACTCAGGGAA-3'	5'-CTGGCCAGCCACTCACTTAT-3'	5'-ATAGACAGATGGGGGTGTCG-3'	VIC-MGB / 20X
4	Tbp (housekeeping gene)	Mm01277042_m1				FAM-MGB/ 20 X

3.2.8 Technical equipment

equipment	source	serial/ catalog number
Centrifuge 5810R	eppendorf	5811CP070979
Centrifuge 5430R	eppendorf	5428JG229937
microplate washer: Immuno Wash 12	Nunc	
ELISA reader: FLUOstar Omega	BMG Labtech	
Flow cytometer: BD LSR II and FACS Flow Supply System	Becton, Dickinson and Company	H48700007
Freezer -80°C: Ultra-low-temperature-freezer, MDF-U73V	Sanyo Electric Co.	08121316
Incubator NU-5510E	Nuaire	144589060611
Labocult Incubator H770	Servoprax GmbH	04/2018/00024
Labgard Biological Safety Bench Class II	Nuaire	

Easy Eights EasySep Magnet	Stemcell Technologies	18103
Microcentrifuge	Roth	068361& 044875
Microscope Type 11090137001	Leica	
Neubauer Chamber Assistent	Karl Hecht	
pH meter Seven Easy	Mettler Toledo	
Pipette filler Pipetus	Hirschmann	
Pipettes Research Plus 0,1-2,5 µL; 0,5-10 µL; 10-100 µL, 30-300 µL, 100-1000 µL	eppendorf	
Multipipette plus	eppendorf	
Water Bath SW-20-c	Julabo	5129346129
Laboratory vacuum pump: Vacusafe	INTEGRA Biosciences AG	180609
C1000 Touch Thermal Cycler	Bio-Rad	CT030356
CFX96 Optical Reaction Module for Real-Time PCR Systems	Bio-Rad	785BR08935
ND1000 Spectrophotometer	Nano Drop Technologies	E926
Vortex-Genie 2 G560E	Scientific Industries	
Vortex REAX 2000	Heidolph	17007
Gel chamber: CompactM	Biometra	070611159
Power PacHC	Bio-Rad	043BR66876
Image Quant 350	GE Healthcare	
Milli-Q, IQ7000	Millipore SAS	F0AB85209E

3.2.9 Software

software	source
BD FacsDIVA Software version 8.0.1	Becton, Dickinson and Company
FlowJo, version 10.7.1	Becton, Dickinson and Company
ImageJ 1.53k	Wayne Rasband and contributors; National Institutes of Health, USA
GraphPad Prism 9.2.0	GraphPad Software
NanoDrop 1000 3.8.1	Thermo Scientific
MARS Data analysis Software	BMG Labtech
R, version 4.0.5	R Foundation for Statistical Computing
CFX Manager Software, version 3.1	Bio-Rad
Mendeley (citation manager)	Elsevier

3.3 Methods

3.3.1 Next-generation sequencing (NGS) analysis

IgE and IgG1 sequences of the mesenteric lymph node of two BALB/c mice on day 15 after primary N. brasiliensis infection (Turqueti-Neves et al., 2015) were uploaded to the international ImMunoGeneTics (IMGT) database (Lefranc et al., 2009). The V, D and J regions were assigned by IMGT/V-QUEST (Brochet & Lefranc, 2008; Giudicelli & Brochet, 2011). The IMGT/V-QUEST output file was used as an input file in the IMGT/StatClonotype database, grouping the assigned VDJ gene rearrangements into clonotypes (Aouinti et al., 2015, 2016). The resulting IMGT/StatClonotype.txt file was further analyzed in Excel: unproductive sequences or sequences containing only one copy number were deleted. Clones or clonotypes were defined as BCRs containing the same VDJ rearrangement with conserved CDR3-IMGT anchors. The productive VDJ genes of IgE and IgG1 were divided into shared clones comprising of the same VDJ genes for IgE and IgG1 and unique clones. The ratio of the copy number of shared IgE/IgG1 was calculated. Depending on the ratio, the IgE clones were divided into IgE or IgG1 biased IgE. The former definition was applied for an IgE/IgG1 copy number of ratio ≥ 2, the latter for an IgG1/IgE copy number ratio ≥2.

This manual Excel analysis, supervised by Christopher C. Udoye, corresponds to the later published Excel VBA Macro (https://mega.nz/file/wwBgAZBD#yrZcvHVpLINE6GYmrEeRDSWiU6XpIeCqnlj425uvzhA).

In addition, the amino acids of the sequences which are part of the IMGT/StatClonotype.txt were investigated for their physiochemical properties, using the “peptide” package (Osorio et al., 2015) in R (Team, 2021).

The results were visualized as diagrams using GraphPad Prism 9.2.0.

3.3.2 Calcium flux assay

First, a single cell suspension of a murine spleen was generated, working on ice. The organ was smashed between the rough sides of two microscope slides over a petri dish covered with cold PBS/0,5% BSA. This homogenous suspension was transferred with a syringe through a 70 µm cell strainer into a 50 ml falcon tube. PBS/0,5% BSA was used to fill the falcon tube up to 50 ml. 30 µL of the cell suspension was pipetted into a 0.5 ml tube and diluted in trypan blue in the ratio of 1 to 10. The total number of cells was determined using a Neubauer counting chamber: *concentration (cells/mL)=(cells per square ×chamber factor ×dilution factor)×volume*. Next, the suspension was centrifuged (350x g, 10 min, 4°C), resuspended in PBS/0,5% and centrifuged again (350x g, 10 min, 4°C). The supernatant was decanted into the waste.

Thereafter, a surface staining was conducted: the suspension was incubated with an anti FcyR2b antibody, diluted in PBS/ 0,5% BSA and stained with the Fixable Viability Dye eFluor 780, as well as PerCP/Cy5.5- and Pacific Blue conjugated anti-mouse antibodies directed against IgM (clone: RMM-1) and IgD (clone: 11-26c.2a), diluted in PBS/0,5% BSA (compare 3.3.5).

After the last centrifugation step of the surface staining, the cells were resuspended in warm RPMI medium to a concentration of 5 x 10^6 cells/mL and incubated for 15 min at 37°C. Then, CalbryteTM 520 AM solution was added to a concentration of 2mM Cal-520 AM/mL cell suspension. Beforehand, the dye was dissolved in DMSO to a working solution of 2µM Cal-520 AM. The mixture was incubated for 1h at 37°C and centrifuged (350xg, 10 min, RT). The supernatant was discarded, the pellet was resuspended in RPMI medium to a concentration of 5 million cells/ 750 µL and the cells rested at room temperature for 10 min. 750 µL of the cell suspension was transferred to each FACS (fluorescence-activated cell-sorting) tube through a 70µm FACS-tube-filter.

Flow cytometry analysis was performed with an LSRII flow cytometer. After measuring a baseline value for 20 seconds, polyclonal AffiniPure $F(ab')_2$ fragments of goat anti-mouse IgM or goat anti-mouse anti-Ig kappa $F(ab')_2$ fragments were added to the cell suspension in titrated concentrations (0-1-2-4-8 µg/ml) and the measurement continued until 3 min/condition. The kinetics of the calcium signal detected in the FITC channel were evaluated using the software Flow Jo 10.7.1., investigating the calcium response of IgD-high/low as well as IgM-high/low cells.

In one experimental setting, the anti-Ig kappa $F(ab')_2$ fragments were purified before starting the experiment. For this procedure, 50µL of the goat anti-mouse anti-Ig kappa $F(ab')_2$ fragments were added with 4 ml of either PBS/BSA or DPBS to the Amicon Ultra filter device and centrifuged (4°C; 20min; 4,000 x g). The supernatant was discarded in a 15 ml tube. Again, 2 ml of either PBS/BSA or DPBS were added to the Amicon Ultra filter device and centrifuged (4°C; 20min; 4,000 x g). The supernatant was discarded in a 15 ml tube. Thirdly, 2 ml of either PBS/BSA or DPBS were added to the Amicon Ultra filter device and centrifuged (4°C; 20min; 4,000 x g). The remaining volume from the filter (after dilution with PBS/BSA: 260 µL, after dilution with DBPS: 160 µL) was transferred to another tube and stored at 4 °C.

The calcium flux experiments were conducted together with Sarah Rümpeler who performed a traineeship during her Master studies in our research group, enabling me to perform the experiments when I broke my arm.

3.3.3 Cell culture

The protocol for the Induced Germinal Center B Cell Culture System using BALB/c 3T3 fibroblasts transfected with CD40L and BAFF was adopted from Hanuida & Kitamura (Haniuda & Kitamura, 2019; Nojima et al., 2011). The cells were cultured in DMEM containing 10% FBS and 1% Penicillin/Streptomycin. 24 hours before B cell isolation, the fibroblast culture was incubated with Mitomycin C to stop proliferation, which is different from the original protocol.

PBS and DMEM were warmed up. The 40 LB cells in the cell culture flasks were detached with a cell scraper and resuspended with a pipette. 10 ml cell suspension was taken from each cell culture and replaced with 10 ml warm DMEM. 30 µL of each cell suspension was transferred in an aliquot to count the cells with a Neubauer chamber (dilution factor 1:2). Cell suspensions were centrifuged (350xg, 10 min, RT) in 50 ml falcon tubes, the supernatant was discarded. Cells were resuspended in 2 ml warm DMEM. 10 µg/mL of Mitomycin C was added to each tube and incubated at 37°C, 5% CO2 for 30 min. Next, 50 ml warm PBS was added to each tube to wash the cells. The cell suspension was centrifuged again (350xg, 10 min, RT) and the supernatant was discarded. The washing was repeated. Cells were resuspended in warm DMEM medium and seeded into 48-well plates (5*10^4 cells / well) or 6 well-plates (5*10^5 cells/well). Cells rested for 24h in the incubator at 37 °C.

3.3.4 B cell isolation from spleen

First, a single cell suspension of the murine spleen was generated, working on ice and under the safety bench class II. The organ was smashed between the rough sides of two microscope slides over a petri dish covered with cold PBS/0,5% BSA. This homogenous suspension was transferred with a syringe through a 70 µm cell strainer into a 50 ml falcon tube. PBS/0,5% BSA was used to fill the falcon tube up to 50 ml. 30 µL of the cell suspension was pipetted into a 0.5 ml tube and diluted in trypan blue in the ratio of 1 to 10. The total amount of cells was counted with a Neubauer chamber (dilution factor 1:10). Next, the volume encompassing the number of needed cells was transferred to a new falcon tube and centrifuged (350x g, 10 min, 4°C). The supernatant was decanted into the waste.

Secondly, B cells were isolated from the single cell suspension using the EasySep™ Mouse Pan-B Cell Isolation Kit: the centrifuged cell pellet was resuspended in MACS buffer to a concentration of 1x10^8 cells/mL and incubated at room temperature (RT) for 10 minutes with 50 µL/mL of Rat serum and Isolation cocktail. Subsequently, the suspension was incubated with 75 µL/mL of Rapid Spheres for 2.5 minutes and filled up to 2.5 ml with MACS buffer. The non- B cells were excluded from the cell suspension

through dual incubation in an EasySep magnet for 2.5 min at RT. After each of these two magnetic incubation steps, the enriched cell suspension was poured into a 10 ml falcon tube. The remaining particles were resuspended in 2,5 ml MACS buffer after the first incubation with the magnet. An aliquot of the cell suspension was diluted in trypan blue in the ratio of 1:2 to count the number of cells with a Neubauer chamber. Again, an appropriate volume was transferred to a new falcon tube and centrifuged (350x g, 10 min, 4°C). The supernatant was decanted into the waste.

Thirdly, a “Germinal Center Culture” was generated: the cell pellet was resuspended in warm RPMI medium to a concentration of 1x 10^6 cells/ml. In general, the RPMI medium in all experiments contained 10% FBS, 1% Penicillin/Streptomycin, and 50 µM ß-Mercaptoethanol. The DMEM medium of the fibroblast pre-culture was replaced with RPMI medium, adding 4.5 ml of RPMI and 0.5 ml of B cells suspension/well to a 6 well-plate or 950 µl RPMI and 50 µl of B cell suspension/well to a 48 well-plate. B cells were stimulated with 2 ng/ml of recombinant mouse IL-4 on day 0 and day 1. Additionally, the Germinal Center Culture was supplemented with different concentrations of the polyclonal AffiniPure F(ab')$_2$ fragment goat anti-mouse IgM or goat anti-mouse anti-Ig kappa F(ab')$_2$ fragments on day 0.

A different stimulation procedure was used for the experiments concerning the role of co-stimulatory factors: various IL-4 concentrations (0.5, 1, 2, 4 and 8 ng/ml) were added on day 0 and 1 of the culture. Moreover, the glucose concentration of the RPMI medium (200 mg/dL) was adjusted by diluting it in glucose free RPMI medium to 50, 100 or 150 mg/dL or by adding a glucose solution to 300 or 400 mg/dL.

On day 3 of the culture, 50 % of the RPMI medium was discarded by pipetting it out of the wells and it was replaced with new RPMI medium.

An aliquot was taken from each condition on day 4 of the cell culture to count the cells with a Neubauer chamber. Cells were stained with trypan blue (dilution 1:2) and counted under the microscope. The total cell number of a condition was multiplied by the frequency of IgE+ and IgG1+ cells in % (measured by flow cytometry, see 3.3.5) and divided by the frequency of FVD positive living cells in % to calculate the counted IgE+ and IgG1+ cells.

3.3.5 Surface staining

All steps were performed on ice. On day 4 of the described co-culture, the cells were strongly resuspended in their medium in each well and transferred into 2 ml tubes. 30 µL of the cell suspension was pipetted into a 0.5 ml tube and diluted in trypan blue in the ratio of 1 to 2. The total amount of cells was counted with a Neubauer chamber.

The cell suspension was centrifuged (350x g, 10 min, 4°C) and the supernatant was discarded. The remaining pellet was incubated with an anti FcyR2b antibody, diluted in PBS including 0,5% BSA, for 5 min at 4 °C. Next, the cell suspension was stained with the Fixable Viability Dye eFluor 780 and PE-Cy7, PE-, PerCP/Cy5.5-, FITC-, APC- and BV785 conjugated anti-mouse antibodies directed against IgG1 (clone: RMG1-1), IgE (clone: RME-1), IgM (clone: RMM-1), IgD (clone: 11-26c.2a), CD138 (clone: 281-2), and CD19 (clone: 6D5), diluted in PBS/0,5% BSA. Afterwards, the stained samples were incubated for 10 min at 4°C. The samples were washed in 1 ml PBS/0,5% BSA, centrifuged (350x g, 10 min, 4°C), and the supernatant was discarded. Finally, 400 µL PBS/0,5% BSA with 1:1000 DNase was added. A flow cytometry analysis was performed with an LSRII flow cytometer, and the compensation was calculated by BD Diva during the FACS measurement.

The gating according to isotype controls was accomplished using Flow Jo 10.7.1 software. A time gate prevented potential irregularities, for example air bubbles. Dead cells were excluded from the analysis by means of the Fixable Viability Dye (FVD), cell doublets and debris by FSC-A versus FSC-H gating. 40LB cells were excluded from the analysis based on FSC-A versus FSC-H and SSC-W versus SSC-H gating. The Pacific-Blue channel (max. excitation 407 nm; Bandpass filter 450/50 nm) was used to rule out autofluorescence. The frequency of the immunoglobulins IgE and IgG1 was analyzed.

3.3.6 Apoptosis staining

The procedure of the surface staining was adjusted to stain for apoptosis. After the last centrifugation step of the surface staining as described above, the cells were resuspended in 250 µL cold Annexin V binding buffer and centrifuged (300xg, 10 min, 4°C). Then, the cells were resuspended in 30 µL cold binding buffer and 1,2 µL of Annexin V- Pacific Blue was added to each tube. These samples were incubated at RT for 15 minutes, before they were placed again on ice. As a last step before the flow cytometry analysis, using LSR II, 300 µL cold binding buffer was added.

The gating was performed as described (chapter 3.3.5), the AF700 channel (max. excitation 696 nm; Bandpass filter 730/45 nm) was measured to rule out autofluorescence. To analyze apoptotic cells, necrotic and dead cells were excluded, using the FVD. To differentiate between apoptotic and viable cells, Annexin V was applied. The decrease in cell volume and size in apoptotic cells is detected by FSC gating, with late apoptotic cells having a more decreased FSC than early apoptotic cells.

3.3.7 Glucose uptake

The procedure of the surface staining was adopted to measure the glucose uptake. After harvesting and centrifuging the cells (compare 3.3.5), the cells were resuspended in 200 µL of warm RPMI medium. Two µl of the 10 mM 2-NBDG stock solution dissolved in PBS was added to the cells, achieving a concentration of 100 µM 2-NBDG. The cells were incubated for 20 min at 37°C. Thereafter, the cells were washed in 1 ml PBS/0,5% BSA, centrifuged (350xg, 10 min, 4°C) and the supernatant was discarded. The surface staining protocol was carried out as described, starting with the incubation of the samples with the anti FcyR2b antibody.

In addition to the explained gating strategy (chapter 3.3.5), the Mean Fluorescence Intensity (MFI) of 2-NBDG (FITC) of IgE+ and IgG1+ cells was analyzed by means of the software Flow Jo 10.7.2.

The data of two experiments was normalized in Graph Pad 9.2.0, defining 0 % as the smallest mean of the data set for each dye and 100 % as the largest mean of the data set for each dye.

3.3.8 Enzyme-linked Immunosorbent Assay (ELISA)

The cell culture supernatant used for the ELISA experiments was generated on day 4 of the Germinal Center Culture (see section 3.3.4): the harvested cells were centrifuged (350xg, 10 min, 4°C) and the cell culture supernatant were stored at -80°C until the day of the ELISA experiments.

An opaque 96-well plate was coated with 50 µL of unlabeled anti-IgE or -IgG1 antibodies diluted in 1X Tris Saline to a concentration of 2,5 µg/ml. After incubation at 4°C overnight, the plate was washed three times using a washing buffer. Remaining uncoated places in the wells were blocked using a blocking buffer. It was incubated for 30 minutes. Next, the wells were incubated overnight at 4°C with 30 µL of the cell culture supernatants from day 4 of the Germinal Center Culture and purified anti-mouse IgE or IgG1 as a standard, titrated in doublets. Again, the plate was washed three times with the washing buffer. Subsequently, the plate was incubated with 50 µL of 200 ng/mL biotinylated anti- IgE or -IgG1 antibodies, diluted in blocking buffer, for 60 minutes. The washing step was repeated before 200 µL of 50 ng/mL Streptavidin-HRP in blocking buffer was added and incubated for 25 minutes. Next, the plates were washed five times. Then, 200 µL of the Super Signal ELISA Substrate was added to the wells. Immediately, the plate was analyzed by means of a luminometer. The MARS data analysis software measured the luminescence and calculated the relative light units of each well. The mean of the cell doublets was visualized using Graph Pad Prism 9.2.0.

3.3.9 RNA isolation and reverse transcription

RNA was obtained on day 3 of the Germinal Center Culture using the RNeasy Mini-Kit, performing all steps at RT and the centrifugation steps at 21 °C. The cells were resuspended in their medium in each well of the 6- well plate and transferred to 15 ml tubes. 30 µL of the cell suspension was pipetted into a 0.5 ml tube and diluted in trypan blue in the ratio of 1 to 2. The total number of cells was counted with a Neubauer chamber. The cells were centrifuged for 5 min at 300 x g and the supernatant was removed by pipetting. Next, 350 or 600 µL of buffer RLT was added, depending on whether the number of counted cells was less or more than 5 million. The sample was vortexed to generate a lysate, transferred to a QIAshredder spin column positioned in a 2 ml collection tube and centrifuged for 2 min at 9000 x g. Then, a volume of 70% ethanol equal to the RLT volume was added and mixed by pipetting. 700 µL of this solution was transferred to the RNeasy spin column placed in a collection tube and centrifuged for 15 s at 8000 x g. The flow-through was discarded. Afterwards, 700 µL of buffer RW1 was added to the RNeasy spin column and centrifuged for 15 s at 8000 x g. The flow through was discarded. Next, 500 µL of the buffer RPE was added to the spin column, followed by a centrifugation for 15 s at 8000 x g and the discard of the flow-through. Again, 500 µL of the buffer RPE was added and it was centrifuged for 2 min at 8000 x g. The RNeasy spin column was placed in a new 2 ml collection tube and centrifuged for 1 min at 9000 x g to dry the membrane. Finally, RNeasy spin column was placed in a new 1.5 ml collection tube, 50 µl RNAse-free water was pipetted directly to the membrane of the spin column and it was centrifuged for 1 min at 8000 x g.

The RNA was quantified by means of the NanoDrop Spectrophotometer, measuring triplets of each sample. In addition to the concentration, the purity was evaluated by the ratio of the absorbance at 260 nm and 280 nm. A 260/280 ration between 2.0 and 2.2 was considered pure.

The DNase digestion and reverse transcription into cDNA were accomplished via PrimeScript RT Reagent Kit with gDNA Eraser, executing all steps on ice. To begin with the genomic DNA elimination reaction, 2 µg of the RNA was pipetted into a 0.2 ml PCR stripe (Nerbe Plus), mixed with 2 µl of 5X gDNA Eraser Buffer, 1.0 µl of gDNA Eraser and RNase free water, resulting in a volume of 10 µl. The samples were centrifuged and they rested in the thermocycler for 2 min at 42 °C.

To continue with the reverse transcription reaction, further components were added to the 10 µl reaction solution of the DNA elimination: 4 µl of 5X PrimeScript Buffer 2, 1 µl of Prime Script RT Enzyme Mix I, 4 µl of RT Primer Mix and 1 µl of RNase free water. The reverse-transcription reaction was performed with a thermocycler at 37°C for 15 min and 85°C for 5 s.

3.3.10 PCR

Three different primer pairs were used to detect switch circles which are excised during the CSR to IgG1 as well as during the direct and indirect CSR to IgE. Each pair consists of a reverse primer in the C_H region downstream of the appropriate donor S region and a forward primer in the intron upstream of the acceptor S region. All sequences are already published (Park et al., 2005; Wesemann et al., 2011): the excised circles of the direct switch from μ to ε consist of a forward primer in Iε (5'-CTGGCCAGCCACTCACTTAT-3') and a reverse primer in Cμ (5'-AGGTGAAGGAAATGGTGCTC-3'), while switch circles resulting from the indirect switch to ε contain a forward primer in Iε(5'-CTGGCCAGCCACTCACTTAT-3') and a reverse primer in Cγ1 (5'-ATAGACAGATGGGGGTGTCG-3'). Moreover, the excised circles derived from the switch from μ to γ1 was defined by a forward primer in Iγ1 (5'-TCGAGAAGCCTGAGGAATGT-3') and a reverse primer in Cμ (5'-AGGTGAAGGAAATGGTGCTC-3'). Tbp (Mm01277042_m1) was used as a housekeeping gene.

The steps of the PCR were carried out on ice. 0.2 ml 8-tube PCR strips were filled with 10 µl of the gene expression master mix, 1 µl of the primer assay and 9 µl of the cDNA template, which was generated from 2 µg RNA. After the centrifugation of the samples, the strips were placed in the PCR instrument. It ran 2 min at 50 °C, then10 min at 95°C, followed by 40 repetitions of the PCR cycle. This PCR cycle consisted of denaturation at 95°C for 15 s and annealing at 60°C for 60 s.

As a last step, the PCR product was visualized by gel electrophoresis. To produce the gel, 1.5 g agarose and 125 ml of 1X TAE buffer were heated in the microwave for 3 min in a 500 ml flask. 2µl GelRed was added into the flask and the suspension was poured into the chamber. After a polymerization time of 45 min, 1 µl of DNA ladder and 3 µl of sample/lane were added. The gel ran for 110 min at 110 V and was photographed using Image Quant. The integrated density of the band of the gene of interest relative to the house keeping gene was measured using ImageJ.

3.4 statistical analysis

The software R was used to calculate statistical tests (Team, 2021). The results of the experiments were saved in different EXCEL tables in a .csv format and imported into R (Wickham & Bryan, 2019).

The descriptive statistics were summed up, applying the package "psych" (Revelle, 2020). Non-parametric tests were chosen after confirmation of a not-normal distribution according to the Shapiro Wilk test. Another aspect is the dependence of the samples considering that the cells of an individual mouse were used in all conditions.

A two-tailed Wilcoxon signed rank test was chosen for experiments which compared two different conditions.

A Friedman test was conducted for experiments that included more than two different conditions. If this global test was significant, a multiple comparison of all conditions was implemented by a two-tailed Wilcoxon signed rank test, adjusting the p-value according to the correction method Holm. A significant result was defined by a p-value of 0.05 or less.

The effect size of the Wilcoxon signed rank test was computed using the package “DSUR.noof” (Aufheimer, 2021). The output of the R console was summarized in a table and exported as a .html file, executing the package “stargazer” (Hlavac, 2018, 2022).

I made use of a biometric consultation, comprising approximately 1,5 hours.

4. Results

4.1 NGS analysis

Experiments of our research group explored the clonal relationship between IgE and IgG1 in a murine food allergy model, indicating that each BCR clonotype varies in its proportion of the two immunoglobulins and that IgE- or IgG1- biased IgE clones show similar physiochemical properties (Udoye et al., 2022).

Net charge, aliphatic index, isoelectric points and hydrophobicity define polyreactive and specific antibodies (Rabia et al., 2019; Boughter et al., 2020). For this reason, my research group chose these physiochemical properties for their analysis.

To verify whether the properties of the IgE and IgG1 repertoire detected in our allergy model can be reproduced in other systems, the IgE and IgG1 sequences originated from mice in a helminth infection-model were analyzed (Turqueti-Neves et al., 2015).

In more detail, IgE and IgG1 sequences of the mesenteric lymph node of two BALB/c mice on day 15 after primary N. brasiliensis infection (Turqueti-Neves et al., 2015) were uploaded to the IMGT database as described. The resulting IMGT/StatClonotype.txt file was analyzed in Excel and the amino acids were analyzed using the “peptide” package in R.

Clones or clonotypes, shared and unique clones were defined as described (Udoye et al., 2022): clones were defined as BCRs containing the same VDJ rearrangement. The VDJ genes of IgE and IgG1 were divided into shared clones covering the same VDJ rearrangement for IgE and IgG1 and into unique clones. A unique IgE clone was defined as an IgE clone which is only present in the IgE- and not in the IgG1- compartment. The ratio of the copy number of shared IgE/IgG1 was calculated. Depending on the ratio, the IgE clones were divided into IgE- or IgG1- biased IgE.

Resembling the findings in the food allergy model, the analysis of the BCR repertoire of the N. brasiliensis infection model demonstrated that shared clones showed a bias to IgE (IgE_E) or IgG1 (IgE_G). Of note, more clones expressed IgE_E than IgE_G in contrast to our allergy model (figure 6 A, B). A large difference in the isoelectric point, the hydrophobicity, the net charge and the aliphatic index was observed between the two mice (figure 6 C), but the mean values of the isoelectric point, the hydrophobicity and the net charge were similar among IgE_E and IgE_G.

All in all, the low number of mice and the variation of the physiochemical properties between the mice limit any general conclusion about the IgE response in the helminth system. Nevertheless, it reveals an observation which is comparable to the findings in the allergy model. The analyzed sequences contained IgE_E and IgE_G clonotypes, reproducing

the finding that individual BCR clonotypes present different proportions of IgG1 and IgE. Moreover, most of the physiochemical properties of IgE_E and IgE_G clonotypes are similar. In conclusion, IgE to IgG1 ratios may be controlled on the level of individual B cell clones in food allergies and during infection.

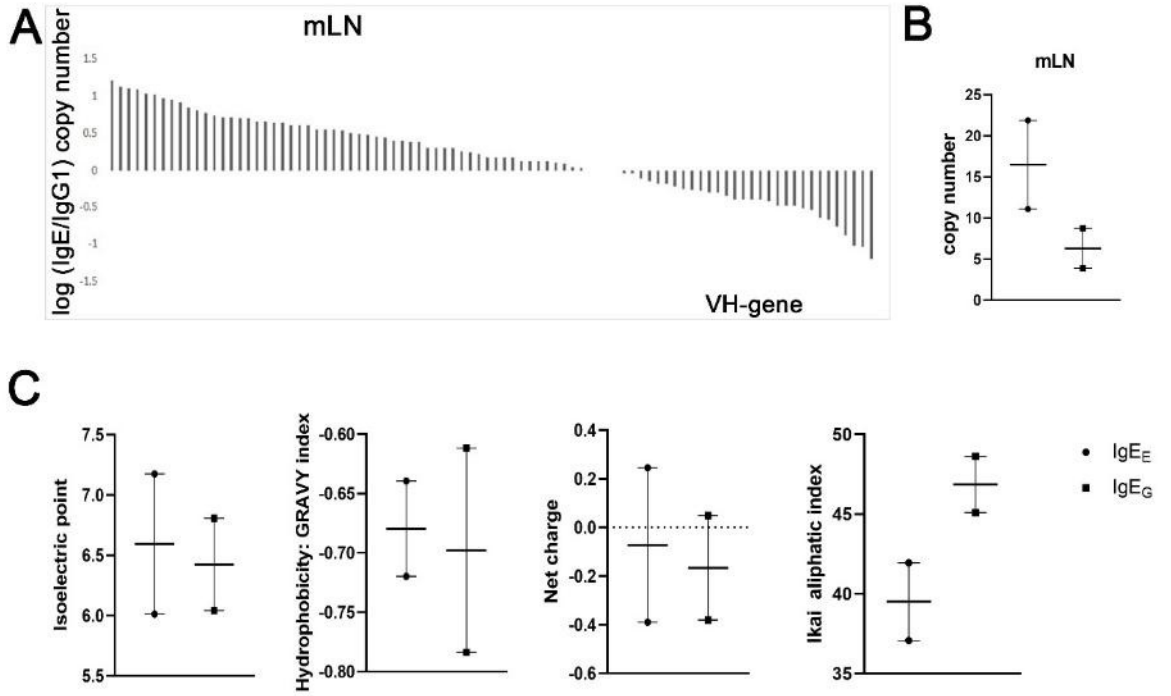

Figure 6: Clonal expansion and physiochemical properties of IgE_G and IgE_E.
Published sequences from the mesenteric lymph node (mLN) from 2 Balb/c mice on day 15 after primary N. brasiliensis infection. (A) Data from one mLN is presented. Shared clonotypes of the VH-gene were categorized in reference to the ratio of the copy number of IgE and IgG1. (B) classification of the shared clones in IgG1 biased (IgE_G, IgG/IgE copy number ratio of ≥ 2) or IgE biased IgE (IgE_E, IgE/IgG copy number ratio of ≥ 2). (C) Physiochemical properties of the amino acids of the sequences were analyzed. The isoelectric point, the hydrophobicity, the net charge and the aliphatic index are shown. Each dot represents the data from one mouse. Mean + SEM are shown.

4.2 BCR stimulation

4.2.1 Calcium flux assay

To investigate the finding that individual B cell clones and probably the BCR itself control the IgE to IgG1 ratio, the impact of BCR signaling strength on the production of IgE and IgG1 should be analyzed. As a first step, it was examined whether the titration of anti Ig $F(ab')_2$ fragments is an appropriate model to represent quantitatively different BCR signaling strengths, inducing calcium signaling pathways in B cells to a greater or lesser extent.

Anti-Ig $F(ab')_2$ fragments which bind directly to the antigen binding site of the BCR can activate an intracellular calcium response (Volkmann et al., 2016). This calcium response was analyzed by measuring the calcium flux. For that purpose, cell suspensions from the spleens of naïve mice were generated, the cell surface was stained for IgD and IgM. Next,

the calcium flux was quantified by flow cytometry. During the flow cytometry analysis, anti-IgM F(ab')$_2$ fragments or anti-Ig kappa F(ab')$_2$ fragments were added to the cell suspensions in titrated concentrations (0-1-2-4-8 µg/ml) and measured immediately. B cells were defined as IgM^{high}IgD^{low}, i.e. marginal zone B cells, or IgM^{low}IgD^{high}, i.e. follicular B cells. Flow Jo 10.7.1 was used to identify IgD$^{high/low}$ as well as IgM$^{high/low}$ cells and to determine their calcium kinetics.

Elaborating further on the method, calcium kinetics are represented by the area under the curve (AUC) because it demonstrates the entire capacity of IgD$^{high/low}$ and IgM$^{high/low}$ B cells to mobilize Ca2+ in response to the activating F(ab')$_2$ fragments. Combining flux measurement and cell-surface staining is in accordance with a new standardized procedure to characterize calcium flux of peripheral human B lymphocytes from healthy individuals by flow cytometry (Bajnok et al., 2023).

A calcium flux could not be detected for BCR-stimulated non-B cells, classified as IgM- and IgD- negative, as well as for non-stimulated B cells. By contrast, upon BCR stimulation, a calcium flux could be measured for all B cell subsets. The highest calcium flux within the B cells was measured while stimulating the cells with the highest concentration of anti-Ig kappa and anti-IgM F(ab')$_2$ fragments. For both anti-BCR antibodies, the AUC was higher for IgM^{high}IgD^{low} than for IgM^{low}IgD^{high} B cells (figure 7 A). There was a statistically significant increase in calcium flux after adding 1, 2, 4 or 8 µg/ml anti-IgM F(ab')$_2$ fragments, comparing each concentration to the condition of no stimulation. The calcium response to anti-Ig F(ab')$_2$ fragments amplified in a dose-dependent manner (figure 7 B).

These results are comparable with a recent study conducted by Berry and colleagues. In vitro stimulation of murine B cells with anti-mouse IgM F(ab')$_2$ fragments revealed that different BCR signaling strengths generated quantitatively different intracellular calcium signals. The stronger the BCR signaling strength, the higher was the quantity of the calcium signal (Berry et al., 2020).

Together, these findings indicate that different concentrations of both, anti-IgM and anti-Ig kappa F(ab')$_2$ fragments, can serve as a model for different BCR signaling strengths, with higher concentrations corresponding to a stronger BCR signaling and a stronger calcium response.

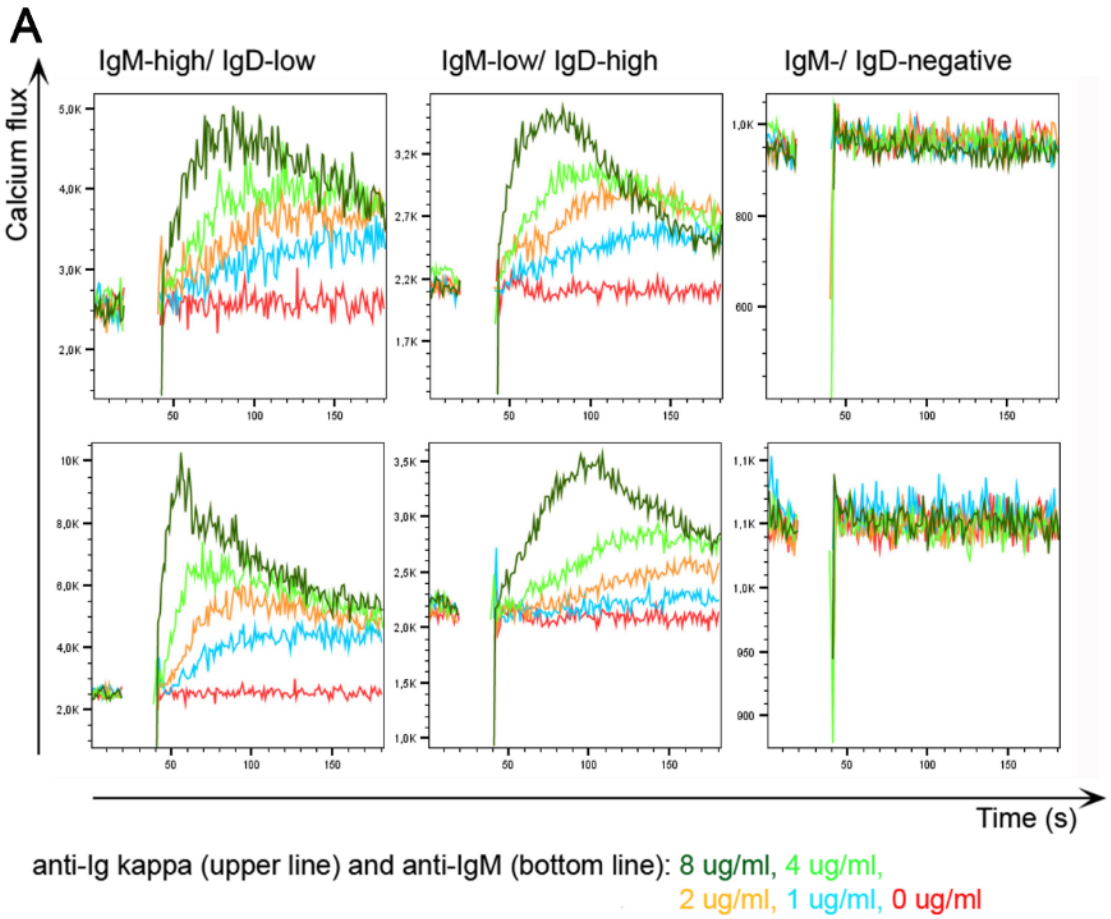

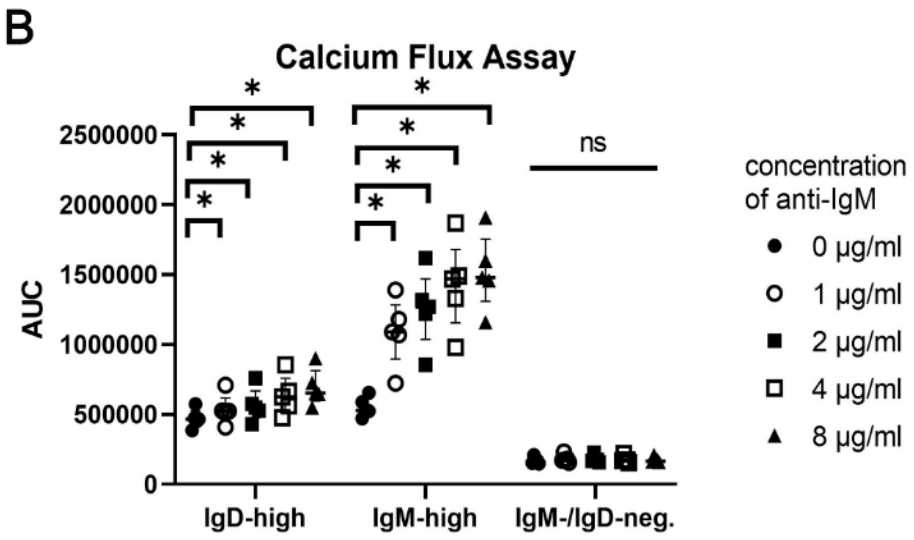

Figure 7: Anti-Ig F(ab')$_2$ fragment induced calcium flux.
Single cell suspensions were generated from spleen and stained for IgM and IgD. After the incubation with CalbryteTM 520 AM, polyclonal anti-IgM or anti-Ig kappa F(ab')$_2$ fragments (0-1-2-4-8 µg/ml) were added to the different samples and the calcium flux was immediately measured by flow cytometry (LSRII). (A) Representative FACS data from IgM^{low}/IgD^{high} follicular B cells, IgM^{high}/IgD^{low} marginal zone B cells and IgM-/IgD-negative splenic cells. (B) Statistical analysis of the calcium flux induced by different concentrations of anti-IgM F(ab')$_2$ fragments for three cell populations as described in A. Calcium flux is depicted as AUC (area under the curve). The summary of three independent experiments is shown, each dot represents data from one mouse. Median and IQR are presented. Statistics: Friedmann-Test: ***p ≤ 0.001, multiple testing after a significant global test: Wilcoxon signed rank test, correction method: Holm (0 and 8 µg/ml, 0 and 4 µg/ml, 0 and 2 µg/ml, 0 and 1 µg/ml), *p ≤ 0.05. Statistical analysis of the calcium flux induced by different concentrations of anti-Ig kappa F(ab')$_2$ fragments was not possible because it was conducted with only two mice in two different experiments.

4.2.2 Anti-IgM F(ab')$_2$ fragments

As a second step to address the hypothesis that individual B cell clones and probably the BCR itself control the IgE to IgG1 ratio, the impact of BCR signaling strength on the production of IgE and IgG1 was analyzed.

The production of pathogenic high-affinity IgE antibodies requires an intermediate germinal center B cell-fate (Haase & Voehringer, 2021; Q. Chen et al., 2023; Xiong et al., 2012). Therefore, a Germinal Center Culture was generated, adopting a protocol from Hanuida & Kitamura (Haniuda & Kitamura, 2019; Nojima et al., 2011). Splenic B cells from BALB/c mice were co-cultured with fibroblasts transfected with CD40L and BAFF, covering the function of feeder cells, and stimulated with IL-4 to induce class switch to IgE and IgG1 (compare method section: chapter 3.3.3). This experimental setting will be termed in subsequent descriptions as “Germinal Center Culture”. Class switch recombination occurs in comparable splenic B-cell cultures within 3 days (Schrader, 2014) and the first step of the germinal center-like reaction is finished on day 4 of the Germinal Center Culture (Nojima et al., 2011).

Focusing on the impact of different BCR signaling strengths, the Germinal Center Culture was supplemented with different concentrations of polyclonal anti-IgM F(ab')$_2$ fragments or not supplemented at all. Cells were harvested on day 4 of the cell culture. Directly afterwards, surface staining was performed to detect IgE+ and IgG1+ B cells and plasmablasts. The cells were characterized using an LSRII for flow cytometry and the software Flow Jo 10.7.1 to analyze the results.

Of note, all harvested cells of the Germinal Center Culture were stained together. To avoid contamination of the measurements with fibroblasts, a flow cytometric analysis of the co-culture versus the fibroblasts alone was performed to establish a gating strategy which includes only B cells and plasmablasts. In detail, fibroblasts could be excluded by their size in FCS and their internal complexity in SSC (side scatter) as well as their missing surface expression for CD19 and CD138. The gating strategy was applied to all experiments, if not indicated otherwise (figure 8 A and B).

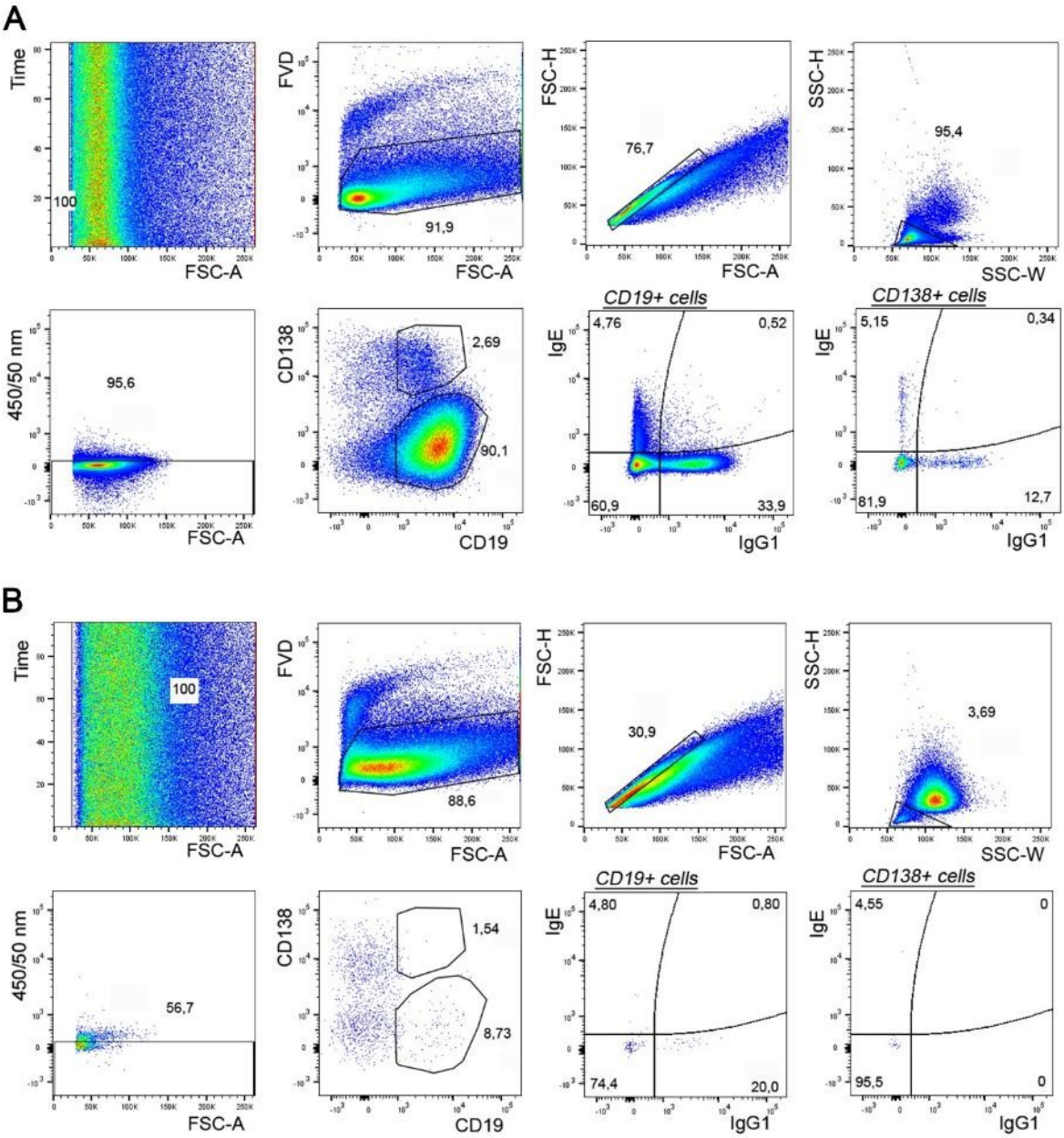

Figure 8: Flow cytometry gating strategy applied for class switched B cells and plasmablasts.
B cells were isolated from murine spleens, cultured in a Germinal Center Culture (BALB/c 3T3 fibroblasts transfected with CD40L and BAFF, stimulated with 2 ng/ml IL-4 (day 0 and 1)). After 4 days, cells were harvested and measured by flow cytometry using an LSRII. Dead cells, debris, doublets and feeder cells were excluded, as indicated. B cells are characterized by the expression of CD19, plasmablasts are characterized by the expression of CD138. Within the B cells and plasmablasts, IgE+ or IgG1+ cells were analyzed. (A) Representative FACS graphs of the Germinal Center Culture. (B) Visualization of the exclusion of the BALB/c 3T3 fibroblasts by applying the gating strategy to a pure fibroblast-culture.

The flow cytometric analysis depicted a decrease in frequencies of IgE+ and IgG1+ CD19+ B cells (figure 9 A) and CD138+ plasmablasts (figure 9 B) depending on the concentration of anti-IgM F(ab')$_2$ fragments. The highest decline in class switched cells can be determined for the highest concentration of anti-IgM F(ab')$_2$ fragments.

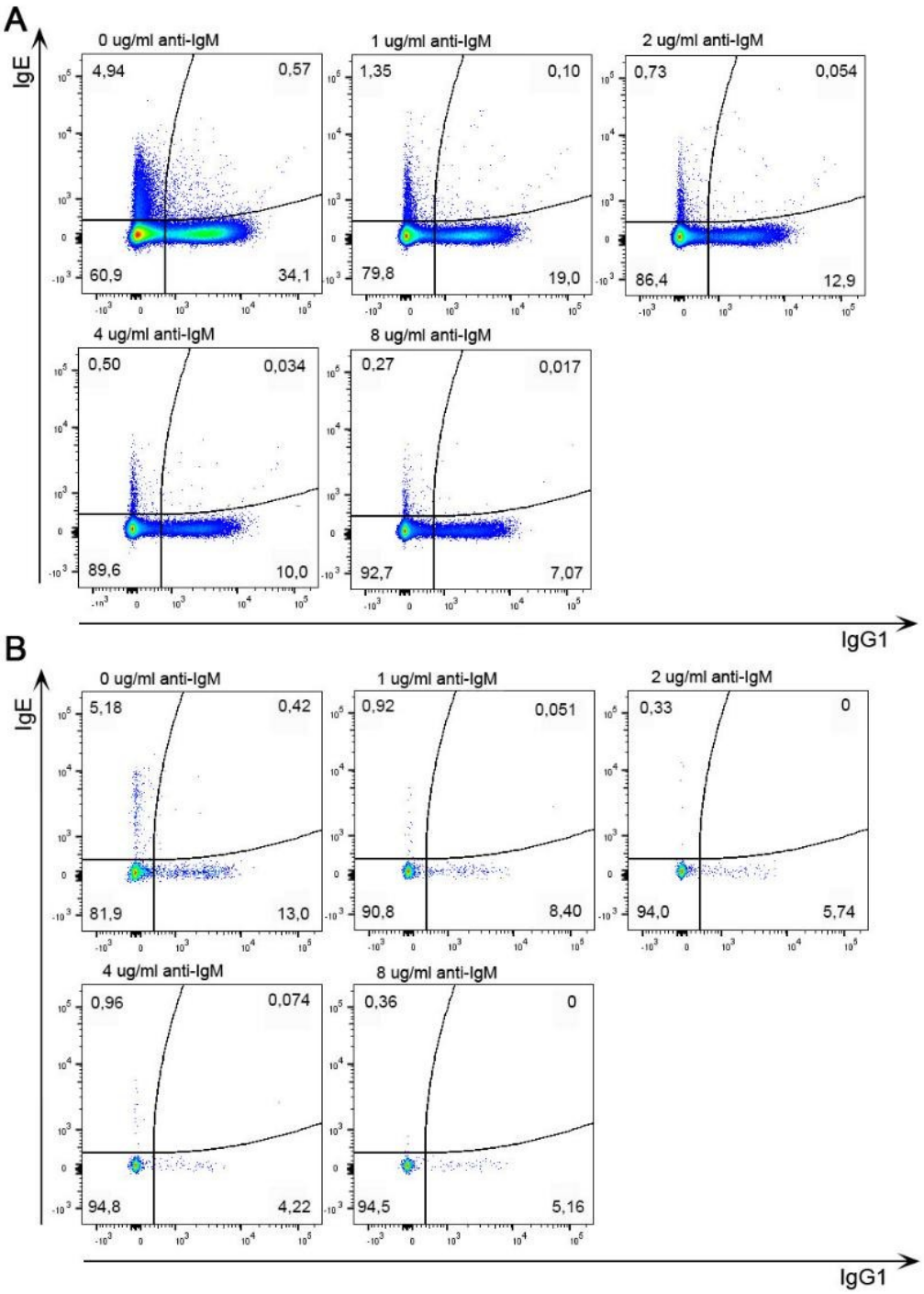
A
0 ug/ml anti-IgM
4,94
0,57
60,9
34,1
1 ug/ml anti-IgM
1,35
0,10
79,8
19,0
2 ug/ml anti-IgM
0,73
0,054
86,4
12,9
4 ug/ml anti-IgM
0,50
0,034
89,6
10,0
8 ug/ml anti-IgM
0,27
0,017
92,7
7,07
IgE
IgG1
B
0 ug/ml anti-IgM
5,18
0,42
81,9
13,0
1 ug/ml anti-IgM
0,92
0,051
90,8
8,40
2 ug/ml anti-IgM
0,33
0
94,0
5,74
4 ug/ml anti-IgM
0,96
0,074
94,8
4,22
8 ug/ml anti-IgM
0,36
0
94,5
5,16
IgE
IgG1

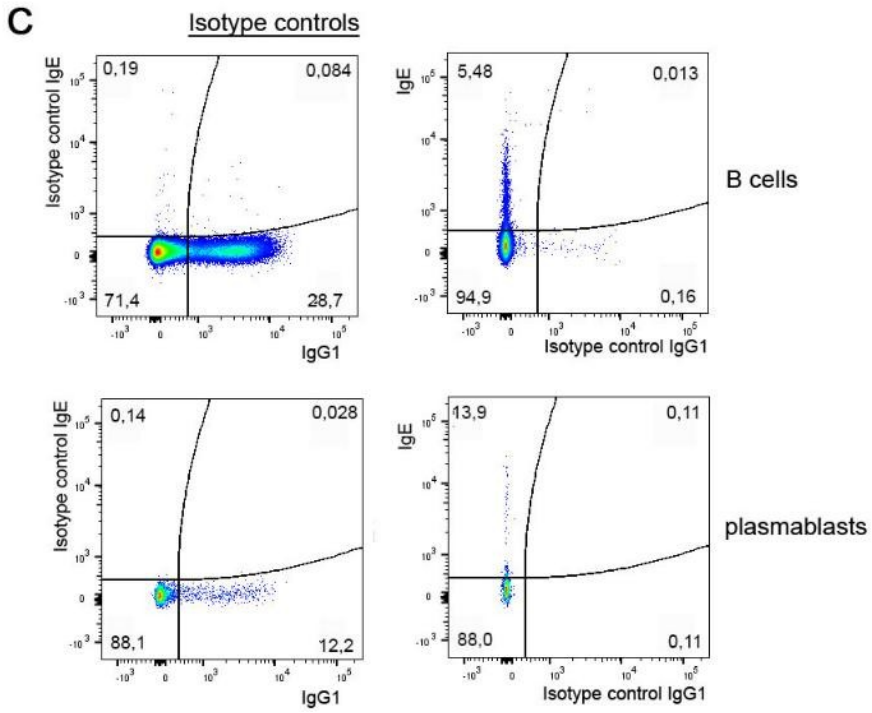

Figure 9: BCR stimulation decreases the frequencies of IgE and IgG1 class switched cells.
B cells were isolated from murine spleens, cultured in a Germinal Center Culture (BALB/c 3T3 fibroblasts transfected with CD40L and BAFF, stimulated with 2 ng/ml IL-4 (day 0 and 1)) and stimulated with several concentrations of polyclonal anti-IgM F(ab')$_2$ fragments (day 0). After 4 days, cells were harvested, the frequencies of IgE+ and IgG1+ cells were measured by flow cytometry using an LSRII. (A) Representative FACS data of the IgE+ and IgG1+ B cells. (B) Representative FACS data of the IgE+ and IgG1+ plasmablasts. (C) Isotype controls for IgE and IgG1.

Simultaneous to an increase in the concentration of anti-IgM F(ab')$_2$ fragments from 0 µg/ml to 8 µg/ml, a decrease in the median frequency of IgE+ B cells from 4,4% to 0,3% was observed (Figure 10 A). Similarly, the median frequency of IgG1+ B cells dropped from 34,9% to 8,1% under the same condition. Calculating the IgE/IgG1 ratio of these frequencies, the median ratio diminished from 0,12 to 0,04 while the stimulation increased from 0 µg/ml to 8 µg/ml anti-IgM F(ab')$_2$ fragments. Consequently, the generation of IgE+ cells seemed to be more inhibited than the formation of IgG1+ cells.

Likewise, the frequencies and the ratio of IgE+ or IgG+ CD138+ plasmablasts decreased in an anti-IgM F(ab')$_2$ fragment dose-dependent manner (figure 10 B). Taking the lower cell number of plasmablasts into account (see figure 9 B), it is difficult to evaluate alterations in frequencies of IgE+ and IgG1+ plasmablasts for concentrations greater than 1 µg/ml anti-IgM F(ab')$_2$ fragments.

In addition to the changes in frequencies, the number of cells were analyzed (figure 10 C). The median total cell number declined from 317.500 to 222.500 as the concentration of anti-IgM F(ab')$_2$ fragments increased from 0 µg/ml to 8 µg/ml. The decrease is more pronounced for the IgE+ B cells. Their median cell number dropped from 15.642 to 863, whereas the median IgG1+ B cell number dropped from 128.106 to 24.924 cells.

These results are in line with a publication of Jabara et al., concluding that BCR-stimulation with anti-IgM F(ab')$_2$ fragments in an in vitro model of splenic B cells from BALB/c mice inhibited the CSR to IgE and IgG1. Their experimental setting was based on ELISA measurements on day 6 of a B cell culture stimulated with IL-4 and LPS (Jabara et al., 2008).

Of note, my results about the frequencies and the ratio of IgE and IgG1 raised another hypothesis, namely that different B cell subclasses are affected differently by the BCR-induced CSR inhibition.

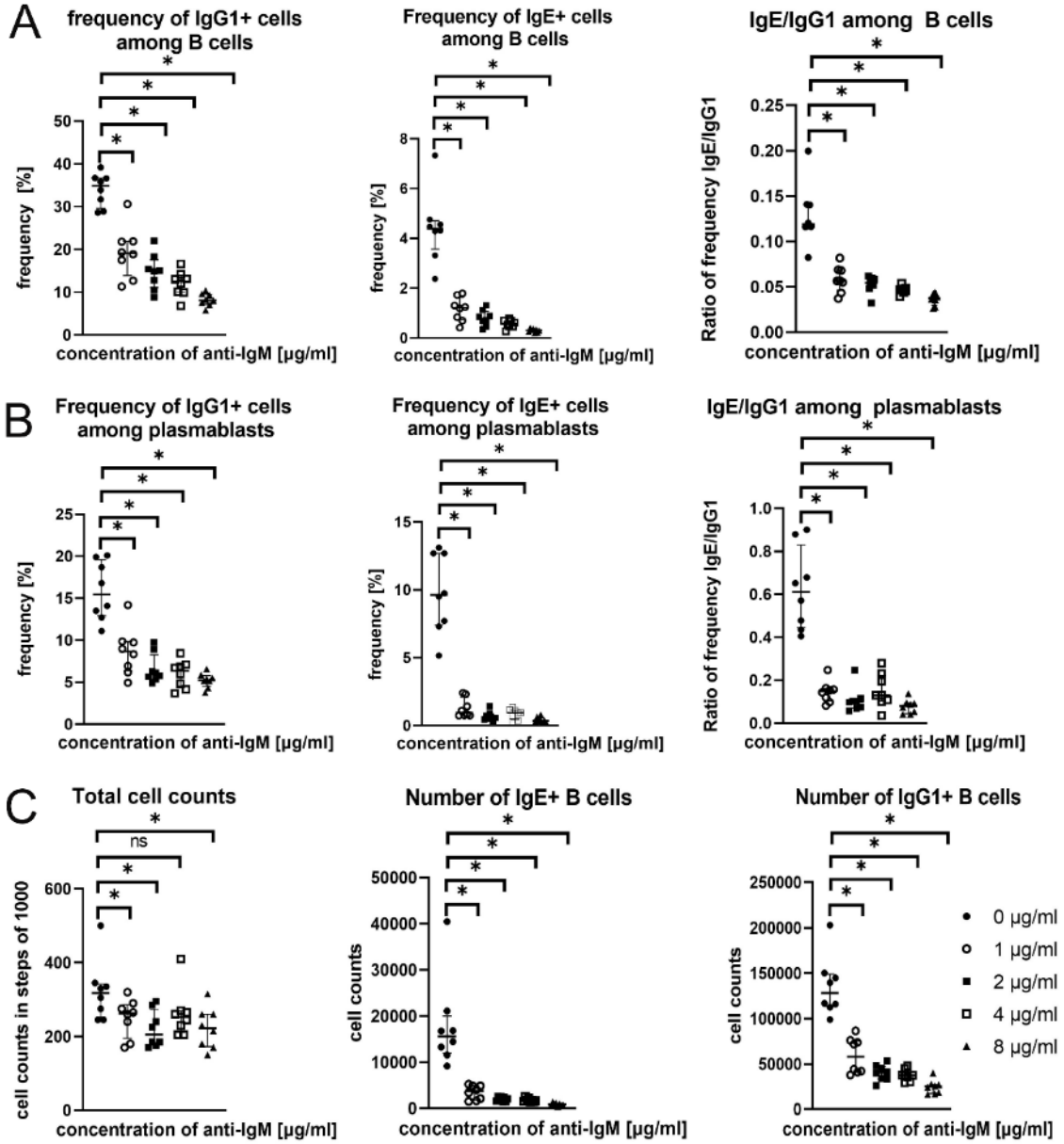

Figure 10: BCR signaling alters the frequency and the ratio of IgE and IgG1 class switched cells.
B cells were isolated from murine spleens, cultured in a Germinal Center Culture and stimulated with several concentrations of anti-IgM F(ab')$_2$ fragments. After 4 days, cells were harvested, the frequencies of IgE+ and IgG1+ cells were measured by flow cytometry using an LSRII. Statistical analysis of frequencies of IgE and IgG1 for B cells (A) and plasmablasts (B). Statistical analysis of the number of counted IgE+ and IgG1+ B cells (C). Data summarizes three independent experiments. Each dot represents the data of one mouse (n=8).

Median and IQR are depicted. Statistics: Friedmann-Test as a global test (not shown), multiple testing after a significant global test: Wilcoxon signed rank test, correction method: Holm, *p ≤ 0.05.

To investigate the dose-dependent effect in more detail, the experiment was executed again using anti-IgM F(ab')$_2$ fragments ≤ 1 µg/ml. A statistically significant difference in the IgE/IgG1 ratio of B cells could not be observed using concentrations < 500 ng/ml of anti-IgM F(ab')$_2$ fragments (figure 11), illustrating the minimal BCR signaling strength required to detect a reduction in the frequency of IgE+ and IgG1+ cells in this model.

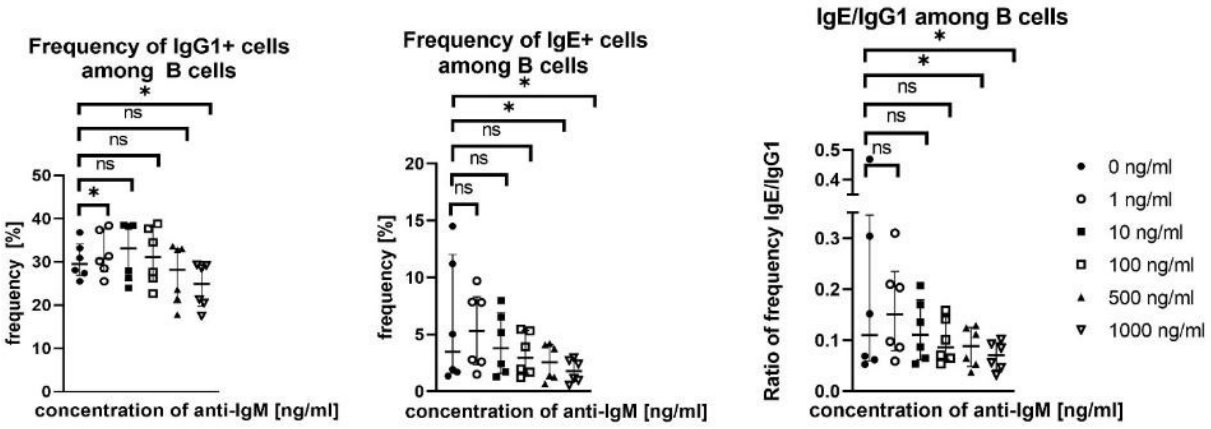

Figure 11: BCR signaling alters the frequency and the ratio of IgE and IgG1 class switched B cells in a dose-dependent manner.
Isolated B cells were cultured in a Germinal Center Culture and stimulated with different concentrations of anti-IgM F(ab')$_2$ fragments. After 4 days, cells were harvested, the frequencies of IgE+ and IgG1+ cells were measured by flow cytometry using an LSRII. Statistical analysis of the frequencies and the ratio of IgE+ and IgG1+ B cells is shown. The data is pooled from two independent experiments. Each dot represents data obtained from one mouse (n=6). Median and IQR are depicted. Statistics: Friedmann-Test as a global test (not shown), multiple testing after a significant global test: Wilcoxon signed rank test, correction method: Holm, *p ≤ 0.05.

All in all, in this model the stimulation of the BCR with anti-IgM F(ab')$_2$ fragments selectively inhibits the formation of IgE+ B cells and plasmablasts more strongly than that of IgG1+ cells. The strength of the inhibition correlates with the BCR signaling strength.

4.2.3 Anti-Ig kappa F(ab')$_2$ fragments

Taking into account that the outcome of BCR stimulation depends on various factors including antigen valency, receptor affinity and duration of the BCR occupancy (Galibert et al., 1996), the experiment was repeated using anti-Ig kappa F(ab')$_2$ fragments instead of anti-IgM F(ab')$_2$ fragments (compare chapter 4.2.2). Approximately 95% of the murine B cells express the Ig kappa light chain (J. Chen et al., 1993). Hence, the repetition ensured a comparable stimulation of different BCR subtypes including IgG and IgE, which might be less stimulated by the polyclonal anti-IgM F(ab')$_2$ fragments than the IgM-BCR.

As described, a Germinal Center Culture was generated, supplemented with different concentrations of anti-Ig kappa F(ab')$_2$ fragments or not supplemented at all. The cell

culture was stained to measure IgE+ and IgG1+ B cells and plasmablasts on day 4 by flow cytometry.

Analogous to the results seen for anti-IgM F(ab')$_2$ fragments, the stimulation of the BCR with anti-Ig kappa F(ab')$_2$ fragments elicited a decrease in frequencies of IgE+ and IgG1+ B cells with a stronger decline in IgE+ cells. The median IgE/IgG1 ratio of B cells diminished from 0,1 to 0,05 with increasing concentrations of anti-Ig kappa F(ab')$_2$ fragments from 0 µg/ml to 4 µg/ml (figure 12 A). Likewise, the IgE/IgG1 ratio of plasmablasts decreased from 0,7 to 0,3 under the same condition. The median frequency of IgE+ plasmablasts dropped depending on the concentration of anti-BCR antibodies, without reaching a statistically significant level. In contrast, the frequency of IgG1+ plasmablasts increased from 12,3% to 17,4%, comparing the condition of no BCR stimulation with the condition of 2 µg/ml anti-Ig kappa F(ab')$_2$ fragments. The frequency re-dropped to 13,5%, analyzing the condition of 4 µg/ml anti-Ig kappa F(ab')$_2$ fragments (figure 12 B).

The frequency and the ratio were not analyzed for an anti-Ig kappa F(ab')$_2$ fragment concentration of 8 µg/ml. The small number of cells, on average 166 IgE+ cells and 1874 IgG1+ cells, did not allow us to draw a conclusion (compare figure 12 C).

Moreover, the median total number of cells in the culture decreased slightly from 282.500 to 211.250, corresponding to a concentration of 0 and 4 µg/ml anti-Ig kappa F(ab')$_2$ fragments. Opposingly, the median cell number of IgE+ B cells declined from 14.158 to 2.855 and from 126.088 to 52.963 for IgG1+ B cells.

In summary, the experiments conducted with anti-Ig kappa F(ab')$_2$ fragments support the finding that the BCR signaling strength reduces the formation of IgE+ cells more than the formation of IgG1+ cells.

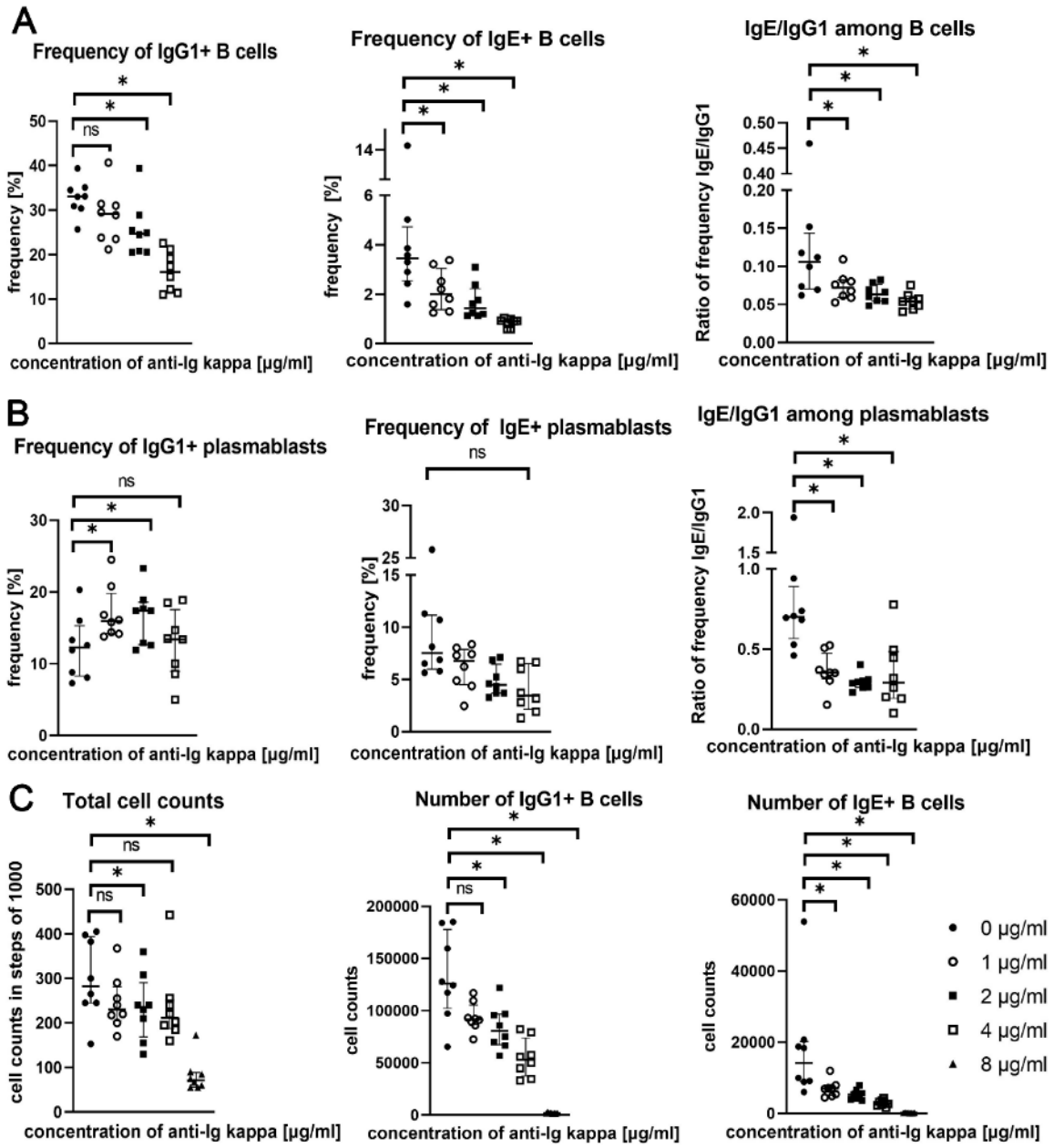

Figure 12: BCR signaling alters the frequency and the ratio of IgE and IgG1 class switched cells.
B cells were isolated from murine spleens, cultured in a Germinal Center Culture and stimulated with several concentrations of anti-Ig kappa F(ab')$_2$ fragments (day 0). After 4 days, cells were harvested, frequencies of IgE+ and IgG1+ cells were measured by flow cytometry using an LSRII. Statistical analysis of the frequencies of IgE+ and IgG1+ B cells and plasmablasts (A) and statistical analysis of the number of counted IgE+ and IgG1+ B cells (B) are shown. Data summarizes three independent experiments. Each dot represents the data of one mouse (n=8). Median and IQR are depicted. Statistics: Friedmann-Test as a global test (not shown), multiple testing after a significant global test: Wilcoxon signed rank test, correction method: Holm, *p ≤ 0.05.

4.2.4 ELISAs of the cell culture supernatant

Next, the question emerged whether the shifts in the proportions of the IgE and IgG1 surface expression correspond to a similar change in the antibody production of these cells. Therefore, two ELISA experiments were performed to measure the content of IgE and IgG1 antibodies in the cell culture supernatants.

A Germinal Center Culture was generated, supplemented with different concentrations of anti-Ig kappa F(ab')$_2$ fragments. After 4 days, the cell culture supernatants were quantified by ELISA.

Two independent experiments (n=6) demonstrated a decrease in relative light units (RLU) of IgE and IgG1 antibodies under increasing concentrations of anti-Ig kappa F(ab')$_2$ fragments. Thus, a dose-dependent decline in antibody secretion was shown (figure 13 A, D). Notably, the cellular expansion rates were different in the two experiments. For this reason, the absolute Ig titers were not comparable, and the results of the ELISA were not pooled but analyzed separately.

In the first experiment, the median ratio of the RLU of IgE/IgG1 rose from 0,06 to 0,2, analyzing an increase in the concentration of anti-Ig kappa F(ab')$_2$ fragments from 0 to 6 µg/ml (figure 13 B).

In comparison, in the second experiment, the ratio of IgE/IgG1 decreased from 0,3 to 0,1, when the concentration of anti-Ig kappa F(ab')$_2$ fragments increased from 0 to 2 µg/ml. Parallel to an increase in the concentration of anti-Ig kappa F(ab')$_2$ fragments to 6 µg/ml, the median ratio of IgE/IgG1 rose to 0,4 (figure 13 E).

In the first experiment, the number of B cells stayed relatively stable between 200.000 and 400.000 cells regardless of the BCR stimulation (figure 13 C). By contrast, the median total number of B cells diminished from 410.000 to 210.000 cells in the second experiment, depending on the concentration of anti-Ig kappa F(ab')$_2$ fragments (figure 13 F).

In conclusion, these experiments could not confirm the finding that BCR stimulation inhibits the formation of IgE more than that of IgG1. Nevertheless, the interpretation of these results was restrained by the very high range of the median IgE/IgG1 ratio and the variations in the cell numbers (figure 13 B, C, E, F). Considering the limitations of inter- and intra-data individuality, a clear interpretation of these experiments is difficult.

Outside of this, the ELISA experiments support the finding of the flow cytometry measurements: BCR stimulation reduces the generation of IgE and IgG1 antibodies in a dose dependent manner which is in line with the ELISA experiments of Jabara and colleagues (Jabara et al., 2008).

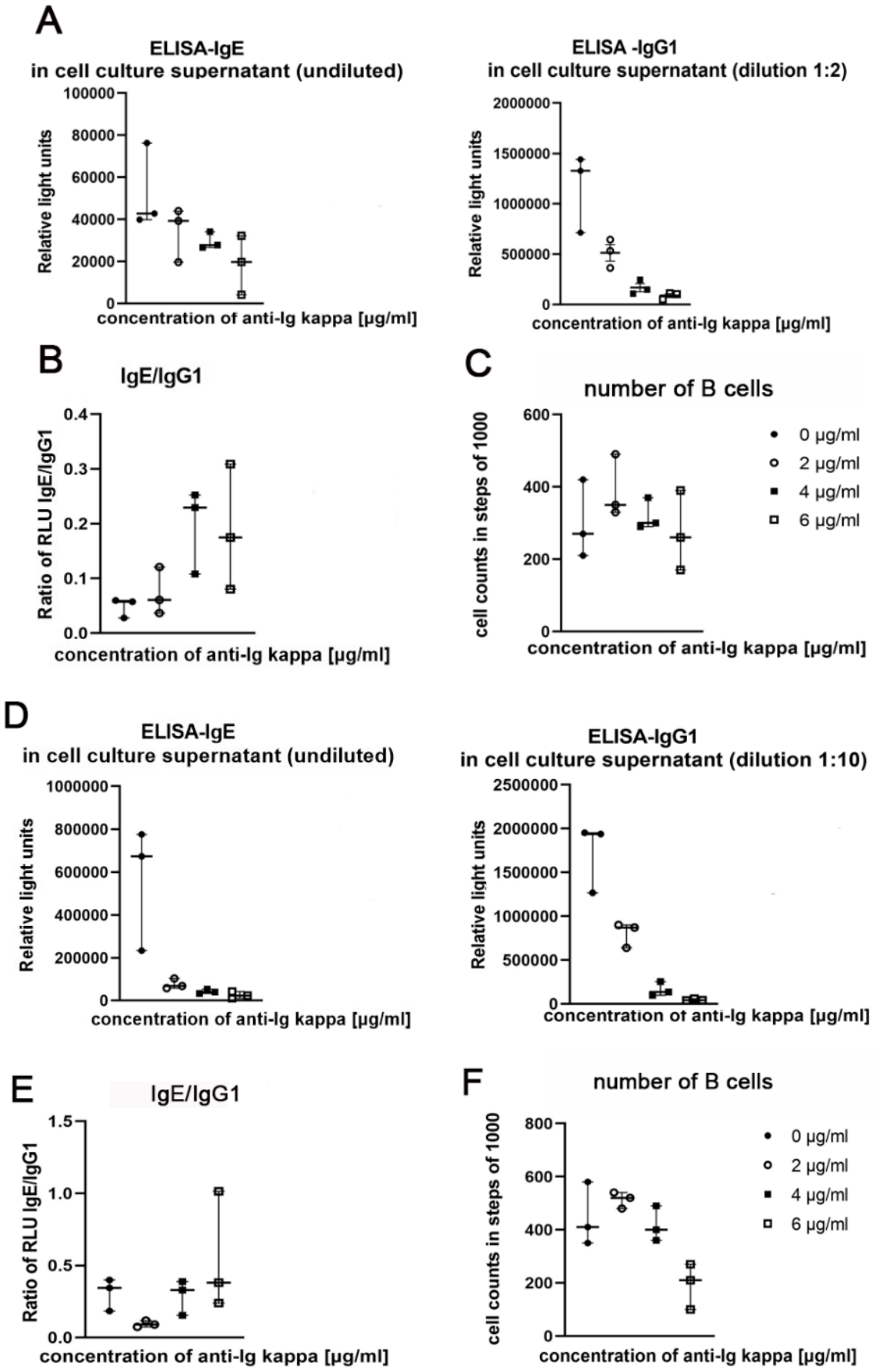

Figure 13: BCR signaling alters the secretion of IgE and IgG1 antibodies.
B cells were isolated from murine spleens, cultured in a Germinal Center Culture and stimulated with several concentrations of anti-Ig kappa $F(ab')_2$ fragments. After 4 days, ELISA experiments of the cell culture supernatant were performed to detect IgE and IgG1 antibodies. Graphs show the summary of two

experiments. The figures A, B and C correspond to one experiment; the figures D, E and F correspond to another experiment. (A) (D) Relative light units (RLU) of IgE and IgG1 antibodies in the cell culture supernatant. (B) (E) Ratio of the RLU of IgE/IgG1. (C) (F) B cells counted in each cell culture condition. Each dot represents data from a single mouse (n=3 for each experiment), the cell culture supernatant was titrated in doublets into the wells. Median and range are depicted.

4.2.5 Apoptosis: Annexin V staining

Investigating the underlying mechanisms of the BCR-signaling induced changes in the proportions of IgE and IgG1, the frequencies of apoptotic cells depending on the BCR stimulation were measured.

To begin with, a Germinal Center Culture was adopted from Hanuida & Kitamura (Haniuda & Kitamura, 2019; Nojima et al., 2011) and supplemented with different concentrations of polyclonal anti-IgM F(ab')$_2$ fragments, as described. Cells were harvested on day 4 of the cell culture. Subsequently, the frequencies of necrotic, dead, early and late apoptotic cells were detected by flow cytometry using an LSRII (compare method section chapter 3.3.6).

In detail, the decrease in cell volume and size of apoptotic cells was detected by FSC gating (Worsley et al., 2022). FSC gating was used to distinguish between early and late apoptotic cells with late apoptotic cells having a more decreased FSC than early apoptotic cells (figure 14 A).

With increasing stimulation of the cell culture with anti-IgM F(ab')$_2$ fragments from 0 to 8 µg/ml, a minor decline in the median frequency of late apoptotic B cells from 6,7% to 5,8% was observed, while the median frequency of early apoptotic cells increased slightly from 7,2% to 9,2% and the median frequency of early apoptotic CD138 intermediate cells increased from 18,4% to 22,2%. The frequency of late apoptotic CD138 intermediate cells and that of apoptotic plasmablasts did not change on a statistically significant level (figure 14 B).

In brief, a modest change in the frequencies of early and late apoptotic cells was detected in a few B cell subpopulations depending on the BCR stimulation. Thus, apoptosis after BCR stimulation might partially regulate the cell survival of different B cell subpopulations. However, it remains elusive whether the modest changes in the frequencies of apoptotic cells after BCR stimulation can explain the altered frequencies of IgE+ and IgG1+ cells.

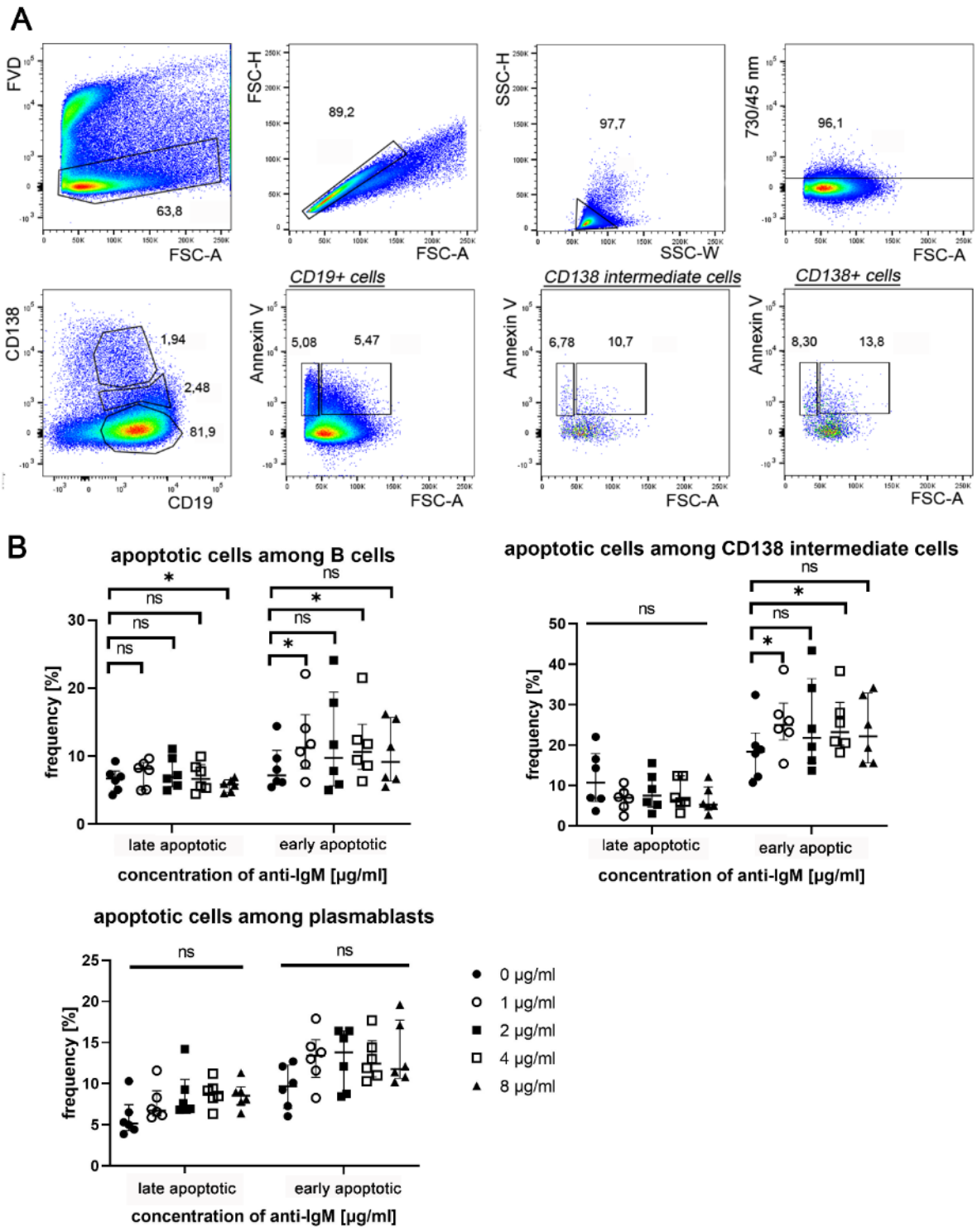

Figure 14: Frequency of apoptotic cells after BCR stimulation.
B cells were isolated from murine spleens, cultured in a Germinal Center Culture and stimulated with various concentrations of anti-IgM F(ab')$_2$ fragments (day 0). After 4 days, cells were harvested and characterized by flow cytometry using an LSRII. Dead cells, debris, doublets and feeder cells were excluded, as indicated. (A) Flow cytometry gating strategy applied for the analysis of the early and late apoptotic, differentiated by Annexin V and the size in the FSC within CD19+ B cells, CD138 intermediate cells and CD138+ plasmablasts. (B) Frequencies of apoptotic cells within the different B cell subpopulations are presented. Data summarizes two independent experiments. Each dot represents data from one mouse (n=6). Median+ IQR are depicted. Statistics: Friedmann-Test ns or *p ≤ 0.05, multiple testing after a significant global test: Wilcoxon signed rank test, correction method: Holm (0 and 8 µg/ml, 0 and 4 µg/ml, 0 and 2 µg/ml, 0 and 1 µg/ml), *p ≤ 0.05

4.2.6 Semiquantitative analysis of switch circles

In order to explore the question of whether the selective inhibition of the IgE production is due to an inhibited class switch, a semiquantitative analysis of switch circles, resulting from the CSR to IgG1 and from both, the direct and indirect CSR to IgE, was performed.

As described, a Germinal Center Culture was generated, supplemented with different concentrations of anti-Ig kappa $F(ab')_2$ fragments. After RNA isolation and reverse transcription into cDNA, the PCR product was visualized by gel electrophoresis using Image Quant.

First, the kinetics of the presence of switch circles were investigated, isolating RNA on day 1, 2, 3 and 4 of the culture system and defining day 3 as time point of analysis for further experiments (figure 15 B).

Comparing all samples, switch circles derived from the direct class switch from IgM to IgE could not be detected except for one single mouse which presented those switch circles on day 2, analyzing a cell culture stimulated with IL4 (figure 15 B). Hence, this might be an indication of the dominance of indirect instead of direct class switch to IgE in our culture system. This interpretation is in accordance with the analysis of circular DNA excision products in cell cultures stimulated with LPS and IL-4, proposing sequential class switch via IgG1 to IgE as the main result of in vitro stimulation (Mandler et al., 1993).

In general, the analysis of switch circles produced by the class swith from IgM to IgG1 is limited because, even after several optimization attempts, not all bands were clearly visible in all samples. By contrast, switch circles excised during the indirect class switch from IgG1 to IgE could be found in all conditions (figure 15 A, B).

In more detail, the median integrated densitiy relative to the house keeping gene of switch circles from the indirect CSR to IgE decreased from to 0,64 to 0,37, comparing the cell cultures stimulated without or with 8 µg/ml anti-Ig kappa $F(ab')_2$ fragments (n=6). This corresponds to a statistically significant decrease in gene expression of switch circles representing IgG1-to-IgE switching. Contrarily, the changes in the integrated density, thus the gene expression, of switch circles derived from the CSR to IgG1 were not statistically significant (figure 15 C).

In addition, the cells stimulated without and with 8 µg/ml anti-IgM $F(ab')_2$ fragments (n=3) demonstrated a stronger decline in the gene expression of switch circles resulting from the indirect class switch to IgE than in the gene expression of switch circles excised during the isotype switching to IgG1 (figure 15 C). These changes in the gene expression did not reach a statistically significant level owing to the low number of mice.

In summary, these results propose that the IgE+ B cells generated by our culture system are originated by indirect class switch. Moreover, BCR stimulation with anti-Ig F(ab')$_2$ fragments inhibited the CSR to IgE more than the CSR to IgG1.

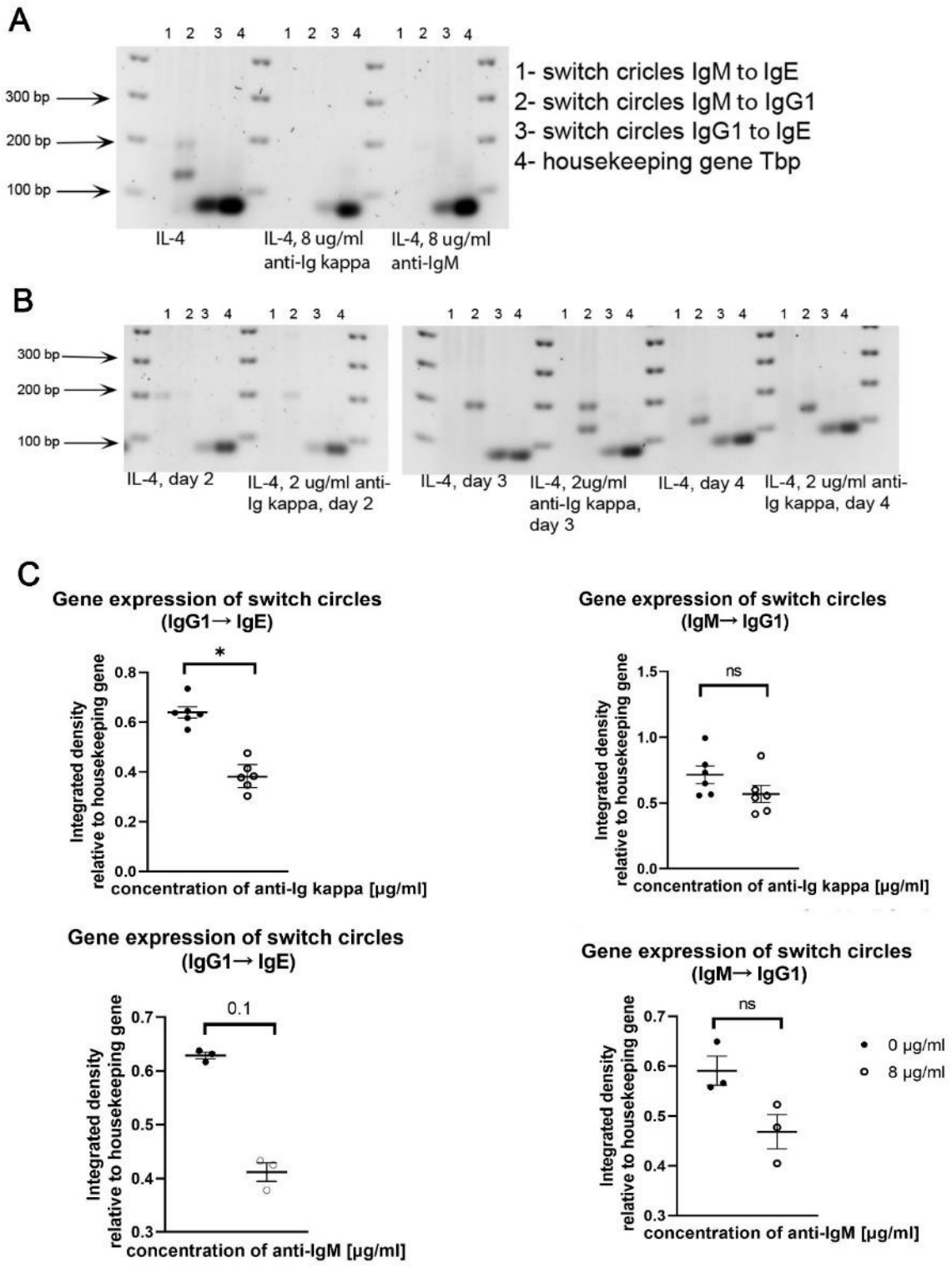

Figure 15: Excised circles resulting from the indirect class switch to IgE or the direct class switch to IgG1.
B cells were isolated from murine spleens, cultured in a Germinal Center Culture and stimulated with anti-IgM or anti-Ig kappa F(ab')$_2$ fragments (day 0). RNA was isolated on day 3 of the cell culture, if not indicated otherwise. (A) Representative PCR gel. (B) Representative PCR gel of the kinetics of the switch circles, isolating RNA on day 2, 3 and 4 of the culture. (C) Statistical analysis of the data pooled from two independent experiments using anti-Ig kappa F(ab')$_2$ fragments (n=6), and of the data of one experiment using anti-IgM

$F(ab')_2$ fragments (n=3). Each dot represents data from one mouse. Mean and SEM are displayed. Statistics: Wilcoxon signed rank test, * p≤ 0.05.

4.1.7 PI3K-Inhibitor LY294002

LY294002 is a chemical probe which inhibits the PI3K/AKT-pathway, among other signaling pathways (Arrowsmith et al., 2015). The PI3K/AKT-pathway is one of the three major pathways activated by BCR stimulation and the only one which has an inhibiting effect. More precisely, it is a negative regulator of the CSR and the AID expression and constrains antibody responses (Z. Chen & Wang, 2019). Hence, the question of whether the removal of the inhibiting pathway by the cell-permeable chemical probe LY294002 counteracts the effects seen by BCR stimulation should be answered.

To begin with the experimental setting, a Germinal Center Culture was generated, supplemented with or without anti-Ig kappa $F(ab')_2$ fragments (anti-BCR) and with or without LY294002 on day 0. On day 4 of the cell culture, the frequencies of IgE+ and IgG1+ cells within the populations of CD19+ B cells and CD138+ plasmablasts were measured by flow cytometry (gating strategy depicted in figure 8 A).

Analyzing IgE+ B cells, the median frequencies did not change on a statistically significant level comparing cells stimulated without or with LY294002. More concretely, the median frequency of IgE+ cells was 4,4% in the Germinal Center Culture and 5,7% in the Germinal Center Culture supplemented with LY294002. In the same way, the median frequency of IgE+ B cells remained at the same level between 1,1% and 1,9%, comparing the cells stimulated with anti-Ig kappa $F(ab')_2$ fragments with the cells which were additionally stimulated with LY294002 (figure 16 A).

Similar to IgE+ B cells, there was no significant difference in the median frequencies of IgE+ plasmablasts, comparing cells stimulated with and without LY294002 as well as comparing anti-BCR stimulated cells with cells which were additionally stimulated with LY294002 (figure 16 B).

The median frequency of IgG1+ B cells increased significantly from 29,9% to 42%, when LY294002 was added to the Germinal Center Culture. When LY294002 was added to the Germinal Center Culture supplemented with anti-Ig kappa $F(ab')_2$ fragments, the frequency amplified from 16% to 20,8% (figure 16 A). Analogously, the frequency of IgG1+ plasmablasts rose from 9,4% to 14,5%, comparing cells from the Germinal Center Culture with additionally LY294002 stimulated cells. Opposingly, there was no statistically significant difference in the frequencies of IgG1+ plasmablasts, analyzing cells stimulated with anti-BCR versus cells stimulated with anti-BCR and LY294002 (figure 16 B).

The ratio of IgE+ to IgG1+ B cells and plasmablasts remained stable for all tested conditions (figure 16 A, B).

All in all, LY294002 increased the frequencies of IgG1+ cells while the frequencies of IgE+ cells increased on a minor and non-significant scale. Consequently, the ratio of IgE/IgG1 was not changed. Of note, LY294002 which was used in this study is a non-selective inhibitor of the PI3K/AKT-pathway.

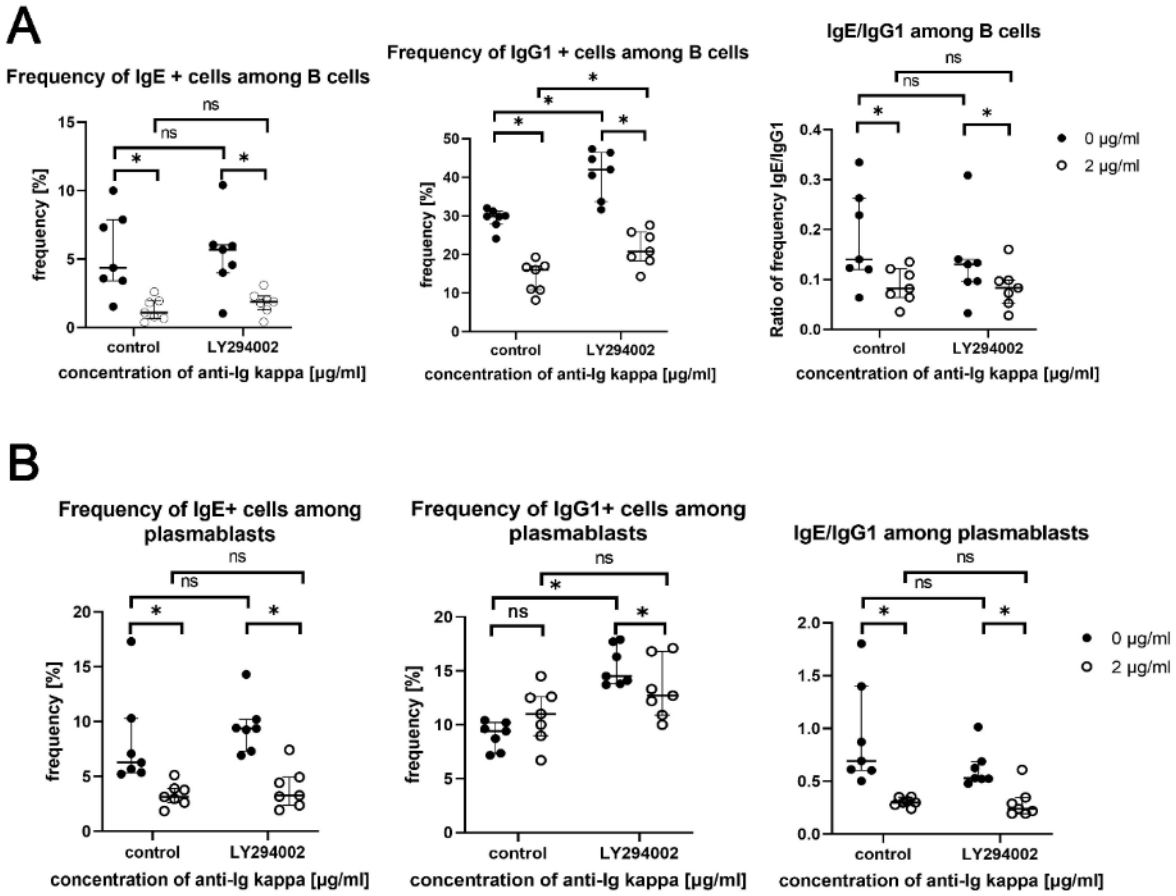

Figure 16: The PI3K-pathway inhibitor LY294002 does not change the ratio of IgE/ IgG1.
Splenic B cells were isolated from BALB/c mice, cultured in a Germinal Center Culture and stimulated with anti-Ig kappa F(ab')$_2$ fragments (0-or 2 µg/ml) and 0 or 1 µM/ml LY294002 (day 0). After 4 days, cells were harvested and characterized by flow cytometry using the LSRII. The frequencies and their ratios were analyzed, gated for CD19+ B cells (A) and CD138+ plasmablasts (B). Summary of the data of three independent experiments is shown. Each dot represents data from one mouse (n=7). Median and IQR depicted. Statistics: Wilcoxon signed rank test *p≤0.05.

4.3 Role of co-stimulating factors

4.3.1 IL-4

Another aim of this thesis was to analyze other factors besides the BCR signaling strength which could facilitate the generation of IgE+ or IgG1+ cells. It is already known that IL-4 binds to its receptor and activates the transcription factor STAT6, promoting the expression of the germline transcripts of IgG1 as well as IgE. IL-4 is secreted by Tfh inside the GC and by Th2 and preTfh cells outside the GC (Haase & Voehringer, 2021),

but it can be produced by other cell types such as mast cells and basophils, too (Nelms et al., 1999).

To introduce the method, a Germinal Center Culture was generated to titrate different concentrations of IL-4, varying from 0,5 ng/ml to 8 ng/ml. In the original protocol from Hanuida and Kitamura, B cells were isolated from C57BL/6 mice and stimulated with 1 ng/ml IL-4 on day 0 (Haniuda & Kitamura, 2019). By contrast, in this experimental approach, B cells were isolated from BALB/c mice and stimulated with IL-4 on day 0 and day 1 of the cell culture. Cells were harvested on day 4 of the cell culture and analyzed by flow cytometry. IgE+ and IgG1+ cells within the population of CD19+ B cells and CD138+ plasmablasts were detected as described (see figure 8 A).

The median frequency of IgE+ B cells increased from 0,4% to 4,8% in response to a stimulation extending from 0,5 ng/ml to 8 ng/ml IL-4 (figure 17 A). Under the same condition, the median frequency of IgG1+ B cells rose from 8,9% to 39%. The median ratio of the frequencies of IgE/IgG1 augmented from 0,04 to 0,13 in B cells. A less pronounced increase in the ratio from 0,44 to 0,7 was observed in plasmablasts (figure 17 B). In plasmablasts, the increase in the frequency of IgG1+ cells was minor from 9,3% to 11,6% and not statistically significant, comparing a stimulation of 0,5 ng/ml IL-4 and 8 ng/ml IL-4. The frequency of IgE+ plasmablasts rose from 4,8% to 6,8% in response to the range of IL-4 concentrations tested.

In conclusion, higher concentrations of IL-4 led to higher proportions of IgE+ cells compared to IgG1+ cells. Of note, the finding was more pronounced in B cells than in plasmablasts.

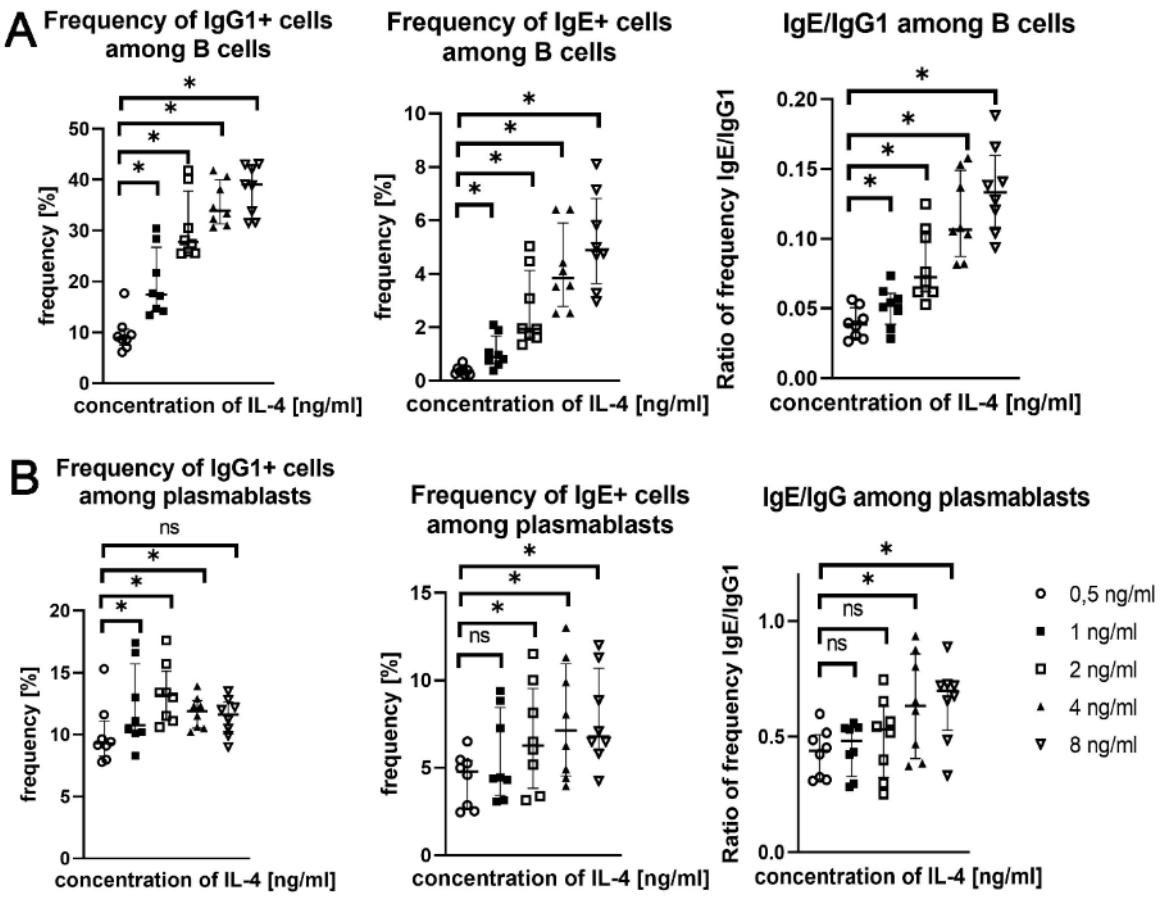

Figure 17: The frequencies and the ratio of IgE and IgG1 change according to the IL-4 stimulation. B cells were isolated from murine spleens, co-cultured with BALB/c 3T3 fibroblasts, transfected with CD40L and BAFF, and stimulated with various concentrations of IL-4 (day 0 and 1), as indicated. After 4 days, cells were harvested and characterized by flow cytometry. The frequencies of IgE and IgG1 and their ratio were analyzed within CD19+ B cells (A) and CD138+ plasmablasts (B). The statistical analysis includes data from three independent experiments (n=8). Each dot represents data from one mouse. Median and IQR are shown. Statistics: Friedmann-Test (not shown), multiple testing after a significant global test: Wilcoxon signed rank test, correction method: Holm *p ≤ 0.05.

4.3.2 Glucose concentration

B cell differentiation requires a multi-step process of changes in their metabolism, depending on the uptake and utilization of glucose, among others (Vivas-García & Efeyan, 2022). Therefore, glucose was analyzed as another co-stimulatory factor which possibly modifies the generation of IgE+ or IgG1+ class switched cells in the presence and absence of anti-Ig F(ab')$_2$ fragments.

To describe the experimental setting, the Germinal Center Culture was adopted to cultivate cells in RPMI media containing different glucose concentrations. For each glucose concentration, the cells were divided into groups stimulated with or without anti-BCR antibodies. Anti-BCR stimulation consisted of 2 µg/ml anti-Ig kappa F(ab')$_2$ fragments, added on day 0 to the cell culture. Cells were harvested and stained on day 4 of the cell culture. In the end, a flow cytometry analysis was performed to characterize

IgE+ and IgG1+ cells within the population of CD19+ B cells and CD138+ plasmablasts (compare figure 8 A).

The different levels of glucose tested in the experiment were adapted to physiological blood sugar levels. 50 mg/dL glucose denotes the border to hypoglycemia, a healthy individual has a blood sugar level below 100 mg/dL on an empty stomach, while a diabetic patient has a blood sugar level of 150 mg/dL or more on an empty stomach. Blood sugar levels of equal or more than 200 mg/dL appear in diabetic patients, especially after eating or after an oral glucose tolerance test (Amboss, 2021). Accordingly, the cell cultures were adjusted to the following glucose concentrations: 50 mg/dL, 100 mg/dL, 150 mg/dL, 200 mg/dl, 300 mg/dL and 400 mg/dL. Results obtained from cells cultured at glucose concentrations of 400 mg/dL were excluded from the analysis due to the low number of cells.

To continue with the results, the frequencies of IgG1+ B cells formed an inverted U-shape: their frequency increased from 21,4% to a peak of 34,9% while the glucose concentration increased from 50 mg/dL to 150 mg/dL. Further addition of glucose resulted in a drop in the frequency of IgG1+ B cells to 18,7% at a glucose concentration of 300 mg/dL.

Similarly, an inverted U-shape was detected analyzing the frequencies of IgG1+ B cells within the cell cultures supplemented with anti-Ig kappa $F(ab')_2$ fragments. More precisely, the frequency of IgG1+ B cells increased from 5,74% to a peak of 17,9%, comparing a glucose concentration of 50 mg/dL and 150 mg/dL. Higher glucose levels in the cell culture led to a decrease in the frequency of IgG1+ B cells to 13,6% at a glucose concentration of 300 mg/dL (figure 18 A).

Contrarily, the frequencies of IgE+ B cells increased almost linearly depending on the glucose concentration. Simultaneous to an increase in the concentration of glucose from 50 µg/ml to 300 µg/ml, an augmentation in the median frequency of IgE+ B cells was observed from 1,2% to 5,8% in the Germinal Center Cultures, as well as from 0,3% to 2,2% in the cell cultures supplemented with anti-Ig kappa $F(ab')_2$ fragments. The median ratio of IgE/IgG1 increased from 0,06 to 0,28 under the former condition and from 0,04 to 0,19 under the latter condition (figure 18 A).

The general shapes of the graphs portraying the frequencies of IgE+ and IgG1+ plasmablasts in dependence on the glucose concentration correspond to the graphs of B cells. In detail, the frequency of IgG1+ plasmablasts rose until it reached a plateau around 10,5% at a glucose concentration of 150 and 200 mg/dL and decreased for higher glucose concentrations. The frequency of IgE+ plasmablasts increased almost linearly, the highest frequency was measured at the highest glucose concentration which was 8,2% at a glucose concentration of 300 mg/dL (figure 18 B). The median ratio of IgE+/IgG1+

plasmablasts increased from 0,25 to 1,1 while the glucose concentration in the Germinal Center Culture rose from 50 mg/dL to 300 mg/dL (figure 18 B).

However, the median frequency of all plasmablasts dropped from approximately 2,6% analyzing a glucose concentration of 200 mg/dL to 0,5% analyzing a glucose concentration of 300 mg/dL (figure 18 C). For the same range of glucose concentrations, the total number of living cells dropped (figure 18 D). Thus, an increase in the frequency of IgE+ plasmablasts between a glucose concentration of 200 mg/dL and 300 mg/dL was not compatible with an increase in the total number of IgE+ plasmablasts.

As a first conclusion, different glucose concentrations modify the frequencies of IgE+ and IgG1+ B cells and plasmablasts in our Germinal Center Culture, possibly raising the IgE/IgG1 ratio.

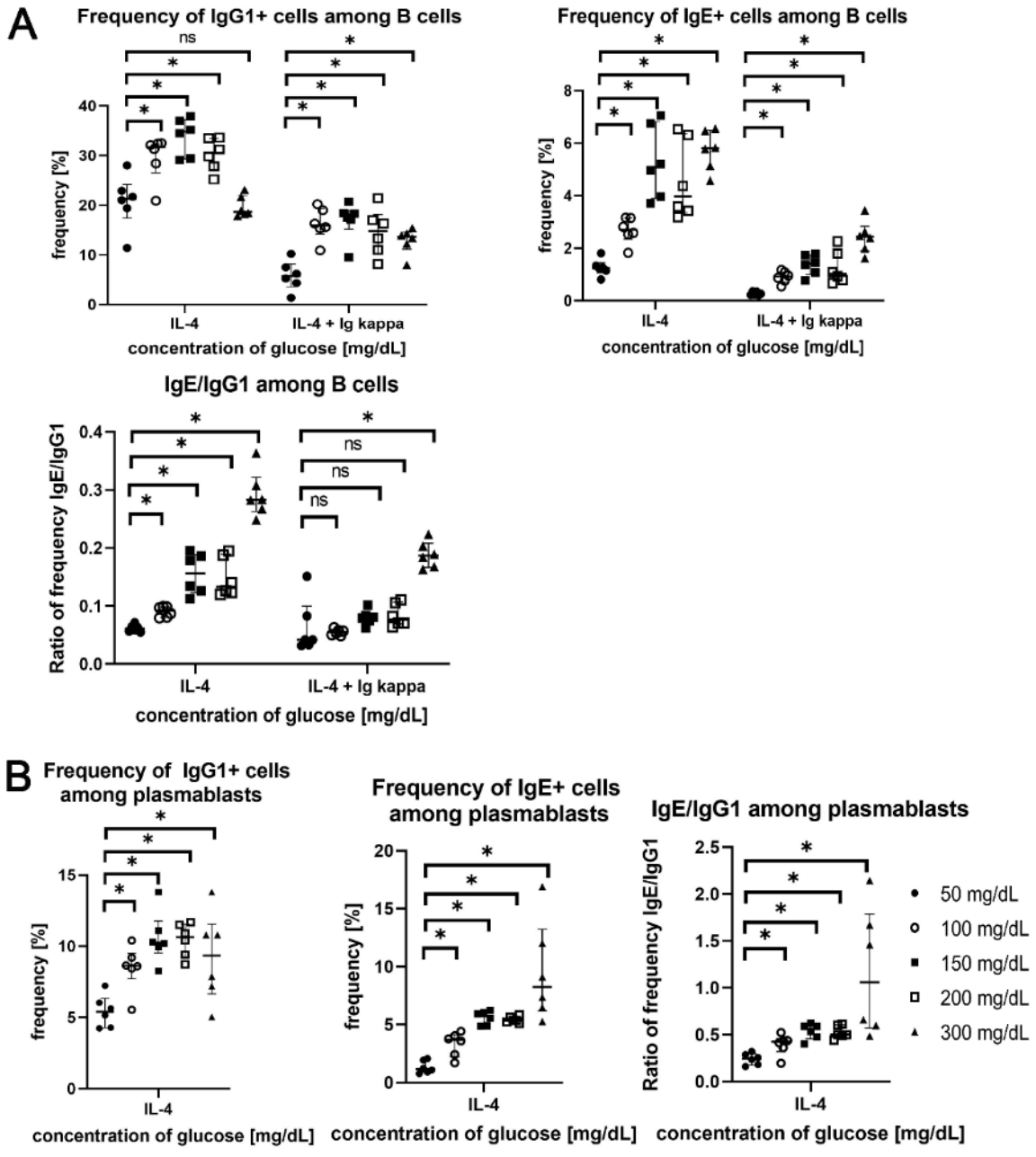

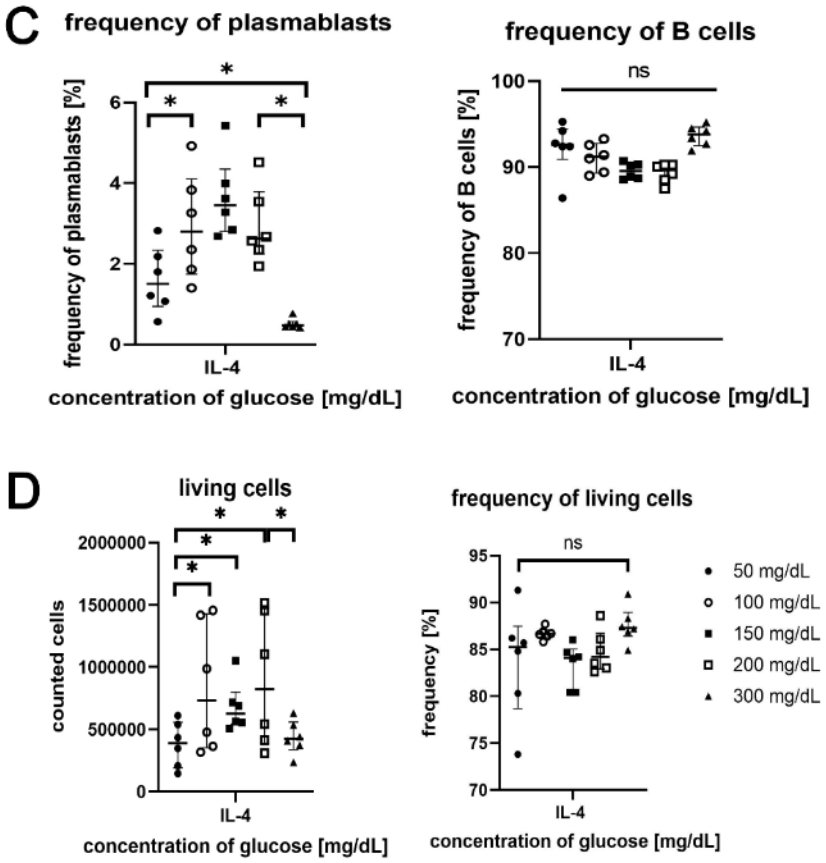

Figure 18: Different glucose concentrations influence the generation of IgE+ and IgG1+ cells.
B cells were isolated from murine spleens, cultured in a Germinal Center Culture and stimulated with or without 2 µg/ml anti-Ig kappa F(ab')$_2$ fragments (day 0), the glucose concentration of the RPMI medium varied, as indicated. After 4 days, cells were harvested and characterized by flow cytometry using an LSRII. The frequencies and the ratio of IgE and IgG1 are shown, gated for CD19+ B cells (A) and CD138+ plasmablasts (B). Results of plasmablasts cultured with anti-Ig kappa F(ab')$_2$ fragments are not depicted due to the low number of cells. Frequencies of plasmablasts and B cells (C). Frequencies of living cells and counted living cells (D). The data is pooled from two independent experiments. Each dot represents data obtained from one mouse (n=6). Median and IQR are depicted. Statistics: Friedmann-Test (not shown); multiple testing after a significant global test: Wilcoxon signed rank test, correction method: Holm *p ≤ 0.05.

Proliferation might vary according to the glucose concentration because the median number of counted living cells increased from 390.280 to 822.983.600, comparing a glucose concentration of 50 mg/dL and 200 mg/dL. In contrast, the frequency of living cells stayed stable at around 85% for each glucose concentration tested (figure 18 D).

The frequency of living cells and therefore the frequency of dead cells was stable without being able to specify the type of cell death. It is of interest to explore the question of whether apoptosis is caused by different glucose concentrations. For this reason, the frequencies of apoptotic cells were analyzed by flow cytometry.

Again, cells were characterized by flow cytometry on day 4 of the Germinal Center Culture, supplemented with or without anti-Ig kappa F(ab')$_2$ fragments. Early and late apoptotic cells were defined as described (see chapter 3.3.6.).

An increase in glucose concentration from 100 mg/dL to 200 mg/dL was associated with a statistically significant decrease in frequencies of early and late apoptotic cells. This could

be found in cells from both, the Germinal Center Culture and that which was supplemented with anti-Ig kappa F(ab')$_2$ fragments (figure 19). In more specific terms, the frequency of early apoptotic cells dropped from 2,6% to 1,4% in the Germinal Center Culture and from 2,7% to 2,1% in the anti-BCR stimulated Germinal Center Culture. Additionally, the frequency of late apoptotic cells decreased from 8,5% to 5,3% in the Germinal Center Culture and from 6,2% to 4,0% in the anti-BCR stimulated Germinal Center Culture.

Hence, it is possible that the cells of the Germinal Center Culture which were stimulated with higher glucose concentrations are less prone to undergo apoptosis, at least for the glucose concentrations tested. Not all glucose concentrations which have been tested to analyze the impact of glucose on the frequencies of IgE+ and IgG1+ cells (see figure 18) could be included in this experiment.

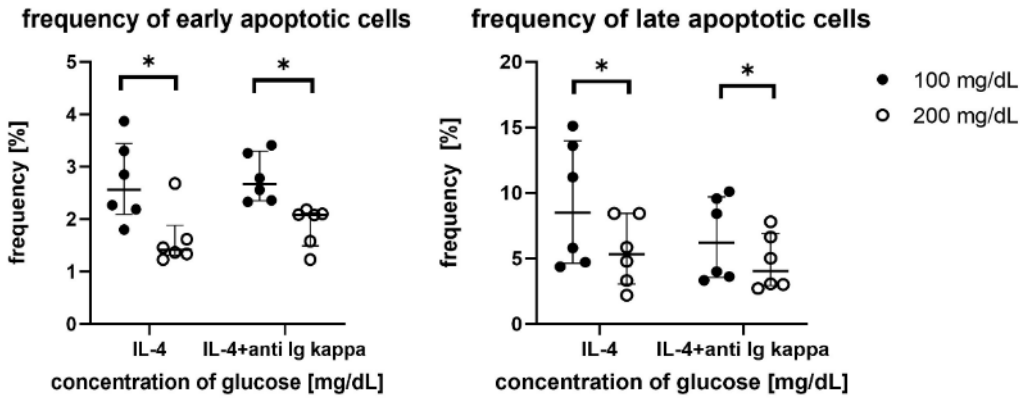

Figure 19: A higher glucose concentration is associated with a lower frequency of apoptotic cells. B cells were isolated from murine spleens, cultured in a Germinal Center Culture and stimulated with or without 2 µg/ml anti-Ig kappa F(ab')$_2$ fragments (day 0), the glucose concentration of the RPMI medium varied, as indicated. After 4 days, cells were harvested and characterized by flow cytometry using an LSRII. Dead cells, debris, doublets and feeder cells were excluded, early and late apoptotic cells were analyzed using Annexin V and FSC (see chapter 3.3.6). Statistical analysis includes data from two independent experiments. Each dot represents data obtained from one mouse (n=6). Median and IQR are depicted. Statistics: Wilcoxon signed rank test *p ≤ 0.05.

A possible reason for the different generation of IgE+ and IgG1+ cells depending on the glucose concentration in the cell culture could be a different glucose uptake of IgE+ and IgG1+ cells. Thus, a flow cytometric analysis of 2-NBDG was performed. 2-NBDG is a fluorescent glucose analogue which was quantified within individual cells (figure 20 A).

As described, a Germinal Center Culture was generated, supplemented with different concentrations of anti-Ig kappa F(ab')$_2$ fragments and characterized on day 4 by flow cytometry.

The normalized MFI of 2-NBDG within IgG1+ cells diminished from 33% to 1,2% while the stimulation of the cells with anti-Ig kappa F(ab')$_2$ fragments increased from 0 µg/ml to 1 µg/ml. Further addition of anti-BCR stimulation in the range of 1 to 6 µg/ml anti-Ig kappa

$F(ab')_2$ fragments led to an increase in the normalized MFI of 2-NBDG within IgG1+ cells to 70%.

Similarly, the normalized MFI of 2-NBDG within IgE+ cells decreased from 19% to 1,3%, comparing cells stimulated with 0 µg/ml and 1 µg/ml anti-Ig kappa $F(ab')_2$ fragments. Additional stimulation until a concentration of 6 µg/ml anti-Ig kappa $F(ab')_2$ fragments correlated with an increase in the normalized MFI of 2-NBDG within IgE+ cells to 74,7% (figure 20 B).

Taken together, a statistically significant difference in the normalized MFI of 2-NBDG between IgE+ and IgG1+ cells could not be determined.

Consequently, it can be suggested that the BCR signaling strength modifies the glucose uptake which is similar for both IgE+ and IgG1+ cells. The finding that higher BCR stimulation increased the glucose uptake more than lower BCR simulation is in line with the conclusion of Doughty and colleagues who cultured splenic B cells from BALB/c mice for 15 hours with anti-IgM $F(ab')_2$ fragments (Doughty et al., 2006). Of note, Doughty and colleagues did not analyze IgE+ or IgG1+ B cells by flow cytometry but analyzed the glucose uptake of all B cells by liquid scintillation spectrometry.

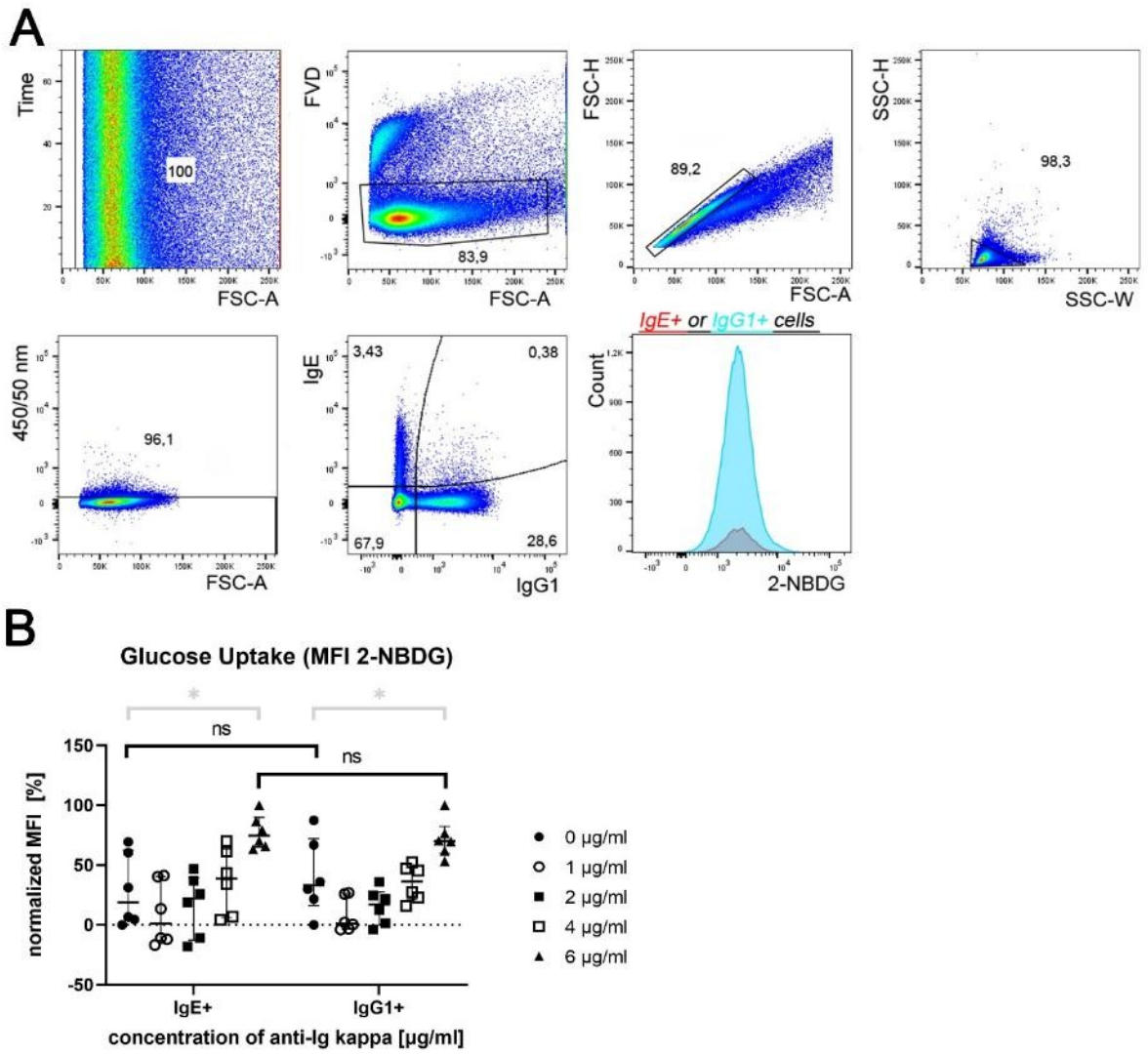

Figure 20: The median fluorescence intensity (MFI) of the glucose uptake.
B cells were isolated from murine spleens, cultured in a Germinal Center Culture and stimulated with various concentrations of anti-Ig kappa F(ab')$_2$ fragments, as indicated. After 4 days, cells were harvested, incubated with 2-NBDG and characterized by flow cytometry using an LSRII. The MFI of 2-NBDG within IgE+ and IgG1+ cells were analyzed using the software Flow Jo 10.7.2. (A) Representative FACS plots of the gating strategy. (B) Statistical analysis, including normalized data from two independent experiments, defining 0 % as the smallest mean of the data set for each dye and 100 % as the largest mean of the data set for each dye. Each dot represents data from one mouse (n=6). Median and IQR are depicted. Statistics: Friedmann-Test (not shown), multiple testing after a significant global test: Wilcoxon signed rank test within the group of IgE+ and IgG1+ cells (grey) and in between these cells (black: ns), correction method: Holm, *p ≤ 0.05.

In summary, IgE+ and IgG1+ B cells demonstrate similar glucose uptake rates, showing their comparable need for this metabolite. Nevertheless, higher glucose concentrations resulted in the formation of higher frequencies of IgE+ cells in comparison to the frequencies of IgG1+ cells.

A selection of the results of this thesis (4.2.1, 4.2.2, 4.2.3, 4.2.6) was published together with experiments of our research group, revealing that BCR signaling strength and physiochemical properties regulate IgE and IgG1 formation on the level of individual B-cell clones:

Udoye CC, Rau CN, **Freye SM**, Almeida LN, Vera-Cruz S, Othmer K, Korkmaz RÜ, Clauder AK, Lindemann T, Niebuhr M, Ott F, Kalies K, Recke A, Busch H, Fähnrich A, Finkelman FD, Manz RA. B-cell receptor physical properties affect relative IgG1 and IgE responses in mouse egg allergy. Mucosal Immunol. 2022 Jun;15(6):1375-1388. doi: 10.1038/s41385-022-00567-y.

5. Discussion

5.1 NGS analysis

My BCR repertoire data revealed that in helminth infected mice different BCR clonotypes varied in their proportion of IgG1 to IgE. Most physiochemical properties were similar for IgE_E and IgE_G clonotypes. This is in accordance with data from my laboratory, indicating that these findings also hold true in a mouse model of food allergy and in naïve mice. According to these analyses, physiochemical properties were not decisive for the individual IgE/IgG1 ratios, but influenced hypermutation rates and clonal selection (Udoye et al., 2022).

However, the aliphatic index was different between IgE_E and IgE_G clonotypes. Certainly, the two helminth infected mice are not representative, and, to my knowledge, there is not any publication analyzing the influence of the aliphatic index on the IgE/IgG1 ratios. Thus, the conclusion about physiochemical properties might not be exhaustive.

In our experimental setting, CDR3 regions of the V_H domain were analyzed instead of complete antibody binding sites. This method is consistent with the finding that CDR3 regions of the V_H domain determine the specificity of the antigen-antibody binding interaction while those of the V_L domain are less diverse and CDR1 and CDR2 regions are more cross-reactive (Davis et al., 1998; Xu & Davis, 2000).

To present the conclusion in the context of other publications, the clonal relationship of IgE and IgG1 and their regulation by individual B cell clones is in accordance with previous studies:

Turqueti-Neves and colleagues analyzed the IgE repertoire in an in vivo mouse model after primary and secondary infection with the helminth N. brasiliensis or after OVA/alum-immunization of BALB/c mice. Their NGS analysis revealed an overlap between the IgG1 and IgE repertoires, including an intersection between CDR3 regions of these antibodies in an individual mouse but not among different mice (Turqueti-Neves et al., 2015).

To consider also data from human beings and not only from the mouse model, Hoof and colleagues analyzed the IgE memory responses in 40 patients with allergic rhinitis during one year of sublingual immunotherapy (SLIT). They concluded that the human IgE memory response after mucosal grass pollen allergen exposure was derived from allergen specific IgG+ memory B cells which could switch to short-lived IgE+ plasmablasts.

baseline time point, revealing the commitment of shared clonotypes to the IgE lineage prior to allergen exposure. On average, the level of SHM in IgE and IgG_E repertoires was

constant for the first 4 weeks, but the number of IgE transcripts increased, demonstrating that IgG switches to IgE without further affinity maturation.

The conclusion of this study is limited by the low number of patients, especially because only a selection of the participating patients was analyzed in each experiment (Hoof, Ilka; Schulten, 2020).

Whether the switch from IgG1 to IgE is independent from somatic hypermutation needs to be further discussed. Data from colleagues in my research group who performed an NGS analysis in an in vivo murine food allergy model described the IgE compartment. It contained unmutated IgE clones as well as hypermutated IgE clones which are clonally less expanded. Hence, these results suggested the co-existence of an extrafollicular response with a germinal center reaction (Udoye et al., 2022). Extrafollicular early type 2 immune responses include a direct switch from IgM to low-affinity IgE. Later type 2 immune responses involve the GC-dependent sequential switch and differentiation from IgG1+ memory B cells to high-affinity IgE-secreting plasma cells (Haase & Voehringer, 2021). To conclude, somatic hypermutation might influence the class switch and the formation of IgE and IgG1.

Another NGS analysis focused on the IgE response for different B cell receptor mutations in a murine helminth infection and immunization model: $CD73^{+}CD80^{+}$ $IgG1^{+}$ memory B cells gave rise to more high affinity mutations in IgE and IgG1 compared to immunoglobulins derived from $CD73^{-}CD80^{-/+}$ $IgG1^{+}$ memory B cells. Thus, specific BCR mutations influenced the IgE affinity. Nevertheless, it remained unclear why IgG1 memory B cells form either IgG1 PCs or IgE PCs (He et al., 2017).

All in all, the clonal relationship between IgE and IgG1 seems to be a common phenomenon in various experimental settings. The switch from IgG1 to IgE does not depend on but might be influenced by somatic hypermutation. BCR mutations are believed to shape the affinity of the produced immunoglobulins. The mechanisms of the sequential class switch from IgE to IgG1 are still incompletely understood. Collectively, the results might demonstrate that individual B cell clones and hence the BCR itself control the IgE to IgG1 ratios.

5.2 BCR stimulation

5.2.1 Calcium flux assay

To further elucidate the role of the BCR, a model to measure the BCR signaling strength was established. Different concentrations of anti-Ig F(ab')$_2$ fragments caused a quantitatively different calcium flux. Hence, the concentration of anti-Ig F(ab')$_2$ fragments can be used as a model for the BCR signaling strength, with higher concentrations reflecting a stronger BCR signaling and potentially mimicking the interaction of an antigen with a high-affinity BCR.

It remains elusive why the calcium response was more pronounced for IgM^{high}IgD^{low} B cells than for IgM^{low}IgD^{high} B cells.

Maity and colleagues created an in vitro B cell line comprising IgD- and IgM- BCRs with different antigen-binding sites. Using two-color direct stochastic optical reconstruction microscopy and transmission electron microscopy, they provided evidence that IgM and IgD receptors are organized in different protein islands within the plasma membranes. Upon B cell activation, the two BCR protein islands shrink and gain proximity. The different IgM and IgD islands could be stimulated separately using monoclonal anti-IgM and anti-IgD F(ab')$_2$ fragments (Maity et al., 2015).

In my experimental setting, IgM and IgD receptors were stimulated by polyclonal antibodies in comparison to Maity and colleague's usage of monoclonal anti-IgD and anti-IgM F(ab')$_2$ fragments. Thus, a specific stimulation cannot explain the lower calcium response for IgD-high B cells. Notably the anti-Ig kappa F(ab')$_2$ fragments are unbiased, but the conclusion is limited by the low number of mice tested (compare figure 7 or appendix 9.2.1). Taking the model of the compartmentalized plasma membrane with various protein islands into account, a different access of the IgM- and IgD- BCRs to the calcium signaling pathway can be suggested:

Considering the higher proximity of the coreceptor CD19 to the IgM- than the IgD- BCR in activated B cells (Kläsener et al., 2014) and CD19's crucial function for B cell activation and generation of a calcium flux (Depoil et al., 2008), it can be speculated that IgM^{high}IgD^{low} B cells show a higher calcium response than IgM^{low}IgD^{high} B cells because their protein island moves closer to the coreceptor CD19, creating a more pronounced calcium flux.

It would be interesting to investigate this hypothesis further, comparing the calcium response of anti-IgM versus anti-IgD F(ab')$_2$ fragments for IgM^{high}IgD^{low} and IgM^{low}IgD^{high} B cells.

5.2.2 Anti-IgM F(ab')$_2$ fragments

Having defined those different concentrations of anti-IgM F(ab')$_2$ fragments as a model for BCR signaling strength, the influence of the BCR signaling strength on the class switch to IgE and IgG1 was measured. In vitro cell culture experiments revealed that the stimulation of the BCR with anti-IgM F(ab')$_2$ fragments selectively inhibited the formation of IgE+ B cells and plasmablasts more strongly than that of IgG1+ cells. Further, both effects, the general inhibition of these Ig subclasses as well as the shift in their ratio, were found to be dose-dependent. Therefore, these results elaborate on previous findings by Jabara and colleagues stating that anti-IgM F(ab')$_2$ fragments inhibit the CSR to IgE and to IgG1 (Jabara et al., 2008).

Studying my experimental setting in more detail, the analysis of the frequencies of IgE+ and IgG1+ cells on day 4 of the Germinal Center Culture cannot evaluate the long-term effect of the BCR stimulation. This is a consequence of the early timepoint of analysis, impeding the detection of memory B cells and long-living plasma cells. Of note, Nojima et al., who established the Germinal Center Culture, could not detect IgE+ memory B cells 30 days after transferring IgG1+ iGB cells into C57BL/6 mice. According to their interpretation, IgE+ iGB cells differentiate into PCs, supported by the finding that the Blimp 1 concentration in IgE+ iGB cells is higher than in IgG1+ iGB cells (Nojima et al., 2011).

This explanation is in line with several studies demonstrating that IgG1+ memory B cells are the predominant precursors for IgE+ plasma cells in mice (He et al., 2017; Jiménez-Saiz et al., 2017; Turqueti-Neves et al., 2015).

Collectively, there are well described pathways explaining the B cell differentiation after the germinal center reaction, but the role of BCR signaling on the development of plasma cells and memory B cells needs to be addressed in long-term culture experiments. Several mechanisms are already known, raising the question of how they shape together the secretion of IgE or IgG1 in vitro or their serum titers in vivo. The group of Nojima et al. stimulated iGB cells with anti-μH F(ab')$_2$ antibodies in vitro which did not result in an altered number of induced memory B cells in the recipient spleens in vivo, concluding that the development of induced memory B cells does not depend on an antigenic stimulation (Nojima et al., 2011). Opposingly, the BCR affinity seems to be important for the development of plasma cells: a higher BCR affinity is associated with enhanced ICOS-ICOSL and CD40L-CD40 interactions between Tfh cells and GC B cells, favoring the PC differentiation (Haase & Voehringer, 2021; Wataru Ise & Kurosaki, 2019).

While in our experimental setting the number of counted cells decreased depending on the BCR stimulation, Jabara and colleagues provided evidence via tritiated thymidine incorporation, CFSE staining and measurement of apoptosis with propidium iodide and

annexin V, that the inhibition of the CSR to IgE and IgG1 is not due to impaired proliferation, cell division or increase in apoptosis (Jabara et al., 2008). In view of the differences in the experimental setting, more precisely the LPS- B cell culture versus the Germinal Center Culture and the time point of analysis, the findings of Jabara and colleagues cannot be transferred to our Germinal Center Culture. Thus, the underlying cause of the reduced number of cells needs to be investigated in our experimental setting.

Together, several limitations of the experimental setting could be identified: long-term effects of the BCR stimulation could not be determined and the comparison of the advanced Germinal Center Culture to LPS- B cell cultures is not fully accomplished.

5.2.3 Anti-Ig kappa F(ab‘)$_2$ fragments

So far, it has been shown that different concentrations of anti-IgM F(ab’)$_2$ fragments, representing differential BCR signaling strength, selectively inhibit the formation of IgE+ B cells and plasmablasts more strongly than that of IgG1+ cells. Questioning whether this result can be repeated with another anti-BCR antibody, it could be demonstrated that anti-Ig kappa F(ab’)$_2$ fragments impede the formation of IgE+ cells more than the formation of IgG1+ cells. Again, the general inhibition of these Ig subclasses as well as the shift in their ratio were found to be dose-dependent.

The condition of 8 µg/ml anti-Ig kappa F(ab’)$_2$ fragments could not be included in the analysis due to the low cell number. Consequently, the question arises how anti-Ig kappa F(ab’)$_2$ fragments reduce the number of cells, for example by means of a toxic component. According to their manufacturer, these fragments do not contain components considered to be either persistent, bioaccumulative and toxic, or very persistent and very bioaccumulative at levels of 0.1% or higher (MERCK, 2023).

Despite the manufacturer’s information, the matter of a toxic ingredient was investigated experimentally. Anti-Ig kappa F(ab’)$_2$ fragments together with either PBS/BSA or DPBS were added to an Amicon Ultra filter device and centrifuged several times. The resulting purified anti-Ig kappa F(ab’)$_2$ fragments did not induce a calcium flux (figure S1). The underlying cause remains subject to speculation. The purification process might change the protein structure by separating the F(ab’)$_2$ fragment from other components of the Sigma Aldrich’s F(ab')$_2$ fragments like disodium tetraborate decahydrate. Thus, altered chemical bonds might influence the protein structure. Therefore, the capacity of the F(ab’)$_2$ fragment to interact with membrane-bound Igs might be impeded. In the end, purified anti-Ig kappa F(ab’)2 fragments could not be used for further cell culture experiments because the original experimental setting could not be reproduced without a BCR-induced calcium response.

Taking all the information into account, it remains elusive why the number of cells was extremely reduced in the cell culture supplemented with 8 µg/ml anti-Ig kappa $F(ab')_2$ fragments.

5.2.4 ELISAs of the cell culture supernatant

ELISA experiments confirmed that not only the surface expression of IgE and IgG1, but also the secretion of IgE and IgG1 antibodies is reduced after BCR stimulation in a dose-dependent manner. A stronger inhibition after BCR stimulation of IgE when compared to IgG1 could not be demonstrated, which might have been influenced by the experimental setting:

The ELISA experiments were performed on day 4 of the cell culture while the ELISA experiments of Jabara and colleagues were performed on day 6 of the cell culture (Jabara et al., 2008). Considering that IgE antibodies are generated by several pathways, the time point of analysis could be an important factor determining the result.

Early type 2 immune responses include the direct switch from IgM to IgE outside the germinal center. The short-lived plasma cells generate low-affinity IgE antibodies. Later type 2 immune responses involve the GC-dependent sequential switch and differentiation from IgG1+ memory B cells to high-affinity IgE-secreting plasma cells (Haase & Voehringer, 2021). All in all, it could be interesting to perform ELISA experiments on different days of cell culture.

Besides the time point of analysis, the anti-Ig kappa $F(ab')_2$ fragments in the cell culture might be a limiting factor of the experimental setting. Anti-Ig kappa F(ab')2 fragments might increase the measured secretion of IgE and IgG1 antibodies by forming immune complexes between the divalent IgE and IgG1 antibodies and the divalent $F(ab')_2$ fragments. The more valent immune complexes might bind better to the coated IgE and IgG1 antibodies in the well plate. In contrast, anti-Ig kappa $F(ab')_2$ fragments might decrease the measured secretion of IgE and IgG1 antibodies by occupying the antigen binding sites of these antibodies and minimizing the interaction between the coated antibodies in the well plate and the secreted antibodies. These opposing effects might also neutralize themselves, hence the anti-Ig kappa $F(ab')_2$ fragments might not change the result at all.

Another factor which needs to be taken into account is the nature of IgE antibodies. The IgE isotype has, in comparison to the other immunoglobulin subtypes, the lowest concentration in the serum and the most limited half-life. (Stone et al., 2010; Haniuda & Kitamura, 2021). Of note, it is difficult to specify the half-life of IgE as it depends on the

tissue and method of measurement: its half-life in murine serum is reported to be in the range of 12 hours and 2 days, while it can extend to several weeks if it is bound on the FcεRI receptor on mast cells (Poulsen & Hummelshoj, 2007; Shade et al., 2019; Vieira & Rajewsky, 1988). Due to the low and temporary limited IgE serum concentration, my ELISAs of the cell culture supernatant might not be sufficiently precise to detect appropriately IgE, especially as it is measured here in relative light units, which is a comparative, but not a quantitative scale.

Additionally, the B cell differentiation process might justify that the frequencies of IgE+ and IgG1+ B cells and plasmablasts, measured by flow cytometry, do not correlate with the quantity of IgE and IgG1 antibodies, secreted by plasma cells and measured by means of ELISA. Yang and colleagues investigated in murine in vivo and in vitro models that IgE+ B cells are, in contrast to IgG1+ B cells, more prone to a short-lived PC fate during primary immune responses due to their upregulation of the transcription factor Blimp-1 (Z. Yang et al., 2012). This is in line with the finding of Erazo and colleagues who described the association of class switch to IgE and differentiation into plasma cells (Erazo et al., 2007). More recent studies indicate that the differentiation into PCs is autonomously promoted by the IgE BCR itself (Haniuda et al., 2016; Z. Yang et al., 2016). Together, the immunological features of the B cell differentiation could explain why the flow cytometry data reveal a shift in the IgE/IgG1 ratio, while the data from the ELISA experiments do not show a decrease in the IgE/IgG1 ratio depending on the BCR stimulation.

5.2.5 Apoptosis: Annexin V staining

Investigating the mechanisms of how BCR stimulation can influence the frequencies of IgE+ and IgG1+ cells, a modest increase in frequency of early apoptotic cells was detected in all B cell subpopulations. Thus, apoptosis after BCR stimulation might partially regulate the cell survival of different B cell subpopulations and it remains subject to speculation whether these changes in the B cell subpopulation contribute to the decrease of IgE+ and IgG1+ cells after BCR stimulation.

This conclusion is limited by the experimental setting which did not allow for specific analysis of the frequency of apoptotic cells within IgE+ and IgG1+ cells, but only within different B cell subpopulations. In essence, it cannot be ruled out that IgE+ cells selectively undergo apoptosis. Generally, it remains controversially discussed whether the autonomous signaling of the IgE BCR selectively induces apoptosis or not (Haniuda et al., 2016; Haniuda & Kitamura, 2021; Wade-Vallance & Allen, 2021; Z. Yang et al., 2016).

Comparing the results of this experiment to other publications is limited by the broad spectrum of methods which can be used to examine apoptosis (Banfalvi, 2017). Jabara

and colleagues performed surface staining with annexin V and propidium iodide after stimulation with anti-IgM F(ab')$_2$ fragments, resulting in a decrease in apoptosis and cell death (Jabara et al., 2008). They used another staining protocol with other dyes and did not divide into early and late apoptotic cells.

The slight decrease in frequencies of late apoptotic cells depending on an increase in the concentration of anti-IgM F(ab')$_2$ fragments is in line with a recent publication from Berry and colleagues showing that BCR signaling strength promotes cell survival in a dose-dependent manner, while apoptosis is prevented by CD40 co-stimulation, activating canonical NF-κB.

In more detail, their cell culture experiments with murine splenic B cells in the presence or absence of anti-BCR antibodies, quantifying anti- and pro-apoptotic genes by qRT-PCR, revealed that strong BCR stimulation and its calcium signal increased the anti-apoptotic gene expression. Hence, the Bcl-xL protein was upregulated and cell survival was promoted. Weak BCR signaling was linked to apoptosis. “Strong” and “weak” BCR signaling were not defined, the range of anti-IgM F(ab')$_2$ fragments included in their experiments comprised concentrations between 0 and 50 µg/ml (Berry et al., 2020).

Consequently, on the one hand, apoptosis might have been prevented in our cell culture system by “strong” BCR stimulation and/or CD40 signaling by the CD40L transfected fibroblasts. On the other hand, apoptosis might have been induced due to “weak” BCR signaling as concentrations from 0 to 8 µg/ml anti-IgM F(ab')$_2$ fragments were used in my experimental setting.

5.2.6 Semiquantitative analysis of switch circles

At first glance, stimulating naïve cells seems like a model for direct CSR from IgM to IgE. However, from a current perspective, the majority of IgE is produced via sequential CSR from IgG1+ memory cells (Haase & Voehringer, 2021). To investigate which type of CSR is dominant in our system and whether the selective inhibition of IgE after BCR stimulation is due to an inhibition of the CSR, a semiquantitative analysis of switch circles was performed. It was shown that the gene expression of switch circles derived from the indirect class switch to IgE decreased more than the gene expression of switch circles from the class switch to IgG1. Thus, a potential conclusion is that the IgE+ B cells generated by our culture system are originated by indirect class switch and that the BCR stimulation with anti-Ig F(ab')$_2$ fragments inhibits the CSR to IgE more than to IgG1.

There are three main limitations of this interpretation: Firstly, the quality of the band for the CSR to IgG1 limits the confidence towards the experimental setting. It was not possible to

perform a quantitative PCR next to the semiquantitative one despite several optimization attempts including different cDNA concentrations, primer concentrations, annealing temperatures, anti-Ig F(ab')$_2$ fragment concentrations during the cell culture and measuring simple and duplex reactions. Conceivable explanations for the failure of the quantitative PCR are the contamination of the primers or a problem with the fluorophore. It is not possible to compare the results with other publications because, to my knowledge, there are no other attempts to quantitatively analyze switch circles in murine cell culture models.

Secondly, the analysis of switch circles was performed on day 3 of the Germinal Center Culture while the long-term presence of switch circles from IgE and IgG1 switching was not evaluated. Therefore, it cannot be ruled out that anti-Ig F(ab')$_2$ fragments delay rather than prevent switching from IgG1 to IgE.

Thirdly, it is questionable how anti-IgM F(ab')$_2$ fragments inhibit the switching from IgG1 to IgE as class-switched IgG1+ B cells do not express IgM on their membrane. Possible explanations include a cross-reactivity of the F(ab')$_2$ fragment to several BCRs or an ongoing inhibition of the F(ab')$_2$ fragment from earlier time points of the experiment, when the IgG1+ B cells were IgM+.

However, the idea of sequential CSR to IgE can be supported by an experiment conducted by Chinweike Christopher Udoye and Kai Othmer, colleagues in my research group, using the Germinal Center Culture. IgG1+ cells were sorted after 4 days of the co-culture and re-cultured together with IL-4 and increasing concentrations of anti-Ig kappa F(ab')$_2$ fragments. After one day, 12-22% of the sorted IgG1+ cells had switched to IgE, if they were not stimulated with anti-Ig kappa F(ab')$_2$ fragments. In contrast, increasing BCR signaling was associated with reduced frequencies of IgE+ cells and higher frequencies of IgG1+ cells. These results indicate that sequential class switch from IgG1+ cells to IgE+ cells is impeded by increasing signals via the BCR, possibly lowering the ratio of IgE+ to IgG1+ cells (Udoye et al., 2022).

These findings are in line with the assumption that class switch to IgE inside a germinal center is sequential (Haase & Voehringer, 2021). Nevertheless, our Germinal Center Culture is not suited to examine the influence of the BCR signaling strength on direct class switch to IgE which occurs outside the GC or on other mucosa-dependent class switch: High-throughput DNA sequencing of immunoglobulin heavy chain transcripts in mucosal gastrointestinal biopsies from peanut allergic, non-allergic and other non-food allergic patients revealed a local class switch in the gastrointestinal tract of peanut allergic patients from IgA2 to IgE (Hoh et al., 2020). Another recent study presented a local direct

and sequential class switch from IgD+ B cells to IgE in the nasal mucosa of patients suffering from allergic rhinitis (Corrado et al., 2021).

Overall, the semiquantitative analysis of switch circles demonstrated the dominance of sequential class switch in our cell culture model and the selective inhibition of the CSR to IgE. Nonetheless, this interpretation is limited by the experimental setting and the Germinal Center Culture which is not suitable to analyze direct or mucosa-dependent class switch.

5.2.7 PI3K-Inhibitor LY294002

The PI3K/AKT-pathway is one of the three major pathways activated by BCR stimulation and the only one with an inhibiting function (Z. Chen & Wang, 2019). Hence, it was investigated whether the removal of the inhibiting pathway by the PI3K-inhibitor LY294002 counteracts the effects seen by BCR stimulation. LY294002 not only increased the frequency of IgG1+ cells but also slightly increased that of IgE+ cells. Nevertheless, it did not change the IgE/IgG1 ratio and did not counteract the effect of BCR stimulation on the IgE/IgG1 ratio.

Comparing the results to other studies and even drawing a consistent conclusion is limited not only by the complexity of the different isoforms of class I PI3K catalytic subunits and their effects on CSR (Chen et al. 2015), but notably by the reagent LY294002 itself.

The usage of LY294002 was inspired by a publication from Doughty and colleagues (Doughty et al., 2006), which was in line with its first report as a PI3K specific inhibitor (Vlahos et al., 1994). LY294002 is used as a specific PI3K inhibitor in many publications (compare for example Cantrell et al., 2018; Lobo EO, Zhang Z, 2009) and is described as a potent and specific inhibitor of the PI3-kinase by the manufacturer (MERCK, 2024). In light of this, it was surprising to discover that LY294002 was declared as an unsuitable probe to abolish the effect of PI3K by the Chemical Probes Portal (Antolin et al., 2023; www.chemicalprobes.org).

LY294002 is not recommended to be used as selective research tool. It inhibits other kinases in the same range of concentrations in which it is applied to inhibit PI3K. Beside the off-target effects, it is considered to be a weak inhibitor, operating with a micromolar potency (Arrowsmith et al., 2015; Workman et al., 2010).

The Chemical Probes Portal is an expert review-based public resource which defines a chemical probe as a small, well characterized molecule which is potent, selective and proven to interact with the protein or cell of interest (Antolin et al., 2023). The website was established to accompany a publication criticizing the wide usage of non-selective,

inadequately characterized probes leading to a waste of public funding, scientific resources and a loss of reliability of scientific publications. One of four factors deemed responsible for the usage of non-specific chemical probes is the difficulty to be informed about the most appropriate and modern probe for a specific target, leading to a choice of chemical probes by precedence and availability (Arrowsmith et al., 2015). This is a suitable description of my experimental conduct and should be adequately addressed in future studies.

The discussed issue should highlight the importance to carefully use appropriate tools as the Chemical Probes Portal or the published checklist for chemical probe-based experiments (Antolin et al., 2023; Arrowsmith et al. 2015) in order to produce robust results.

5.3 Role of co-stimulating factors

5.3.1 IL-4

Analyzing the influence of co-stimulating factors on the IgE/IgG1 ratio, the cytokine IL-4 increased the frequency of IgE+ and IgG1+ B cells and plasmablasts, raising the ratio of IgE to IgG1. In the context of our cell culture which is dominated by sequential class switch (see 4.2.6), it can be suggested that the switch from IgG1 to IgE is more stimulated than the switch from IgM to IgG1.

A possible reason explaining the higher increase in frequency of IgE+ cells relative to IgG1+ cells could be the induction of the low-affinity IgE-receptor, CD23, by IL-4 (Nelms et al., 1999), leading to a higher surface expression of IgE. However, free IgE tends to bind to the FcεRI, while IgE- immune complexes interact preferentially with CD23 (FcεRII) (Engeroff et al., 2020). Therefore, the higher surface expression of CD23 cannot be the principal reason for the enhanced IgE+ frequency because of the absence of immune complexes in the culture. Moreover, cross-linking the CD23 receptor with IgE leads to internalization. Therefrom, it is uncertain whether the IgE antibodies which bind to the CD23 receptor increase the surface expression of IgE (Engeroff & Vogel, 2021).

Snapper and colleagues performed ELISA experiments of B cell cultures supplemented with LPS detecting that IL-4 activates the production of IgE and IgG1 in two different ways. They described a dose-dependent increase in IgE production in contrast to a bimodal curve of the IgG1 production in response to IL-4. In more detail, the IgG1 secretion decreased at IL-4 concentrations between 100 and 1000 U/ml before increasing again with higher concentrations (Snapper CM, Finkelman FD, 1988). On the contrary, in my experiments, the frequencies of IgG1 measured by flow cytometry increased constantly for all tested concentrations of IL-4 (0,5 ng/ml- 8ng/ml ˜100-1600 U/ml). Of note, the ELISA of the cell culture supernatant was performed on day 6 of an LPS-B cell culture, while I analyzed a flow cytometry experiment performed on day 4 of a Germinal Center Culture. Hence, the different concentrations of IgG1 could be due to the time point of analysis, the comparison of a T-cell-independent and a T-cell-dependent stimulation system or a difference between secretion and surface expression of immunoglobulins. The latter does not appear to be a reliable reason because the paper describes that the surface expression of B cells is in accordance with their secretion: the frequency of membrane IgG1 on day 4 was 40-50% mIgG1+ B cells which secreted eleven-fold more IgG1 than mIgG1- B cells (Snapper CM, Finkelman FD, 1988). It is difficult to compare the frequencies with my experiments as the highest IL-4 concentration I recorded was 1600 U/ml in contrast to 10000 U/ml described by Snapper et al. A possible remaining hypothesis is that IL-4 regulates IgE and IgG1 differently in T-cell-independent systems in

comparison to T cell-dependent- systems which include a constant synergistic effect of IL-4 and CD40L.

The effects seen in the studies of Snapper et al. after IL-4 stimulation seem to be caused by this cytokine because the change in the Ig concentration could be reversed by an anti-IL-4 antibody in vitro. Opposingly, the anti-IL-4 antibody inhibits in vivo IgE responses without suppressing IgG1 responses. Different models of explanations are discussed, including a possible alternative pathway to induce IgG1 or a stronger IL-4 dependence of IgE induction compared to IgG1 activation (Snapper CM, Finkelman FD, 1988). It can be speculated that the higher dependency of IgE on IL-4 is due to the different length and number of tandem repeats of the IL-4 transcription factor binding sites in IgE versus IgG1 switch regions (James, 2022). These theories can be adapted as hypotheses to elucidate the increase in the ratio of IgE/IgG1 by enhancing IL-4 concentrations in my experimental setting.

One of the alternative pathways for the generation of IgG1 has been detected by Yang et al.: The IL-21 mediated STAT3 signal promotes in murine B cells with low doses of IL-4 or anti CD-40 the CSR to IgG1+, while the IgE response is reduced (Z. Yang et al., 2020). My colleagues found a similar result for our Germinal Center Culture, concluding that the ratio of IgE to IgG1 is not only influenced by the BCR signaling strength but also determined by the interaction of B cells and T follicular helper cells which provides IL-21 (Udoye et al., 2022). This example illustrates the complexity of interactions between cytokines. Further in vitro experiments could evaluate the influence of certain combinations of cytokines in different concentrations on the IgE/IgG1 ratio, for example combining IL-4 with IL-13. The latter is known to promote the generation of high-affinity IgE (Haase & Voehringer, 2021).

5.3.2 Glucose concentration

Elucidating the role of different glucose levels on the formation of IgE+ and IgG1+ cells, it could be demonstrated that higher glucose concentrations increased the frequency of IgE+ cells, possibly raising the IgE/IgG1 ratio in the Germinal Center Culture. IgE+ and IgG1+ cells displayed similar glucose uptake rates. This finding suggests that a different glucose uptake is not the mechanism behind the shifted IgE/IgG1 ratio.

Analyzing an additional mechanism, apoptosis might be induced or inhibited depending on the glucose concentrations. The frequency of early and late apoptotic cells diminished between the two tested glucose concentrations: 100 mg/dL and 200 mg/dL. Only cells cultured with 100 mg/dL, or 200 mg/dL glucose were analyzed due to time constraints in the context of my doctoral thesis. It could be of interest to specifically analyze the

frequency of IgE+ and IgG1+ apoptotic cells in the range of different glucose concentrations: 50 mg/dL, 100 mg/dL, 150 mg/dL, 200 mg/dl, 300 mg/dL.

To my knowledge, there is no other published in vitro analysis of the effect of different glucose concentrations on the class switch to IgE and IgG1. Thus, it is difficult to compare the results to other studies and to explain why the IgE/IgG1 ratio rose depending on the glucose concentration.

The closest model of different glucose concentrations is a recent in vivo study in a murine food allergy model which divided mice (n=30) into a free diet group and two intermittent fasting groups (24 h fasting/24 h feeding vs. 16 h fasting/8 h feeding). All mice were sensitized to and subsequently challenged with ovalbumin (OVA). Symptoms of food allergy were measured (reduction of the rectal temperature and diarrhea). After 56 days, the intermittent fasting groups showed less food allergic symptoms in terms of frequency and severity, decreased levels of serum OVA-sIgG1 and -sIgE, IL-4 and IL-5 and a differently comprised gut microbiota in comparison to the free diet group (Ma et al., 2023). The protective effect of the altered gut microbiota cannot be adopted for my in vitro stimulation system. Nevertheless, lower serum IgE and IgG1 levels in the intermittent fasting group are comparable to lower frequencies of IgE+ and IgG1+ cells in Germinal Center Cultures with lower glucose levels in my experimental setting.

On the whole, it is possible that the level of glucose shapes the Th2 response. This conclusion is supported firstly by the reduction of Th2 cytokines in the intermittent fasting groups in the in vivo experiment. As discussed above, the formation of IgE might be more sternly dependent on the Th2 cytokine IL-4 (chapter 5.3.1). Secondly, the frequency of IgE+ cells rose more than that of IgG1+ cells depending on the glucose concentration in my in vitro experiments. Further in vitro and in vivo studies are needed to clarify the role of different glucose levels on the ratio of IgE/IgG1 as well as the Th2 response in general.

The interaction between Th2 response and physiological or pathological glucose levels is of interest for human beings, too. A prospective case control study comparing 94 children suffering from diabetes mellitus type 1 with a control group, consisting of 188 children, reported a higher prevalence of IgE-mediated allergies in diabetic children (Klamt et al., 2015). Whether the pathological glucose levels caused the IgE-mediated diseases or vice versa can be discussed. To my knowledge, there are not more recent pediatric publications addressing this question. In contrast, two Chinese studies conducted in 55 to 75 years old adults demonstrated a correlation between plasma IgE levels and glucose tolerance status, describing high IgE levels as a risk factor for pre-diabetes and diabetes type 2 (Z. Wang et al., 2011; Z. Wang et al., 2013).

In the long term, further investigation is required to determine whether and how different diets or diabetic disorders influence the development of IgE-mediated allergies and how IgE shapes the glucose metabolism.

6. Conclusion and outlook

This thesis aimed to analyze how the ratio of the immunoglobulins IgE and IgG1, which are crucial for the development of food allergies, can be influenced on a cellular level. The two main research questions were defined in the following way:

1. *What is the impact of BCR signaling strength on class switch to IgE and IgG1 in murine B cell cultures?*

2. *What is the impact of differential IL-4 levels and differential glucose levels on the ratio of IgE/IgG1 in murine B cell cultures?*

Elucidating the first aim, calcium flux experiments showed that various concentrations of anti-IgM and anti-Ig kappa $F(ab')_2$ fragments were an appropriate model for different BCR signaling strengths. Further in vitro stimulation experiments of murine B cell cultures revealed that higher BCR signaling strengths selectively inhibited the generation of IgE+ cells more strongly than that of IgG1+ cells. Strong BCR signaling does not only inhibit CSR to IgE and IgG1 (Jabara et al., 2008), but also affects distinct Ig-expressing B cells differently. Deepening the understanding of how BCR signaling influences the generation of IgE and IgG1, a semiquantitative analysis of CSR excision products was performed. In combination with the results of cell sorting experiments of my research group, this analysis suggested an inhibition of the indirect class switch from IgG1 to IgE in our cell culture model by strong BCR signaling, possibly reducing the IgE/IgG1 ratio.

Nevertheless, the main limitations of the experiments lie in the absence of analysis of both the long-term effect of BCR stimulation and the impact of BCR signaling on direct or mucosa-dependent class switch. Notably, the findings in a mouse model cannot be automatically transferred to human beings. Thus, it would be of interest to perform further in vitro and, afterwards, in vivo studies analyzing the long-term effect of different BCR signaling strengths on the IgE response in GC-dependent and GC-independent settings. Research aims of these future studies could be the examination of possible pharmaceutical uses of differential BCR signaling strengths, potentially representing different affinities or avidities of the BCR towards the antigen, in clinical desensitization therapies of allergic patients. To be more precise, it is worth exploring the question of whether differential BCR signaling strengths can contribute to overcome the temporary success of the desensitization therapies.

Elaborating on the second research question, in vitro stimulation experiments of murine B cell cultures demonstrated that rising concentrations of the cytokine IL-4 as well as rising concentrations of glucose were associated with an increase in the ratio of IgE to IgG1. The glucose uptake of IgE+ and IgG1+ cells was similar. To my knowledge, the role of

different glucose levels on class switch to IgE and IgG1 in an in vitro setting was described for the first time. It remains elusive by which mechanism different glucose concentrations shape the class switch to IgE and IgG1.
Therefore, more in vitro and in vivo experiments are required to explain how different glucose levels change the nature of the IgE response and how different diets or diabetic disorders might influence the development of IgE mediated diseases.

7. Abstract

Background: IgE-mediated food allergy is a common disease affecting up to one tenth of the population, especially in industrialized nations, and provoking symptoms that range from mild skin manifestations to life-threatening anaphylaxis. Curative and preventive treatment is very limited, creating a danger for the patients and an economic burden for the patients and their stakeholders. Therefore, an advanced knowledge of immunological mechanisms which could serve as a future treatment target is necessary. A promising target is the ratio of the immunoglobulins IgE and IgG4 in humans, or respectively IgE and IgG1 in mice. Several studies describe that sensitized but tolerant patients presented a higher ratio of food-specific IgG4 to IgE as opposed to food allergic patients. Hence, it is of great interest to understand which factors influence the ratio of these immunoglobulins, contributing to a more allergy-releasing or allergy-protective immune response.

Objective: This thesis aims to evaluate the impact of B cell receptor (BCR) signaling strength, differential IL-4 and glucose levels on the ratio of membrane-bound and secreted IgE and IgG1 in murine B cell cultures.

Methods: The experiments are based on an in vitro B cell culture system that mimics a T cell-dependent germinal center reaction: splenic B cells from BALB/c mice were co-cultured with cells from the feeder cell line 40 LB and stimulated with cytokines and, if applicable, $F(ab')_2$ fragments of anti-Ig antibodies, among others. The frequencies of IgE- and IgG1-expressing cells were evaluated by flow cytometry, the secretion of these antibodies by ELISA and the class switch recombination generating these antibodies by semiquantitative analysis of switch circles.

Results: Calcium flux experiments revealed that $F(ab')_2$ fragments of anti-IgM and anti-Ig kappa antibodies could serve as a model for different BCR signaling strengths. Flow cytometric analysis of IgE+ and IgG1+ B cells and plasmablasts showed that stimulation with both $F(ab')_2$ fragments decreased the frequencies of these isotype-switched cells. The ratio of IgE+ to IgG1+ B cells diminished with increased BCR signaling which was similar for BCR stimulation with $F(ab')_2$ fragments of anti-IgM and anti-Ig kappa antibodies. In contrast, increasing concentrations of IL-4 or glucose in cell cultures raised the ratio of IgE/IgG1.

Conclusion: In our germinal center model, the stimulation of the BCR with $F(ab')_2$ fragments of anti-Ig antibodies selectively inhibited the formation of IgE+ B cells and plasmablasts more strongly than that of IgG1+ cells. The strength of this inhibition corresponded to the BCR signaling strength. Semiquantitative analysis of switch circles showed that indirect class switching from IgM to IgG1 to IgE was the principal mechanism of IgE+ B cell generation in our cell culture system. IL-4 and glucose levels seemed to

influence the IgE/IgG1 ratio, too. All in all, these findings suggest that complex B cell-extrinsic environmental stimuli differently influence the generation of IgG1- vs. IgE-switched cells, even though Th2-cytokines, especially IL-4, promote switching to both isotypes.

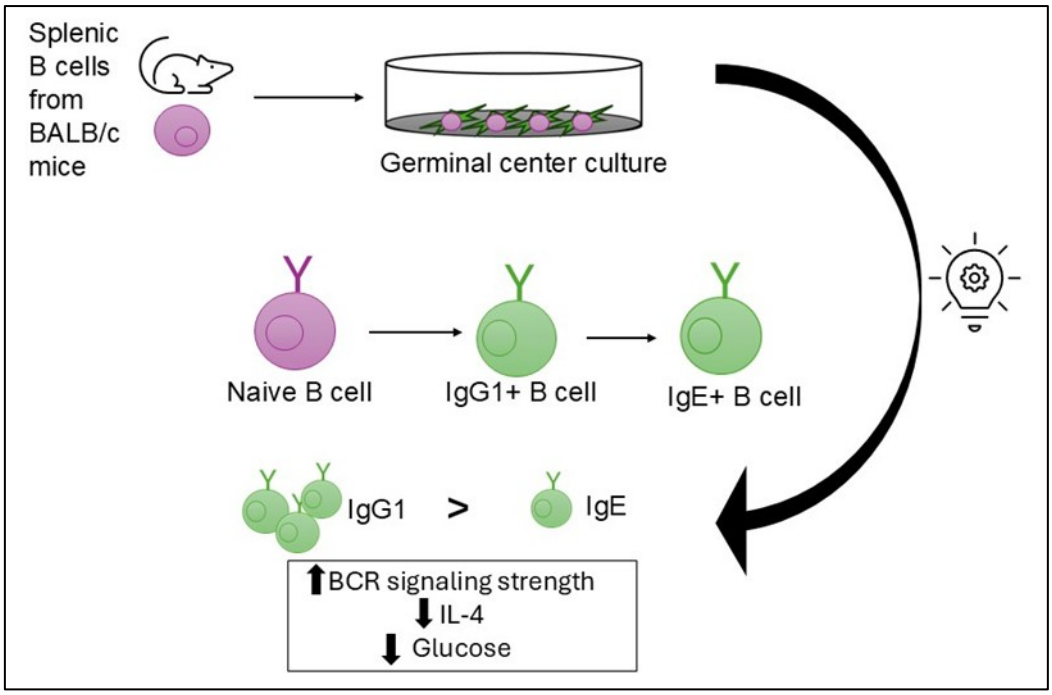

Figure 21: Graphical abstract.
Splenic B cells from BALB/c mice were co-cultured with cells of the feeder cell line 40 LB which are BALB/c3T3 fibroblasts transfected with CD40L and BAFF (B cell activation factor). This cell culture was supplemented with IL-4 and anti-Ig $F(ab')_2$ fragments, among other stimuli. The cells were harvested and analyzed by flow cytometry, ELISA and semiquantitative PCR, revealing that the ratio of IgE to IgG1 can be changed. Higher B cell receptor signaling strength was associated with a decrease in the ratio of IgE to IgG1, while higher IL-4 concentrations and glucose concentrations in the cultures resulted in an increase in this ratio. Cell sorting experiments performed by colleagues in my research group and semiquantitative analysis of switch circles suggest that indirect class switch from IgM to IgE via an IgG1 intermediate is the dominant class switch pathway in our culture system.

8. Extended Abstract (German)

Regulation von IgE- und IgG-Antikörpern im Kontext muriner Nahrungsmittelallergien

1. Einleitung

1.1 Klinischer Hintergrund

Nahrungsmittelallergien sind unerwünschte Gesundheitsreaktionen, die wiederholt nach der Exposition gegenüber einem bestimmten Nahrungsmittel auftreten (Boyce et al., 2010). Die Gruppe der IgE-vermittelten Nahrungsmittelallergien gehört zu den Typ-I-Allergien (Anvari et al., 2019), bei der eine IgE-vermittelte Reaktion innerhalb von einer Stunde nach Exposition gegenüber eines Allergens auftritt. Allergenspezifisches IgE bewirkt eine Freisetzung von Mediatoren wie Histamin und Leukotriene aus Mastzellen und Basophilen. Die darauffolgende Vasodilatation manifestiert sich klinisch unter anderem als Hypotension, Angioödem, Atemnot oder als lebensbedrohliche Anaphylaxie (Ashraf Uzzaman, 2012; Maker et al., 2019; Mike Kulis, Benjamin L. Wright, 2015).

Epidemiologische Angaben zur Prävalenz hängen von verschiedenen Variablen ab, beispielsweise der geografischen Region (Sicherer & Sampson, 2014; Warren et al., 2020). Insgesamt wird von einer Zunahme der Prävalenz in den letzten drei Jahrzehnten, vor allem in Industrieländern, ausgegangen (Sicherer & Sampson, 2018).

Für die Schwere der Symptome sowie die Frage, ob sensibilisierte Personen tolerant oder allergisch auf ein Allergen reagieren, ist nicht allein der IgE Titer sondern das Verhältnis von IgE zu IgG4 im Menschen entscheidend (Datema et al., 2019; Santos et al., 2015). Funktionell entspricht menschliches IgG4 murinem IgG1(Lilienthal et al., 2018).

1.2 Immunologischer Hintergrund

Immunglobuline oder Antikörper sind sekretierte B-Zell-Rezeptoren (BZR), die aus schweren und leichten Polypeptidketten aufgebaut sind (Murphy & Weaver, 2018). Mittels Pepsin kann ein Antikörper in 2 antigenbindende Fab Fragmente und ein die Antikörperklasse (IgM, IgD, IgG, IgA und IgE) bestimmendes Fc Fragment gespalten werden. Fab Fragmente bestehen aus der leichten und Anteile der schweren Kette und binden Antigene über die Antigenbindungsstelle, die für jeden B-Zellklon einzigartig ist (James, 2022; Mix et al., 2006). Effektorfunktionen der Antikörper werden ausgeführt, wenn das Fc Fragment an den Fc Rezeptor (FcR) oder den C-Typ-Lektin Rezeptor von Immunzellen bindet, beispielsweise das Fc Fragemnt von IgE an den FcεRI Rezeptor auf Mastzellen (Lu et al., 2018; Pincetic et al., 2014).

Nach Primärexposition gegenüber einem Nahrungsallergen können naive B-Zellen direkt die Antikörperklasse zu IgE oder indirekt über einen intermediären IgG1+ B-Zellstatus zu IgE wechseln. IgE+ B-Zellen differenzieren sich zu IgE sekretierenden Plasmazellen beziehungsweise können IgG1+ Gedächtniszellen sich bei Re-Exposition gegenüber einem Antigen zu IgE+ Plasmazellen entwickeln (Haase & Voehringer, 2021; Satitsuksanoa et al., 2021). Die gebildeten Antikörper unterscheiden sich in ihrer Affinität: Pathogen wirkende, hoch-affine IgE Antikörper setzen eine Keimzentrumsreaktion der B-Zellen voraus (Haase & Voehringer, 2021; Q. Chen et al., 2023; Xiong et al., 2012). Das Keimzentrum ist eine transiente Mikrostruktur, die zum Beispiel als Reaktion auf ein Pathogen in Follikeln des sekundär lymphatischen Gewebes gebildet wird (Huang, 2020a).

1.3 Experimenteller Hintergrund

Meine Forschungsgruppe analysierte in einem murinen Nahrungsmittelallergie-Modell Sequenzierungsdaten der Antigenbindungsstelle von IgG1 und IgE. Diese zeigten, dass die Bildung von IgE und IgG1 auf der Ebene individueller B-Zellklone reguliert wird (Udoye et al., 2022). Um zu untersuchen, warum individuelle B-Zellklone die Antikörperklasse zu IgE oder IgG1 wechseln, soll der Einfluss von B-Zellrezeptor (BZR)-Signalstärke und ko-stimulierenden Faktoren auf das Verhältnis von IgE und IgG1 analysiert werden.

2. Methoden

Die in vitro Experimente basieren auf einem innovativen B-Zellkultursystem, welches eine T-Zell abhängige Keimzentrumsreaktion imitiert. BALB/c3T3 Fibroblasten, welche mit Oberflächenmarker von T-Zellen (CD40L, BAFF) transfiziert sind, bilden die Interaktion von B- und T-Zellen nach (Haniuda & Kitamura, 2019; Nojima et al., 2011). B-Zellen wurden aus Milzen von BALB/c Mäusen isoliert, mit dem Zytokin IL-4 und verschiedenen Konzentrationen von anti-Ig $F(ab')_2$ Fragmenten stimuliert und in der Zellkultur für drei bis vier Tage kultiviert. Danach wurde mittels Durchflusszytometrie die Expression und mittels ELISA die Sekretion von IgE und IgG1 analysiert. Um die Art des Klassenwechsels beurteilen zu können, wurde eine semiquantitative Analyse der „switch circles“, die entsprechend des Ziel-Immunoglobulins aus dem Gen deletiert werden, durchgeführt.

3. Ergebnisse

3.2 Stimulation des B-Zellrezeptors

Durchflusszytometrieanalysen mit dem LSR II von B-Zellen, die mit steigenden Konzentrationen von anti-IgM oder anti-Ig kappa $F(ab')_2$ Fragmenten (0-1-2-4-8 µg/ml) stimuliert wurden, zeigten einen dosisabhängigen steigenden Calciumfluss. Daher können

unterschiedliche Konzentrationen dieser F(ab')$_2$ Fragmente als ein Modell für quantitativ unterschiedliche BZR- Signalstärken genutzt werden.

Um den Einfluss der BZR-Signalstärke auf das Verhältnis von IgE und IgG1 zu überprüfen, wurden B-Zellen in der Keimzentrums-Zellkultur mit IL-4 und anti-IgM oder anti-Ig kappa F(ab')$_2$ Fragmenten (0-1-2-4-8 µg/ml) stimuliert und vier Tage in der Kultur belassen. Fluoreszenz-Durchflusszytometrie von angefärbten IgE+ und IgG1+ B-Zellen und Plasmablasten zeigte eine Abnahme der Frequenz dieser Zellen in Abhängigkeit von der Stimulation mit den zwei Fragmenten. Das Verhältnis von IgE+ und IgG1+ B-Zellen verminderte sich mit Zunahme der BZR- Signalstärke, welches für die Stimulation des BZR mit anti-IgM- und anti-Ig kappa F(ab')$_2$ Fragmenten ähnlich war. ELISA Experimente der Überstände der mit anti-Ig kappa F(ab')$_2$ Fragmenten stimulierten Zellkulturen zeigten eine konzentrationsabhängige Abnahme von IgE und IgG1.

Um festzustellen, ob die selektive Inhibition von IgE im Vergleich zu IgG1 auf einen inhibierten Klassenwechsel zurückzuführen ist, wurde eine semiquantitative Analyse von „switch circles" aus dem direkten und indirekten Klassenwechsel zu IgE durchgeführt. „Switch circles" des direkten Klassenwechsels waren am Tag drei der Keimzentrums-Zellkultur nicht detektierbar. Demgegenüber nahm die integrierte Dichte der Banden der „switch circles" des indirekten Klassenwechsels zu IgE im Vergleich zum Kontrollgen durch die Stimulation mit den F(ab')$_2$ Fragmenten ab.

3.3 Einfluss von ko-stimulierenden Faktoren

Stimulation der Keimzentrum-Zellkultur mit ansteigenden Konzentrationen von IL-4 (0,5 ng/ml bis 8 ng/ml) resultierte in einen Anstieg der Frequenzen und des Verhältnisses von IgE zu IgG1. Ebenso führten steigende Glucose-Konzentrationen (50 mg/dL bis 300 mg/dL) in der Keimzentrums-Zellkultur mit und ohne zusätzliche Stimulation mit anti-Ig kappa F(ab')$_2$ Fragmenten zu einem zugunsten zu IgE verschobenen IgE/IgG1. Dabei war die mit 2-NBDG, einem fluoreszierenden Glucose-Analogon, gemessene Glucose-Aufnahme ähnlich für IgE+ und IgG1+ B-Zellen.

4. Diskussion

Die Interpretation, dass IgE+ B-Zellen in unserem Zellkultursystem Produkt von indirektem Klassenwechsel sind und, dass Stimulation des BZR mit anti-Ig F(ab')$_2$ Fragmenten den Klassenwechsel zu IgE mehr als zu IgG1 inhibiert, kann mit weiteren Experimenten meiner Forschungsgruppe illustriert werden. Am vierten Tag der Keimzentrumskultur wurden IgG1+ B-Zellen FACS-gesteuert sortiert und mit IL-4 und steigenden Konzentrationen von anti-Ig kappa F(ab')$_2$ Fragmenten rekultiviert. Nach einem Tag waren 12-22% der IgG1+ Zellen IgE+, während die Frequenz von IgE+ in den mit F(ab')$_2$

Fragmenten stimulierten Zellkulturen konzentrationsabhängig abnahm (Udoye et al., 2022).

Dennoch ist die Keimzentrumskultur nicht geeignet, um den Einfluss der B-Zellrezeptorsignalstärke auf den direkten oder den Mukosa-abhängigen Klassenwechsel zu IgE außerhalb des Keimzentrums zu evaluieren, zum Beispiel ist ein lokaler Klassenwechsel von IgA2 zu IgE in der gastrointestinalen Mukosa beschrieben (Hoh et al., 2020).

5. Schlussfolgerung und Ausblick

In unserem Keimzentrumsmodell inhibierte die Stimulation des BZR mit anti-Ig $F(ab')_2$ Fragmenten selektiv mehr die Bildung von IgE+ B-Zellen und Plasmablasten als die Bildung von IgG1+ Zellen. Die Stärke der Inhibition entsprach der BZR-Signalstärke. Eine Semiquantitative Analyse der „switch circles“ zeigte, dass IgE+ B-Zellen in unserem Zellkultursystem aus indirektem Klassenwechsel (IgM→IgG1→ IgE) entstehen.

Um die Erkenntnisse zu vertiefen, wären weitere *in vitro*- und anschließend *in vivo*-Studien notwendig, um die Langzeitwirkung unterschiedlicher BZR-Signalstärken auf die IgE-Reaktion in Keimzentrums-abhängigen und -unabhängigen Umgebungen zu analysieren. Forschungsziele dieser zukünftigen Studien könnten die Untersuchung möglicher pharmazeutischer Anwendungen unterschiedlicher BZR-Signalstärken sein, die möglicherweise unterschiedliche Affinitäten oder Aviditäten des BZR gegenüber dem Antigen darstellen und in bisher nur temporär wirkenden Desensibilisierungstherapien eingesetzt werden können.

Ferner beeinflussten IL-4 und verschiedene Glucose-Konzentrationen das Verhältnis von IgE/IgG1. Zusammengefasst zeigen diese Ergebnisse, dass komplexe B-Zell-extrinsische Umweltstimuli auf verschiedene Weise die Bildung von IgG1+ vs. IgE+ Zellen beeinflussen, obwohl Th2-Zytokine, vor allem IL-4, den Klassenwechsel zu beiden Immunoglobulinen fördern.

9. Appendix

9.1 Figures

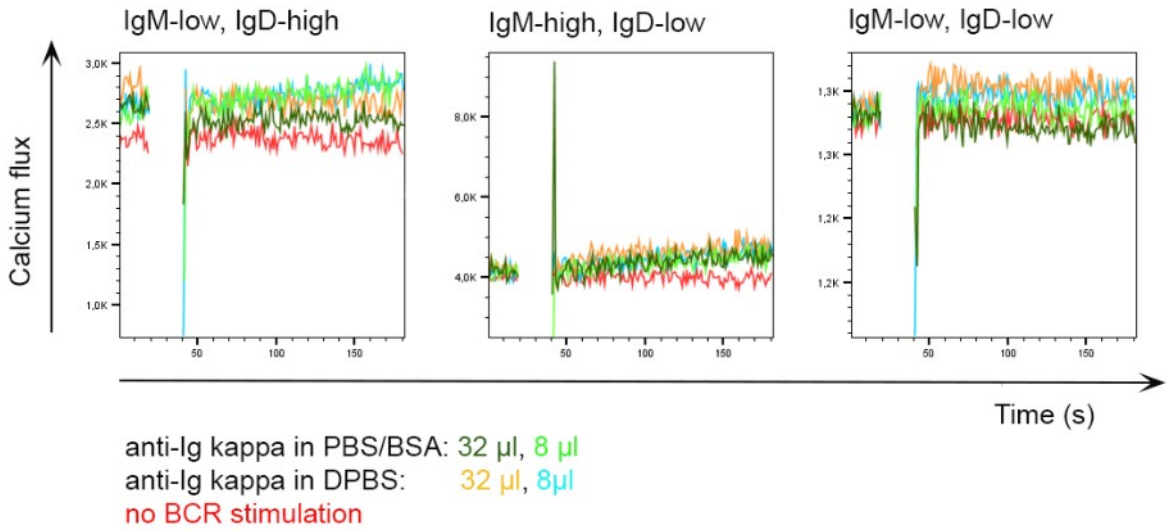

Figure S1: Purified anti Ig F(ab')$_2$ fragments did not induce a calcium flux.
Single cell suspensions were generated from spleen and stained for IgM and IgD. Subsequent to the incubation with CalbryteTM 520 AM, polyclonal and purified anti Ig kappa F(ab')2 fragments (0-8-32 µl) were added to the different samples and the calcium flux was immediately measured by flow cytometry (LSRII). Representative FACS data from IgMhigh/IgDlow naive B cells, IgMhigh/IgDlow marginal zone B cells and IgM-/IgD-negative splenic cells.

9.2 Descriptive statistics

9.2.1 Statistics fig. 22: Anti-Ig F(ab')$_2$ fragment induced calcium flux

anti-IgM F(ab`)$_2$ fragments: IgD-high

Friedman test: p-value = 0.0004994

Descriptive statistics											
	n	mean	sd	median	mad	min	max	range	skew	kurtosis	se	IQR
0 µg/ml	5	469,731.400	67,364.110	465,000	20,756.400	386,657	574,000	187,343	0.362	-1.388	30,126.150	21,000
1 µg/ml	5	536,600	108,527.900	523,000	11,860.800	409,000	710,000	301,000	0.489	-1.314	48,535.140	11,000
2 µg/ml	5	567,800	119,857.000	548,000	40,030.200	431,000	759,000	328,000	0.505	-1.362	53,601.680	49,000
4 µg/ml	5	636,800	141,514.000	627,000	97,851.600	476,000	855,000	379,000	0.411	-1.519	63,286.960	104,000
8 µg/ml	5	695,600	131,595.200	654,000	108,229.800	549,000	902,000	353,000	0.481	-1.475	58,851.170	81,000

	Wilcoxon-signed-Rank-Test, correction method: Holm
0-8 µg/ml	p.value = 0.0431144467830754; r= 0.904534
0-4 µg/ml	p.value = 0.0431144467830754; r= 0.904534
0-2 µg/ml	p.value = 0.0431144467830754; r= 0.904534
0-1 µg/ml	p.value = 0.0431144467830754; r= 0.904534
1-8 µg/ml	p.value = 0.0431144467830754; r= 0.904534
1-4 µg/ml	p.value = 0.0431144467830754; r= 0.904534
1-2 µg/ml	p.value = 0.042168197097156; r= 0.9086738

2-8 µg/ml	p.value = 0.0431144467830754; r= 0.904534
2-4 µg/ml	p.value = 0.0431144467830754; r= 0.904534
4-8 µg/ml	p.value = 0.0431144467830754; r= 0.904534

anti-IgM F(ab`)$_2$ fragments: IgM-high

Friedman test: p-value = 0.0006677

Descriptive statistics												
	n	mean	sd	median	mad	min	max	range	skew	kurtosis	se	IQR
0 µg/ml	5	553,800	70,357.660	528,000	83,025.600	472,000	656,000	184,000	0.298	-1.724	31,464.900	63,000
1 µg/ml	5	1,090,600	241,447.300	1,090,000	133,434	723,000	1,390,000	667,000	-0.314	-1.449	107,978.500	110,000
2 µg/ml	5	1,257,000	273,349.600	1,270,000	74,130	855,000	1,620,000	765,000	-0.166	-1.442	122,245.700	100,000
4 µg/ml	5	1,428,200	320,306.400	1,470,000	207,564	981,000	1,870,000	889,000	-0.023	-1.514	143,245.400	160,000
8 µg/ml	5	1,522,000	270,776.700	1,480,000	177,912	1,160,000	1,910,000	750,000	0.112	-1.516	121,095.000	140,000

	Wilcoxon-signed-Rank-Test, correction method: Holm
0-8 µg/ml	p.value = 0.0431144467830754; r= 0.904534
0-4 µg/ml	p.value = 0.0431144467830754; r= 0.904534
0-2 µg/ml	p.value = 0.0431144467830754; r= 0.904534
0-1 µg/ml	p.value = 0.0431144467830754; r= 0.904534
1-8 µg/ml	p.value = 0.0431144467830754; r= 0.904534
1-4 µg/ml	p.value = 0.0431144467830754; r= 0.904534
1-2 µg/ml	p.value = 0.0431144467830754; r= 0.904534
2-8 µg/ml	p.value = 0.0431144467830754; r= 0.904534
2-4 µg/ml	p.value = 0.0431144467830754; r= 0.904534
4-8 µg/ml	p.value = 0.0796158014601134; r= 0.7839295

anti-IgM F(ab`)$_2$ fragments: IgD-low, IgM-low

Friedman test: p-value = 0.05817

Descriptive statistics												
	n	mean	sd	median	mad	min	max	range	skew	kurtosis	se	IQR
0 µg/ml	5	168,592.600	24,495.520	162,165	14,149.930	148,766	209,943	61,177	0.797	-1.253	10,954.730	16,847
1 µg/ml	5	183,241.400	28,417.020	176,829	7,498.991	156,563	231,530	74,967	0.800	-1.171	12,708.480	7,743
2 µg/ml	5	179,583.400	27,352.210	168,534	12,548.730	157,760	226,968	69,208	0.908	-1.105	12,232.280	9,341
4 µg/ml	5	177,980.400	24,105.560	172,920	5,522.685	155,514	219,131	63,617	0.820	-1.146	10,780.330	3,947
8 µg/ml	5	174,273.400	20,629.700	165,954	10,855.600	158,632	209,944	51,312	0.905	-1.126	9,225.884	9,749

anti-Ig kappa F(ab`)$_2$ fragments: IgD-high

Friedman test: p-value = 0.1468

Descriptive statistics												
	n	mean	sd	median	mad	min	max	range	skew	kurtosis	se	IQR

0 µg/ml	2	416,828.500	42,668.940	416,828.500	44,732.270	386,657	447,000	60,343	0	-2.750	30,171.500	30,171.500
1 µg/ml	2	491,000	66,468.040	491,000	69,682.200	444,000	538,000	94,000	0	-2.750	47,000	47,000
2 µg/ml	2	533,500	57,275.650	533,500	60,045.300	493,000	574,000	81,000	0	-2.750	40,500	40,500
4 µg/ml	2	546,500	51,618.790	546,500	54,114.900	510,000	583,000	73,000	0	-2.750	36,500	36,500
8 µg/ml	2	554,500	23,334.520	554,500	24,462.900	538,000	571,000	33,000	0	-2.750	16,500	16,500

anti-Ig kappa F(ab`)$_2$ fragments: IgM-high

Friedman test: p-value = 0.09158

Descriptive statistics												
	n	mean	sd	median	mad	min	max	range	skew	kurtosis	se	IQR
0 µg/ml	2	508,000	50,911.690	508,000	53,373.600	472,000	544,000	72,000	0	-2.750	36,000	36,000
1 µg/ml	2	608,500	62,932.500	608,500	65,975.700	564,000	653,000	89,000	0	-2.750	44,500	44,500
2 µg/ml	2	667,000	63,639.610	667,000	66,717	622,000	712,000	90,000	0	-2.750	45,000	45,000
4 µg/ml	2	712,500	55,861.440	712,500	58,562.700	673,000	752,000	79,000	0	-2.750	39,500	39,500
8 µg/ml	2	761,500	19,091.880	761,500	20,015.100	748,000	775,000	27,000	0	-2.750	13,500	13,500

anti-Ig kappa F(ab`)$_2$ fragments: IgD-low, IgM-low

Friedman test: p-value = 0.1074

Descriptive statistics												
	n	mean	sd	median	mad	min	max	range	skew	kurtosis	se	IQR
0 µg/ml	2	179,593	14,318.910	179,593	15,011.330	169,468	189,718	20,250	0	-2.750	10,125	10,125
1 µg/ml	2	187,964.500	25,093.100	187,964.500	26,306.510	170,221	205,708	35,487	0	-2.750	17,743.500	17,743.500
2 µg/ml	2	189,689.500	24,814.500	189,689.500	26,014.440	172,143	207,236	35,093	0	-2.750	17,546.500	17,546.500
4 µg/ml	2	185,287.500	22,322.650	185,287.500	23,402.100	169,503	201,072	31,569	0	-2.750	15,784.500	15,784.500
8 µg/ml	2	183,077	22,853.690	183,077	23,958.820	166,917	199,237	32,320	0	-2.750	16,160	16,160

9.2.2 Statistics fig. 10: BCR signaling alters the frequency and the ratio of IgE and IgG1 class switched cells

IgE/IgG1 among B cells

Friedman test: p-value = 1.435x 10^{-5}

Descriptive statistics												
	n	mean	sd	median	mad	min	max	range	skew	kurtosis	se	IQR
0 µg/ml	8	0.129	0.034	0.119	0.018	0.082	0.200	0.117	0.792	-0.154	0.012	0.024
1 µg/ml	8	0.058	0.014	0.057	0.017	0.037	0.082	0.045	0.064	-1.305	0.005	0.016
2 µg/ml	8	0.053	0.009	0.055	0.007	0.032	0.062	0.029	-1.130	0.055	0.003	0.008
4 µg/ml	8	0.047	0.004	0.047	0.002	0.040	0.054	0.014	0.053	-0.508	0.001	0.002
8 µg/ml	8	0.036	0.006	0.038	0.005	0.027	0.044	0.017	-0.439	-1.477	0.002	0.007

	Wilcoxon-signed-Rank-Test, correction method: Holm
0-8 µg/ml	p.value = 0.0117186855997686; r= 0.8911328
0-4 µg/ml	p.value = 0.0117186855997686; r= 0.8911328
0-2 µg/ml	p.value = 0.0117186855997686; r= 0.8911328
0-1 µg/ml	p.value = 0.0117186855997686; r= 0.8911328
1-8 µg/ml	p.value = 0.0117186855997686; r= 0.8911328
1-4 µg/ml	p.value = 0.0928919408837053; r= 0.5940885
1-2 µg/ml	p.value = 0.262618290442521; r= 0.396059
2-8 µg/ml	p.value = 0.0117186855997686; r= 0.8911328
2-4 µg/ml	p.value = 0.161429462367083; r= 0.4950738
4-8 µg/ml	p.value = 0.0117186855997686; r= 0.8911328

IgE/IgG1 among plasmablasts

Friedman test: p-value = 7.283×10^{-5}

Descriptive statistics												
	n	mean	sd	median	mad	min	max	range	skew	kurtosis	se	IQR
0 µg/ml	8	0.625	0.190	0.611	0.230	0.406	0.901	0.495	0.305	-1.655	0.067	0.262
1 µg/ml	8	0.146	0.051	0.149	0.032	0.082	0.248	0.165	0.665	-0.507	0.018	0.044
2 µg/ml	8	0.109	0.059	0.100	0.031	0.058	0.247	0.189	1.456	0.819	0.021	0.033
4 µg/ml	8	0.152	0.079	0.131	0.071	0.036	0.279	0.243	0.230	-1.368	0.028	0.098
8 µg/ml	8	0.078	0.033	0.081	0.031	0.041	0.138	0.097	0.391	-1.147	0.012	0.042

	Wilcoxon-signed-Rank-Test, correction method: Holm
0-8 µg/ml	p.value = 0.0117186855997686; r= 0.8911328
0-4 µg/ml	p.value = 0.0117186855997686; r= 0.8911328
0-2 µg/ml	p.value = 0.0117186855997686; r= 0.8911328
0-1 µg/ml	p.value = 0.0117186855997686; r= 0.8911328
1-8 µg/ml	p.value = 0.0117186855997686; r= 0.8911328
1-4 µg/ml	p.value = 1; r= 0
1-2 µg/ml	p.value = 0.161429462367083; r= 0.4950738
2-8 µg/ml	p.value = 0.207578442335624; r= 0.4455664
2-4 µg/ml	p.value = 0.0928919408837053; r= 0.5940885
4-8 µg/ml	p.value = 0.0687035743228782; r= 0.6435959

IgE frequency among B cells

Friedman test: p-value = 7.119×10^{-6}

Descriptive statistics												
	n	mean	sd	median	mad	min	max	range	skew	kurtosis	se	IQR
0 µg/ml	8	4.428	1.415	4.390	0.400	2.380	7.330	4.950	0.642	-0.188	0.500	0.562
1 µg/ml	8	1.151	0.480	1.215	0.660	0.420	1.790	1.370	-0.062	-1.544	0.170	0.603
2 µg/ml	8	0.797	0.322	0.785	0.311	0.340	1.310	0.970	0.136	-1.383	0.114	0.310
4 µg/ml	8	0.564	0.165	0.570	0.170	0.270	0.780	0.510	-0.350	-1.238	0.058	0.225
8 µg/ml	8	0.300	0.077	0.305	0.096	0.200	0.410	0.210	0.017	-1.694	0.027	0.110

	Wilcoxon-signed-Rank-Test, correction method: Holm
0-8 µg/ml	p.value = 0.0117186855997686; r= 0.8911328
0-4 µg/ml	p.value = 0.0117186855997686; r= 0.8911328
0-2 µg/ml	p.value = 0.0116160448992625; r= 0.8922269
0-1 µg/ml	p.value = 0.0117186855997686; r= 0.8911328
1-8 µg/ml	p.value = 0.0117186855997686; r= 0.8911328
1-4 µg/ml	p.value = 0.0250618443438836; r= 0.792118
1-2 µg/ml	p.value = 0.0356919001168044; r= 0.7426107

2-8 µg/ml	p.value = 0.0117186855997686; r= 0.8911328
2-4 µg/ml	p.value = 0.0687035743228782; r= 0.6435959
4-8 µg/ml	p.value = 0.0117186855997686; r= 0.8911328

IgE frequency among plasmablasts

Friedman test: p-value = 8.365×10^{-5}

Descriptive statistics												
	n	mean	sd	median	mad	min	max	range	skew	kurtosis	se	IQR
0 µg/ml	8	9.742	2.927	9.635	3.996	5.150	13.100	7.950	-0.150	-1.676	1.035	5.090
1 µg/ml	8	1.288	0.705	0.955	0.319	0.740	2.410	1.670	0.689	-1.466	0.249	0.890
2 µg/ml	8	0.695	0.346	0.600	0.215	0.330	1.430	1.100	1.012	-0.223	0.122	0.275
4 µg/ml	8	0.860	0.388	0.945	0.326	0.250	1.360	1.110	-0.375	-1.495	0.137	0.485
8 µg/ml	8	0.410	0.208	0.355	0.141	0.210	0.810	0.600	0.800	-0.943	0.074	0.178

	Wilcoxon-signed-Rank-Test, correction method: Holm
0-8 µg/ml	p.value = 0.0117186855997686; r= 0.8911328
0-4 µg/ml	p.value = 0.0117186855997686; r= 0.8911328
0-2 µg/ml	p.value = 0.0117186855997686; r= 0.8911328
0-1 µg/ml	p.value = 0.0117186855997686; r= 0.8911328
1-8 µg/ml	p.value = 0.0117186855997686; r= 0.8911328
1-4 µg/ml	p.value = 0.262618290442521; r= 0.396059
1-2 µg/ml	p.value = 0.0499499764547464; r= 0.6931033
2-8 µg/ml	p.value = 0.0356919001168044; r= 0.7426107
2-4 µg/ml	p.value = 0.262618290442521; r= 0.396059
4-8 µg/ml	p.value = 0.0499499764547464; r= 0.6931033

IgG1 frequency among B cells

Friedman test: p-value = 5.129×10^{-6}

Descriptive statistics												
	n	mean	sd	median	mad	min	max	range	skew	kurtosis	se	IQR
0 µg/ml	8	33.925	3.868	34.850	3.707	28.600	39.200	10.600	-0.205	-1.681	1.368	5.625
1 µg/ml	8	19.250	5.996	19.100	4.077	11.300	30.600	19.300	0.411	-0.821	2.120	5.525
2 µg/ml	8	14.715	4.187	14.950	4.077	8.820	22	13.180	0.249	-1.161	1.480	3.900
4 µg/ml	8	11.969	2.997	12.500	3.039	6.830	16.600	9.770	-0.176	-1.118	1.060	3.320
8 µg/ml	8	8.236	1.506	8.115	1.727	5.780	10.400	4.620	-0.111	-1.397	0.532	1.995

	Wilcoxon-signed-Rank-Test, correction method: Holm
0-8 µg/ml	p.value = 0.0117186855997686; r= 0.8911328
0-4 µg/ml	p.value = 0.0117186855997686; r= 0.8911328
0-2 µg/ml	p.value = 0.0117186855997686; r= 0.8911328
0-1 µg/ml	p.value = 0.0117186855997686; r= 0.8911328
1-8 µg/ml	p.value = 0.0117186855997686; r= 0.8911328
1-4 µg/ml	p.value = 0.0172902805929063; r= 0.8416254
1-2 µg/ml	p.value = 0.0117186855997686; r= 0.8911328
2-8 µg/ml	p.value = 0.0117186855997686; r= 0.8911328
2-4 µg/ml	p.value = 0.0687035743228782; r= 0.6435959
4-8 µg/ml	p.value = 0.0117186855997686; r= 0.8911328

IgG1 frequency among plasmablasts

Friedman test: p-value = 6.34×10^{-5}

Descriptive statistics												
	n	mean	sd	median	mad	min	max	range	skew	kurtosis	se	IQR
0 µg/ml	8	15.863	3.476	15.450	4.448	11.100	20.100	9	0.022	-1.879	1.229	5.700
1 µg/ml	8	8.650	2.840	8.670	2.172	4.940	14.200	9.260	0.562	-0.717	1.004	3.015
2 µg/ml	8	6.595	1.759	5.945	0.726	4.900	9.740	4.840	0.814	-1.178	0.622	1.367
4 µg/ml	8	5.976	1.627	6.345	1.661	3.680	8.440	4.760	-0.059	-1.575	0.575	2.240
8 µg/ml	8	5.215	0.870	5.270	0.615	3.770	6.580	2.810	-0.168	-1.110	0.308	0.658

	Wilcoxon-signed-Rank-Test, correction method: Holm

0-8 µg/ml	p.value = 0.0117186855997686; r= 0.8911328
0-4 µg/ml	p.value = 0.0117186855997686; r= 0.8911328
0-2 µg/ml	p.value = 0.0117186855997686; r= 0.8911328
0-1 µg/ml	p.value = 0.0117186855997686; r= 0.8911328
1-8 µg/ml	p.value = 0.0117186855997686; r= 0.8911328
1-4 µg/ml	p.value = 0.0172902805929063; r= 0.8416254
1-2 µg/ml	p.value = 0.0356919001168044; r= 0.7426107
2-8 µg/ml	p.value = 0.0250618443438836; r= 0.792118
2-4 µg/ml	p.value = 0.123485272144549; r= 0.5445811
4-8 µg/ml	p.value = 0.123485272144549; r= 0.5445811

Number of all counted cells

Friedman test: p-value = 0.008098

Descriptive statistics												
	n	mean	sd	median	mad	min	max	range	skew	kurtosis	se	IQR
0 µg/ml	8	322.500	81.766	317.500	51.891	245	500	255	1.043	-0.007	28.909	70
1 µg/ml	8	250	51.893	262.500	37.065	170	320	150	-0.384	-1.414	18.347	53.750
2 µg/ml	8	220	49.642	205	48.184	170	295	125	0.412	-1.703	17.551	68.750
4 µg/ml	8	261.250	65.233	252.500	29.652	205	410	205	1.306	0.525	23.063	42.500
8 µg/ml	8	222.500	55.162	222.500	59.304	150	315	165	0.219	-1.439	19.503	82.500

	Wilcoxon-signed-Rank-Test, correction method: Holm
0-8 µg/ml	p.value = 0.0250618443438836; r= 0.792118
0-4 µg/ml	p.value = 0.14932461032049; r= 0.5097961
0-2 µg/ml	p.value = 0.0117186855997686; r= 0.8911328
0-1 µg/ml	p.value = 0.0356919001168044; r= 0.7426107
1-8 µg/ml	p.value = 0.0924914701126299; r= 0.5948179
1-4 µg/ml	p.value = 0.94411409557764; r= 0.02478408
1-2 µg/ml	p.value = 0.262618290442521; r= 0.396059
2-8 µg/ml	p.value = 0.94411409557764; r= 0.02478408
2-4 µg/ml	p.value = 0.067685673432768; r= 0.6459752
4-8 µg/ml	p.value = 0.207578442335624; r= 0.4455664

Number of counted IgE+ B cells

Friedman test: p-value = 1.435×10^{-5}

Descriptive statistics												
	n	mean	sd	median	mad	min	max	range	skew	kurtosis	se	IQR
0 µg/ml	8	17,973.330	9,794.271	15,641.820	4,748.067	9,200.253	40,497.240	31,296.980	1.380	0.609	3,462.798	5,031.682
1 µg/ml	8	3,480.408	1,529.807	3,758.421	1,936.262	1,519.737	5,221.607	3,701.870	-0.172	-1.936	540.868	2,862.737
2 µg/ml	8	2,043.962	500.160	2,130.008	682.373	1,412.058	2,605.263	1,193.206	-0.167	-1.908	176.833	908.644
4 µg/ml	8	1,808.820	404.405	1,686.039	220.726	1,433.780	2,600	1,166.220	0.899	-0.848	142.979	312.599
8 µg/ml	8	861.345	304.532	863.336	320.164	414.129	1,365.854	951.725	0.160	-1.322	107.668	332.884

	Wilcoxon-signed-Rank-Test, correction method: Holm
0-8 µg/ml	p.value = 0.0117186855997686; r= 0.8911328
0-4 µg/ml	p.value = 0.0117186855997686; r= 0.8911328
0-2 µg/ml	p.value = 0.0117186855997686; r= 0.8911328
0-1 µg/ml	p.value = 0.0117186855997686; r= 0.8911328
1-8 µg/ml	p.value = 0.0117186855997686; r= 0.8911328
1-4 µg/ml	p.value = 0.0499499764547464; r= 0.6931033
1-2 µg/ml	p.value = 0.0250618443438836; r= 0.792118

2-8 µg/ml	p.value = 0.0117186855997686; r= 0.8911328
2-4 µg/ml	p.value = 0.207578442335624; r= 0.4455664
4-8 µg/ml	p.value = 0.0117186855997686; r= 0.8911328

Number of counted IgG1+ B cells

Friedman test: p-value = $4.803x\ 10^{-5}$

Descriptive statistics												
	n	mean	sd	median	mad	min	max	range	skew	kurtosis	se	IQR
0 µg/ml	8	135,124.500	32,641.500	128,106.400	24,052.280	98,755.510	202,762.400	104,006.900	0.865	-0.439	11,540.510	31,059.100
1 µg/ml	8	59,057.610	19,654.200	57,923.780	24,396.380	37,719.870	86,357.830	48,637.960	0.104	-2.030	6,948.811	32,497.210
2 µg/ml	8	40,089.790	8,773.940	40,567.200	10,332.680	26,194.690	53,293.590	27,098.900	-0.060	-1.402	3,102.056	11,910.120
4 µg/ml	8	37,549.570	6,344.056	37,293.480	6,196.140	29,350.220	47,731.630	18,381.410	0.255	-1.370	2,242.962	4,849.281
8 µg/ml	8	24,516.050	7,703.211	24,924.450	6,722.639	16,348.770	39,945.300	23,596.530	0.689	-0.661	2,723.496	9,000.970

	Wilcoxon-signed-Rank-Test, correction method: Holm
0-8 µg/ml	p.value = 0.0117186855997686; r= 0.8911328
0-4 µg/ml	p.value = 0.0117186855997686; r= 0.8911328
0-2 µg/ml	p.value = 0.0117186855997686; r= 0.8911328
0-1 µg/ml	p.value = 0.0117186855997686; r= 0.8911328
1-8 µg/ml	p.value = 0.0117186855997686; r= 0.8911328
1-4 µg/ml	p.value = 0.0250618443438836; r= 0.792118
1-2 µg/ml	p.value = 0.0687035743228782; r= 0.6435959
2-8 µg/ml	p.value = 0.0172902805929063; r= 0.8416254
2-4 µg/ml	p.value = 0.674424072235294; r= 0.1485221
4-8 µg/ml	p.value = 0.0172902805929063; r= 0.8416254

9.2.3 Statistics fig.11: BCR signaling alters the frequency and the ratio of IgE and IgG1 class switched B cells in a dose-dependent manner

IgE frequency among B cells

Friedman test: p-value = 0.000247

Descriptive statistics												
	n	mean	sd	median	mad	min	max	range	skew	kurtosis	se	IQR
0 ng/ml	6	5.955	5.600	3.490	2.913	1.350	14.500	13.150	0.501	-1.792	2.286	7.900
1 ng/ml	6	5.382	3.469	5.305	3.884	1.510	9.710	8.200	0.055	-2.134	1.416	5.187
10 ng/ml	6	4.185	2.776	3.805	3.425	1.290	7.980	6.690	0.183	-1.999	1.133	4.310
100 ng/ml	6	3.273	1.887	2.950	2.194	1.230	5.470	4.240	0.124	-2.111	0.770	3.205
500 ng/ml	6	2.567	1.625	2.580	2.105	0.670	4.230	3.560	-0.033	-2.214	0.663	2.720
1000 ng/ml	6	1.805	1.022	1.790	1.282	0.560	2.980	2.420	-0.018	-2.120	0.417	1.612

	Wilcoxon-signed-Rank-Test, correction method: Holm
0-1000 ng/ml	p.value = 0.0277078493580799; r= 0.898717
0-500 ng/ml	p.value = 0.0277078493580799; r= 0.898717
0-100 ng/ml	p.value = 0.463071015014588; r= 0.2995723
0-10 ng/ml	p.value = 0.500184257070794; r= 0.2752409
0-1 ng/ml	p.value = 0.916511907863894; r= 0.04279605
1-1000 ng/ml	p.value = 0.0277078493580799; r= 0.898717
1-500 ng/ml	p.value = 0.0277078493580799; r= 0.898717
1-100 ng/ml	p.value = 0.0277078493580799; r= 0.898717
1-10 ng/ml	p.value = 0.0463994618709046; r= 0.8131249
10-1000 ng/ml	p.value = 0.0277078493580799; r= 0.898717

10-500 ng/ml	p.value = 0.0277078493580799; r= 0.898717
10-100 ng/ml	p.value = 0.248863874937922; r= 0.4707565
100-1000 ng/ml	p.value = 0.0277078493580799; r= 0.898717
100-500 ng/ml	p.value = 0.0463994618709046; r= 0.8131249
500-1000 ng/ml	p.value = 0.0277078493580799; r= 0.898717

IgG1 frequency among B cells

Friedman test: p-value = 0.001237

Descriptive statistics												
	n	mean	sd	median	mad	min	max	range	skew	kurtosis	se	IQR
0 ng/ml	6	30.317	4.179	29.500	4.300	25.500	36.800	11.300	0.341	-1.649	1.706	5.050
1 ng/ml	6	31.883	5.065	30.750	5.560	25.500	38.400	12.900	0.181	-1.853	2.068	6.950
10 ng/ml	6	32.233	6.838	33.100	7.932	24	38.500	14.500	-0.078	-2.206	2.792	11.625
100 ng/ml	6	31.267	6.639	31.100	8.525	22.700	38.800	16.100	-0.044	-2.035	2.710	10.325
500 ng/ml	6	27.050	6.923	28.200	7.561	17.800	33.600	15.800	-0.162	-2.086	2.826	10.925
1000ng/ml	6	24.383	5.221	24.900	6.449	17.500	29.300	11.800	-0.133	-2.109	2.131	8.325

	Wilcoxon-signed-Rank-Test, correction method: Holm
0-1000 ng/ml	p.value = 0.0277078493580799; r= 0.898717
0-500 ng/ml	p.value = 0.11585149752593; r= 0.6419407
0-100 ng/ml	p.value = 0.753152364765915; r= 0.1283881
0-10 ng/ml	p.value = 0.345447530469226; r= 0.3851644
0-1 ng/ml	p.value = 0.0431144467830754; r= 0.8257228
1-1000 ng/ml	p.value = 0.0277078493580799; r= 0.898717
1-500 ng/ml	p.value = 0.0463994618709046; r= 0.8131249
1-100 ng/ml	p.value = 0.345447530469226; r= 0.3851644
1-10 ng/ml	p.value = 0.753152364765915; r= 0.1283881
10-1000 ng/ml	p.value = 0.027281171477618; r= 0.9011963
10-500 ng/ml	p.value = 0.0277078493580799; r= 0.898717
10-100 ng/ml	p.value = 0.248863874937922; r= 0.4707565
100-1000 ng/ml	p.value = 0.027281171477618; r= 0.9011963
100-500 ng/ml	p.value = 0.0277078493580799; r= 0.898717
500-1000 ng/ml	p.value = 0.0277078493580799; r= 0.898717

IgE/ IgG1 among B cells

Friedman test: p-value = 0.0005459

Descriptive statistics												
	n	mean	sd	median	mad	min	max	range	skew	kurtosis	se	IQR
0 ng/ml	6	0.185	0.169	0.110	0.078	0.053	0.469	0.416	0.659	-1.463	0.069	0.202
1 ng/ml	6	0.161	0.096	0.151	0.092	0.059	0.310	0.251	0.330	-1.727	0.039	0.119
10 ng/ml	6	0.120	0.062	0.111	0.077	0.054	0.207	0.154	0.225	-1.899	0.025	0.091
100 ng/ml	6	0.099	0.043	0.086	0.039	0.054	0.159	0.104	0.308	-1.936	0.018	0.065
500 ng/ml	6	0.087	0.040	0.089	0.053	0.038	0.129	0.091	-0.066	-2.126	0.016	0.065
1000ng/ml	6	0.069	0.028	0.071	0.035	0.032	0.102	0.070	-0.095	-2.002	0.011	0.042

	Wilcoxon-signed-Rank-Test, correction method: Holm
0-1000 ng/ml	p.value = 0.0277078493580799; r= 0.898717
0-500 ng/ml	p.value = 0.0463994618709046; r= 0.8131249
0-100 ng/ml	p.value = 0.172954917988421; r= 0.5563486
0-10 ng/ml	p.value = 0.463071015014588; r= 0.2995723
0-1 ng/ml	p.value = 0.916511907863894; r= 0.04279605
1-1000 ng/ml	p.value = 0.0277078493580799; r= 0.898717
1-500 ng/ml	p.value = 0.0277078493580799; r= 0.898717
1-100 ng/ml	p.value = 0.0277078493580799; r= 0.898717
1-10 ng/ml	p.value = 0.0277078493580799; r= 0.898717
10-1000 ng/ml	p.value = 0.0277078493580799; r= 0.898717
10-500 ng/ml	p.value = 0.0463994618709046; r= 0.8131249
10-100 ng/ml	p.value = 0.345447530469226; r= 0.3851644

100-1000 ng/ml	p.value = 0.0277078493580799; r= 0.898717
100-500 ng/ml	p.value = 0.172954917988421; r= 0.5563486
500-1000 ng/ml	p.value = 0.0277078493580799; r= 0.898717

9.2.4 Statistics fig. 12: BCR signaling alters the frequency and the ratio of IgE and IgG1 class switched cells

IgE frequency among B cells

Friedman test: p-value = 0.0003307

Descriptive statistics												
	n	mean	sd	median	mad	min	max	range	skew	kurtosis	se	IQR
0 µg/ml	8	4.610	4.005	3.440	1.149	1.590	14.200	12.610	1.626	1.168	1.416	1.368
1 µg/ml	8	2.160	0.824	2.010	0.904	1.250	3.380	2.130	0.322	-1.685	0.291	1.178
2 µg/ml	8	1.695	0.711	1.430	0.445	1.130	3.100	1.970	0.874	-0.842	0.252	0.733
4 µg/ml	8	0.854	0.171	0.915	0.096	0.590	1.040	0.450	-0.664	-1.367	0.061	0.153

	Wilcoxon-signed-Rank-Test, correction method: Holm
0-4 µg/ml	p.value = 0.0117186855997686; r= 0.8911328
0-2 µg/ml	p.value = 0.0356919001168044; r= 0.7426107
0-1 µg/ml	p.value = 0.0499499764547464; r= 0.6931033
1-4 µg/ml	p.value = 0.0117186855997686; r= 0.8911328
1-2 µg/ml	p.value = 0.0117186855997686; r= 0.8911328
2-4 µg/ml	p.value = 0.0117186855997686; r= 0.8911328

IgG1 frequency among B cells

Friedman test: p-value = 8.465×10^{-5}

Descriptive statistics												
	n	mean	sd	median	mad	min	max	range	skew	kurtosis	se	IQR
0 µg/ml	8	32.350	4.308	32.450	2.817	24.700	39.700	15	-0.085	-0.661	1.523	3.325
1 µg/ml	8	27.663	5.495	28.850	4.744	20.900	38.300	17.400	0.525	-0.819	1.943	6.200
2 µg/ml	8	24.512	6.188	22.550	3.855	19.600	37.900	18.300	1.131	-0.116	2.188	5.575
4 µg/ml	8	15.350	4.584	15.650	6.301	10.300	22	11.700	0.063	-1.850	1.621	8.350

	Wilcoxon-signed-Rank-Test, correction method: Holm
0-4 µg/ml	p.value = 0.0117186855997686; r= 0.8911328
0-2 µg/ml	p.value = 0.0179604775260788; r= 0.83666
0-1 µg/ml	p.value = 0.0928919408837053; r= 0.5940885
1-4 µg/ml	p.value = 0.0117186855997686; r= 0.8911328
1-2 µg/ml	p.value = 0.0117186855997686; r= 0.8911328
2-4 µg/ml	p.value = 0.0117186855997686; r= 0.8911328

IgE/IgG1 among B cells

Friedman rank sum test: p-value = 0.00521

Descriptive statistics												
	n	mean	sd	median	mad	min	max	range	skew	kurtosis	se	IQR
0 µg/ml	8	0.143	0.131	0.106	0.051	0.062	0.460	0.398	1.672	1.260	0.046	0.054
1 µg/ml	8	0.074	0.018	0.072	0.016	0.053	0.109	0.057	0.678	-0.739	0.006	0.020
2 µg/ml	8	0.064	0.012	0.063	0.013	0.048	0.082	0.034	0.209	-1.626	0.004	0.017
4 µg/ml	8	0.054	0.011	0.054	0.010	0.040	0.075	0.035	0.511	-0.901	0.004	0.011

	Wilcoxon-signed-Rank-Test, correction method: Holm
0-4 µg/ml	p.value = 0.0117186855997686; r= 0.8911328
0-2 µg/ml	p.value = 0.0356919001168044; r= 0.7426107
0-1 µg/ml	p.value = 0.0499499764547464; r= 0.6931033
1-4 µg/ml	p.value = 0.0687035743228782; r= 0.6435959
1-2 µg/ml	p.value = 0.0499499764547464; r= 0.6931033

2-4 µg/ml	p.value = 0.161429462367083; r= 0.4950738

IgE frequency among plasmablasts

Friedman rank sum test: p-value = 0.1357

Descriptive statistics												
	n	mean	sd	median	mad	min	max	range	skew	kurtosis	se	IQR
0 µg/ml	8	10.092	6.697	7.505	2.661	5.630	25.800	20.170	1.507	0.846	2.368	4.520
1 µg/ml	8	6.126	2.060	6.760	2.113	2.460	8.350	5.890	-0.502	-1.370	0.728	2.825
2 µg/ml	8	4.846	1.456	4.455	1.149	3.270	7.120	3.850	0.514	-1.534	0.515	1.953
4 µg/ml	8	4.035	2.143	3.450	2.735	1.300	6.690	5.390	0.151	-1.867	0.758	3.593

IgG1 frequency among plasmablasts

Friedman rank sum test: p-value = 0.001577

Descriptive statistics												
	n	mean	sd	median	mad	min	max	range	skew	kurtosis	se	IQR
0 µg/ml	8	12.291	4.369	12.250	5.323	7.310	20.300	12.990	0.490	-1.156	1.545	5.335
1 µg/ml	8	17.050	3.738	15.950	2.446	13.800	24.500	10.700	0.927	-0.753	1.322	3.450
2 µg/ml	8	16.512	3.862	17.400	4.448	11.900	23.300	11.400	0.270	-1.305	1.365	5.175
4 µg/ml	8	12.825	4.788	13.450	6.153	5	18.900	13.900	-0.186	-1.444	1.693	6

	Wilcoxon-signed-Rank-Test, correction method: Holm
0-4 µg/ml	p.value = 0.779434528427275; r= 0.09901475
0-2 µg/ml	p.value = 0.0117186855997686; r= 0.8911328
0-1 µg/ml	p.value = 0.0117186855997686; r= 0.8911328
1-4 µg/ml	p.value = 0.0248839951339654; r= 0.7930906
1-2 µg/ml	p.value = 0.674424072235294; r= 0.1485221
2-4 µg/ml	p.value = 0.0250618443438836; r= 0.792118

IgE/IgG1 among plasmablasts

Friedman rank sum test: p-value = 0.007915

Descriptive statistics												
	n	mean	sd	median	mad	min	max	range	skew	kurtosis	se	IQR
0 µg/ml	8	0.836	0.468	0.701	0.156	0.460	1.940	1.480	1.523	0.929	0.166	0.145
1 µg/ml	8	0.363	0.116	0.352	0.049	0.153	0.523	0.370	-0.185	-0.927	0.041	0.073
2 µg/ml	8	0.293	0.051	0.290	0.035	0.229	0.402	0.173	0.902	-0.105	0.018	0.041
4 µg/ml	8	0.349	0.218	0.290	0.189	0.101	0.778	0.677	0.723	-0.817	0.077	0.260

	Wilcoxon-signed-Rank-Test, correction method: Holm
0-4 µg/ml	p.value = 0.0356919001168044; r= 0.7426107
0-2 µg/ml	p.value = 0.0117186855997686; r= 0.8911328
0-1 µg/ml	p.value = 0.0117186855997686; r= 0.8911328
1-4 µg/ml	p.value = 0.888637860895008; r= 0.04950738
1-2 µg/ml	p.value = 0.0687035743228782; r= 0.6435959
2-4 µg/ml	p.value = 0.575403022912754; r= 0.1980295

Number of all counted cells

Friedman rank sum test: p-value = 0.0003315

Descriptive statistics												
	n	mean	sd	median	mad	min	max	range	skew	kurtosis	se	IQR
0 µg/ml	8	299.167	89.537	282.500	101.929	153.333	405	251.667	-0.130	-1.565	31.656	141.250
1 µg/ml	8	245	61.164	230	40.771	170	367.500	197.500	0.754	-0.624	21.625	50.625
2 µg/ml	8	234.062	74.641	235	72.277	130	360	230	0.228	-1.239	26.390	60.625

4 µg/ml	8	237.500	88.186	211.250	40.771	160	442.500	282.500	1.437	0.751	31.178	51.250
8 µg/ml	8	82.500	38.661	71.250	22.239	55	172.500	117.500	1.455	0.753	13.669	27.500

	Wilcoxon-signed-Rank-Test, correction method: Holm
0-8 µg/ml	p.value = 0.0116160448992625; r= 0.8922269
0-4 µg/ml	p.value = 0.0796880256742914; r= 0.619602
0-2 µg/ml	p.value = 0.0499499764547464; r= 0.6931033
0-1 µg/ml	p.value = 0.0924914701126299; r= 0.5948179
1-8 µg/ml	p.value = 0.0117186855997686; r= 0.8911328
1-4 µg/ml	p.value = 0.674424072235294; r= 0.1485221
1-2 µg/ml	p.value = 0.362137574847986; r= 0.322193
2-8 µg/ml	p.value = 0.0116160448992625; r= 0.8922269
2-4 µg/ml	p.value = 0.888502029228298; r= 0.04956816
4-8 µg/ml	p.value = 0.0116160448992625; r= 0.8922269

Number of counted IgE+ B cells

Friedman rank sum test: p-value = 5.129×10^{-6}

Descriptive statistics												
	n	mean	sd	median	mad	min	max	range	skew	kurtosis	se	IQR
0 µg/ml	8	18,210.650	15,415.870	14,158.120	7,646.107	6,020.866	53,855.880	47,835.010	1.412	0.664	5,450.334	10,192.070
1 µg/ml	8	6,982.219	2,361.053	7,038.064	1,844.974	4,452.756	11,969.390	7,516.632	0.908	-0.242	834.758	2,053.484
2 µg/ml	8	5,314.596	1,428.440	5,273.420	1,762.345	3,625.899	7,864.943	4,239.043	0.438	-1.248	505.030	1,763.506
4 µg/ml	8	2,889.526	834.759	2,855.472	773.253	1,602.790	4,252.036	2,649.246	0.089	-1.289	295.132	976.412
8 µg/ml	8	153.256	55.916	166.109	71.990	83.279	238.318	155.039	0.045	-1.621	19.769	73.816

	Wilcoxon-signed-Rank-Test, correction method: Holm
0-8 µg/ml	p.value = 0.0117186855997686; r= 0.8911328
0-4 µg/ml	p.value = 0.0117186855997686; r= 0.8911328
0-2 µg/ml	p.value = 0.0117186855997686; r= 0.8911328
0-1 µg/ml	p.value = 0.0499499764547464; r= 0.6931033
1-8 µg/ml	p.value = 0.0117186855997686; r= 0.8911328
1-4 µg/ml	p.value = 0.0117186855997686; r= 0.8911328
1-2 µg/ml	p.value = 0.0687035743228782; r= 0.6435959
2-8 µg/ml	p.value = 0.0117186855997686; r= 0.8911328
2-4 µg/ml	p.value = 0.0117186855997686; r= 0.8911328
4-8 µg/ml	p.value = 0.0117186855997686; r= 0.8911328

Number of counted IgG1+ B cells

Friedman rank sum test: p-value = 2.753×10^{-5}

Descriptive statistics												
	n	mean	sd	median	mad	min	max	range	skew	kurtosis	se	IQR
0 µg/ml	8	132,608.400	41,773.840	126,088.900	46,099.800	65,459.110	185,070.900	119,611.700	-0.086	-1.477	14,769.280	53,440.330
1 µg/ml	8	93,826.610	13,763.890	91,715.050	6,228.241	72,614.170	116,864.000	44,249.830	0.289	-1.080	4,866.271	8,882.421
2 µg/ml	8	83,602.040	20,898.060	80,601.160	21,485.390	56,893.060	121,954.400	65,061.330	0.455	-1.133	7,388.579	26,796.960

4 µg/ml	8	54,716.140	18,364.490	52,963.200	19,573.230	33,142.440	82,283.100	49,140.670	0.334	-1.537	6,492.828	20,666.620
8 µg/ml	8	1,925.903	550.257	1,874.019	564.253	1,277.692	2,979.030	1,701.337	0.579	-0.941	194.545	688.845

	Wilcoxon-signed-Rank-Test, correction method: Holm
0-8 µg/ml	p.value = 0.0117186855997686; r= 0.8911328
0-4 µg/ml	p.value = 0.0117186855997686; r= 0.8911328
0-2 µg/ml	p.value = 0.0250618443438836; r= 0.792118
0-1 µg/ml	p.value = 0.0687035743228782; r= 0.6435959
1-8 µg/ml	p.value = 0.0117186855997686; r= 0.8911328
1-4 µg/ml	p.value = 0.0172902805929063; r= 0.8416254
1-2 µg/ml	p.value = 0.161429462367083; r= 0.4950738
2-8 µg/ml	p.value = 0.0117186855997686; r= 0.8911328
2-4 µg/ml	p.value = 0.0356919001168044; r= 0.7426107
4-8 µg/ml	p.value = 0.0117186855997686; r= 0.8911328

9.2.5 Statistics fig. 14: Frequency of apoptotic cells after BCR stimulation

Early apoptotic B cells

Friedman test: p-value = 0.02306

Descriptive Statistics												
	n	mean	sd	median	mad	min	max	range	skew	kurtosis	se	IQR
0 µg/ml	6	6.573	1.760	6.720	1.698	4.290	9.260	4.970	0.145	-1.530	0.719	1.857
1 µg/ml	6	7.477	1.991	8.125	1.720	4.950	9.670	4.720	-0.330	-1.928	0.813	2.940
2 µg/ml	6	7.575	2.370	6.965	2.394	4.980	11.100	6.120	0.365	-1.767	0.967	3.128
4 µg/ml	6	6.928	2.120	6.695	2.268	4.460	9.960	5.500	0.183	-1.876	0.866	2.843
8 µg/ml	6	5.722	0.922	5.840	1.223	4.560	6.920	2.360	-0.084	-1.852	0.376	1.303

	Wilcoxon-signed-Rank-Test, correction method: Holm
0-8 µg/ml	p.value = 0.0463994618709046; r= 0.8131249
0-4 µg/ml	p.value = 0.753152364765915; r= 0.1283881
0-2 µg/ml	p.value = 0.172954917988421; r= 0.5563486
0-1 µg/ml	p.value = 0.11585149752593; r= 0.6419407
1-8 µg/ml	p.value = 0.0277078493580799; r= 0.898717
1-4 µg/ml	p.value = 0.345447530469226; r= 0.3851644
1-2 µg/ml	p.value = 0.600179487140554; r= 0.2139802
2-8 µg/ml	p.value = 0.0277078493580799; r= 0.898717
2-4 µg/ml	p.value = 0.345447530469226; r= 0.3851644
4-8 µg/ml	p.value = 0.11585149752593; r= 0.6419407

Late apoptotic B cells

Friedman test: p-value= 0.03251

Descriptive statistics												
	n	mean	sd	median	mad	min	max	range	skew	kurtosis	se	IQR
0 µg/ml	6	8.355	3.329	7.195	2.024	5.470	14.400	8.930	0.817	-1.039	1.359	3.040
1 µg/ml	6	12.290	5.498	11.250	3.914	6.220	22.100	15.880	0.682	-1.034	2.245	4.235
2 µg/ml	6	12.077	7.544	9.775	6.405	5.030	24.100	19.070	0.494	-1.646	3.080	9.977
4 µg/ml	6	11.692	5.284	10.635	2.787	6.340	21.500	15.160	0.849	-0.822	2.157	3.402
8 µg/ml	6	10.358	4.711	9.150	4.559	5.500	16.200	10.700	0.206	-2.068	1.923	7.762

	Wilcoxon-signed-Rank-Test, correction method: Holm
0-8 µg/ml	p.value = 0.248863874937922; r= 0.4707565
0-4 µg/ml	p.value = 0.0277078493580799; r= 0.898717

0-2 µg/ml	p.value = 0.172954917988421; r= 0.5563486
0-1 µg/ml	p.value = 0.0277078493580799; r= 0.898717
1-8 µg/ml	p.value = 0.172954917988421; r= 0.5563486
1-4 µg/ml	p.value = 0.0796158014601134; r= 0.7156264
1-2 µg/ml	p.value = 0.753152364765915; r= 0.1283881
2-8 µg/ml	p.value = 0.463071015014588; r= 0.2995723
2-4 µg/ml	p.value = 0.916511907863894; r= 0.04279605
4-8 µg/ml	p.value = 0.248863874937922; r= 0.4707565

Early apoptotic CD138- intermediate cells

Friedman test: p-value = 0.08681

Descriptive statistics											
	n	mean	sd	median	mad	min	max	range	skew	kurtosis	se
0 µg/ml	6	11.710	7.021	10.645	7.205	3.690	22	18.310	0.229	-1.833	2.866
1 µg/ml	6	6.675	2.842	6.965	2.572	2.450	10.700	8.250	-0.098	-1.465	1.160
2 µg/ml	6	8.477	4.683	7.500	4.996	3.020	15.500	12.480	0.294	-1.737	1.912
4 µg/ml	6	7.783	3.787	6.450	2.891	3.190	12.400	9.210	0.262	-1.881	1.546
8 µg/ml	6	6.513	3.371	5.285	2.231	2.760	12.100	9.340	0.545	-1.430	1.376

Late apoptotic CD138- intermediate cells

Friedman test: p-value= 0.03072

Descriptive statistics												
	n	mean	sd	median	mad	min	max	range	skew	kurtosis	se	IQR
0 µg/ml	6	18.667	7.695	18.400	5.708	10.700	32.400	21.700	0.664	-1.034	3.141	6.025
1 µg/ml	6	25.817	7.587	25	3.262	15.400	38.700	23.300	0.378	-1.019	3.098	3.800
2 µg/ml	6	25.167	11.459	21.800	10.156	13.700	43.400	29.700	0.484	-1.631	4.678	14.525
4 µg/ml	6	25.233	7.336	23.200	5.560	18.200	38.300	20.100	0.725	-1.130	2.995	6.775
8 µg/ml	6	23.683	8.248	22.200	9.859	15.500	34.200	18.700	0.198	-2.023	3.367	14.050

	Wilcoxon-signed-Rank-Test, correction method: Holm
0-8 µg/ml	p.value = 0.11585149752593; r= 0.6419407
0-4 µg/ml	p.value = 0.0277078493580799; r= 0.898717
0-2 µg/ml	p.value = 0.11585149752593; r= 0.6419407
0-1 µg/ml	p.value = 0.0277078493580799; r= 0.898717
1-8 µg/ml	p.value = 0.463071015014588; r= 0.2995723
1-4 µg/ml	p.value = 0.753152364765915; r= 0.1283881
1-2 µg/ml	p.value = 0.892738400944348; r= 0.05504819
2-8 µg/ml	p.value = 0.463071015014588; r= 0.2995723
2-4 µg/ml	p.value = 0.753152364765915; r= 0.1283881
4-8 µg/ml	p.value = 0.345447530469226; r= 0.3851644

Early apoptotic plasmablasts

Friedman test: p-value = 0.1395

Descriptive statistics												
	n	mean	sd	median	mad	min	max	range	skew	kurtosis	se	IQR
0 µg/ml	6	5.897	2.334	5.145	1.483	3.860	10.300	6.440	0.958	-0.760	0.953	1.630
1 µg/ml	6	7.568	2.148	6.740	1.075	5.880	11.600	5.720	0.958	-0.826	0.877	1.693
2 µg/ml	6	8.615	2.894	7.270	0.652	6.820	14.200	7.380	1.081	-0.618	1.182	2.012
4 µg/ml	6	8.810	1.590	8.820	0.852	6.350	11.200	4.850	-0.049	-1.189	0.649	1.027
8 µg/ml	6	8.598	1.633	8.530	0.934	6.410	11.300	4.890	0.333	-1.200	0.667	1.160

Late apoptotic plasmablasts

Friedman test: p-value = 0.1211

Descriptive statistics												
	n	mean	sd	median	mad	min	max	range	skew	kurtosis	se	IQR
0 µg/ml	6	9.580	2.618	9.680	3.573	6.040	12.700	6.660	-0.093	-1.865	1.069	3.825
1 µg/ml	6	13.177	3.198	13.400	2.150	8.260	17.900	9.640	-0.076	-1.261	1.306	2.375
2 µg/ml	6	12.940	3.704	13.800	3.855	8.450	16.400	7.950	-0.207	-2.085	1.512	6.557
4 µg/ml	6	13.050	2.703	12.450	2.520	10.300	17.700	7.400	0.608	-1.291	1.104	2.825
8 µg/ml	6	13.533	3.866	11.750	1.853	10.200	19.600	9.400	0.573	-1.716	1.578	4.900

9.2.6 Statistics fig. 15: Excised circles resulting from the indirect class switch to IgE or the direct class switch to IgG1

Switch circles for indirect switch to IgE (anti-Ig kappa F(ab')$_2$ fragments)

Wilcoxon signed rank test: p-value = 0.02771; r= 0.898717

Descriptive statistics												
	n	mean	sd	median	mad	min	max	range	skew	kurtosis	se	IQR
0 µg/ml	6	0.639	0.054	0.635	0.021	0.569	0.735	0.166	0.556	-0.896	0.022	0.022
8 µg/ml	6	0.365	0.076	0.366	0.082	0.264	0.476	0.211	0.091	-1.663	0.031	0.092

Switch circles for direct switch to IgG1 (anti-Ig kappa F(ab')$_2$ fragments)

Wilcoxon signed rank test: p-value = 0.07474; r= 0.7275328

Descriptive statistics												
	n	mean	sd	median	mad	min	max	range	skew	kurtosis	se	IQR
0 µg/ml	6	0.715	0.165	0.690	0.167	0.558	0.995	0.437	0.552	-1.354	0.067	0.190
8 µg/ml	6	0.569	0.159	0.549	0.119	0.417	0.860	0.443	0.785	-0.920	0.065	0.124

Switch circles for indirect switch to IgE (anti-IgM F(ab')$_2$ fragments)

Wilcoxon signed rank test: p-value = 0.1088; r= 0.9258201

Descriptive statistics												
	n	mean	sd	median	mad	min	max	range	skew	kurtosis	se	IQR
0 µg/ml	3	0.629	0.011	0.632	0.009	0.617	0.638	0.021	-0.247	-2.333	0.006	0.010
8 µg/ml	3	0.412	0.030	0.425	0.012	0.378	0.433	0.055	-0.353	-2.333	0.017	0.028

Switch circles for direct switch to IgG1 (anti-IgM F(ab')$_2$ fragments)

Wilcoxon signed rank test: p-value = 0.1088; r= 0.9258201

Descriptive statistics												
	n	mean	sd	median	mad	min	max	range	skew	kurtosis	se	IQR
0 µg/ml	3	0.591	0.051	0.566	0.012	0.558	0.649	0.091	0.373	-2.333	0.029	0.046
8 µg/ml	3	0.468	0.059	0.477	0.068	0.405	0.523	0.118	-0.145	-2.333	0.034	0.059

9.2.7 Statistics fig. 16: The PI3K-pathway inhibitor LY294002 does not change the ratio of IgE/ IgG1

IgE frequency among B cells (non- anti-BCR stimulated cells)

Descriptive statistics												
	n	mean	sd	median	mad	min	max	range	skew	kurtosis	se	IQR
control	7	5.443	3.007	4.370	4.211	1.530	10	8.470	0.209	-1.701	1.137	4.100
LY294002	7	5.387	2.815	5.690	1.661	1.030	10.400	9.370	0.260	-0.733	1.064	1.715

Wilcoxon-signed-rank test: p-value = 0.6121, r= 0.191663

IgE frequency among B cells (anti-BCR stimulated cells)

Descriptive statistics												
	n	mean	sd	median	mad	min	max	range	skew	kurtosis	se	IQR
control	7	1.327	0.811	1.090	1.053	0.380	2.610	2.230	0.308	-1.683	0.307	1.155
LY294002	7	1.830	0.842	1.880	0.623	0.400	3.110	2.710	-0.209	-1.006	0.318	0.640

Wilcoxon-signed-rank test: p-value = 0.398, r= 0.3194383

- Wilcoxon-signed-rank test (LY294002 group) comparing cells stimulated without and with anti-Ig kappa $F(ab')_2$ fragments: p-value = 0.01796, r= 0.8944272
- Wilcoxon-signed-rank test (control group) comparing cells stimulated without and with anti-Ig kappa $F(ab')_2$ fragments: p-value = 0.01796, r= 0.8944272

IgG1 frequency among B cells (non- anti-BCR stimulated cells)

Descriptive statistics												
	n	mean	sd	median	mad	min	max	range	skew	kurtosis	se	IQR
control	7	29.257	2.623	29.900	1.927	24.100	32	7.900	-0.882	-0.636	0.991	1.800
LY294002	7	40.886	6.128	42	6.523	31.600	47.300	15.700	-0.424	-1.690	2.316	8.450

Wilcoxon-signed-rank test: p-value = 0.01796, r=0.8944272

IgG1 frequency among B cells (anti-BCR stimulated cells)

Descriptive statistics												
	n	mean	sd	median	mad	min	max	range	skew	kurtosis	se	IQR
control	7	14.141	4.108	16	4.893	8.190	19.300	11.110	-0.196	-1.843	1.553	5.950
LY294002	7	21.543	4.673	20.800	5.486	14.300	27.600	13.300	-0.134	-1.616	1.766	6.250

Wilcoxon-signed-rank test: p-value = 0.01796, 0.8944272

- Wilcoxon-signed-rank test (LY294002 group) comparing cells stimulated without and with anti-Ig kappa F(ab')2 fragments: p-value = 0.01796, r= 0.8944272
- Wilcoxon-signed-rank test (control group) comparing cells stimulated without and with anti-Ig kappa F(ab')2 fragments: p-value = 0.01776; r= 0.8960287

IgE/IgG1 among B cells (non- anti-BCR stimulated cells)

Descriptive statistics												
	n	mean	sd	median	mad	min	max	range	skew	kurtosis	se	IQR
control	7	0.182	0.096	0.140	0.114	0.063	0.334	0.271	0.329	-1.615	0.036	0.124
LY294002	7	0.134	0.085	0.130	0.050	0.033	0.309	0.276	0.960	-0.199	0.032	0.041

Wilcoxon-signed-rank test: p-value = 0.1763, r= 0.5111013

IgE/IgG1 among B cells (anti-BCR stimulated cells)

Descriptive statistics												
	n	mean	sd	median	mad	min	max	range	skew	kurtosis	se	IQR
control	7	0.088	0.035	0.082	0.040	0.035	0.135	0.100	-0.064	-1.653	0.013	0.048
LY294002	7	0.085	0.042	0.083	0.023	0.028	0.160	0.132	0.436	-0.913	0.016	0.035

Wilcoxon-signed-rank test: p-value=0.499, r= 0.2555506

- Wilcoxon-signed-rank test (LY294002 group) comparing cells stimulated without and with anti-Ig kappa F(ab')2 fragments: p-value = 0.01796, r= 0.8944272
- Wilcoxon-signed-rank test (control group) comparing cells stimulated without and with anti-Ig kappa F(ab')2 fragments: p-value = 0.01796, r= 0.8944272

IgE frequency among plasmablasts (non- anti-BCR stimulated cells)

Descriptive statistics												
	n	mean	sd	median	mad	min	max	range	skew	kurtosis	se	IQR
control	7	8.169	4.390	6.270	1.364	5.220	17.300	12.080	1.181	-0.243	1.659	3.175
LY294002	7	9.539	2.417	9.370	1.231	6.930	14.300	7.370	0.802	-0.549	0.914	1.535

Wilcoxon-signed-rank test: p-value= 0.398, r= 0.3194383

IgE frequency among plasmablasts (anti-BCR stimulated cells)

Descriptive Statistics												
	n	mean	sd	median	mad	min	max	range	skew	kurtosis	se	IQR
control	7	3.347	1.048	3.140	0.949	1.860	5.130	3.270	0.275	-1.173	0.396	1.040
LY294002	7	3.936	1.866	3.270	1.705	1.940	7.430	5.490	0.689	-0.967	0.705	1.905

Wilcoxon-signed-rank test: p-value = 0.398, r= 0.3194383

- Wilcoxon-signed-rank test (LY294002 group) comparing cells stimulated without and with anti-Ig kappa F(ab')2 fragments: p-value = 0.01796, r= 0.8944272
- Wilcoxon-signed-rank test (control group) comparing cells stimulated without and with anti-Ig kappa F(ab')2 fragments: p-value = 0.01796, r= 0.8944272

IgG1 frequency among plasmablasts (non- anti-BCR stimulated cells)

Descriptive statistics												
	n	mean	sd	median	mad	min	max	range	skew	kurtosis	se	IQR
control	7	8.983	1.291	9.410	1.171	7.180	10.400	3.220	-0.344	-1.771	0.488	1.855
LY294002	7	15.429	1.839	14.500	1.186	13.700	17.900	4.200	0.341	-1.947	0.695	3.050

Wilcoxon-signed-rank test: p-value = 0.01796, 0.8944272

IgG1 frequency among plasmablasts (non- anti-BCR stimulated cells)

Descriptive statistics												
	n	mean	sd	median	mad	min	max	range	skew	kurtosis	se	IQR
control	7	10.897	2.598	11	2.372	6.710	14.500	7.790	-0.207	-1.416	0.982	3.065
LY294002	7	13.286	2.736	12.700	2.669	10	17.100	7.100	0.337	-1.688	1.034	3.500

Wilcoxon-signed-rank test: p-value = 0.3105, r= 0.3833259

• Wilcoxon-signed-rank test (LY294002 group) comparing cells stimulated without and with anti-Ig kappa F(ab')2 fragments: p-value = 0.01796, r= 0.8944272

• Wilcoxon-signed-rank test (control group) comparing cells stimulated without and with anti-Ig kappa F(ab')2 fragments: p-value = 0.1763; r= 0.5111013

IgE/IgG1 among plasmablasts (non- anti-BCR stimulated cells)

Descriptive statistics												
	n	mean	sd	median	mad	min	max	range	skew	kurtosis	se	IQR
control	7	0.926	0.488	0.693	0.267	0.502	1.802	1.300	0.764	-1.258	0.185	0.529
LY294002	7	0.626	0.186	0.529	0.076	0.478	1.014	0.536	1.171	-0.173	0.070	0.134

Wilcoxon-signed-rank test: p-value = 0.1763, 0.5111013

IgE/IgG1 among plasmablasts (anti-BCR stimulated cells)

Descriptive statistics												
	n	mean	sd	median	mad	min	max	range	skew	kurtosis	se	IQR
control	7	0.304	0.040	0.300	0.034	0.239	0.354	0.115	-0.184	-1.399	0.015	0.044
LY294002	7	0.299	0.148	0.238	0.066	0.194	0.609	0.415	1.198	-0.121	0.056	0.112

Wilcoxon-signed-rank test: p-value = 0.398, r= 0.3194383

• Wilcoxon-signed-rank test (LY294002 group) comparing cells stimulated without and with anti-Ig kappa F(ab')2 fragments: p-value = 0.01796, r= 0.8944272

• Wilcoxon-signed-rank test (control group) comparing cells stimulated without and with anti-Ig kappa F(ab')2 fragments: p-value = 0.01796, r= 0.8944272

9.2.8 Statistics fig. 17: The frequency and the ratio of IgE and IgG1 changes according to the IL-4 stimulation

IgE+ frequency among B cells

Friedman test: p-value = 1.913×10^{-6}

Descriptive Statistics												
	n	mean	sd	median	mad	min	max	range	skew	kurtosis	se	IQR
0.5 ng/ml	8	0.379	0.156	0.370	0.148	0.230	0.700	0.470	0.831	-0.515	0.055	0.170
1 ng/ml	8	1.067	0.607	0.885	0.326	0.380	2.090	1.710	0.644	-1.318	0.215	0.545
2 ng/ml	8	2.643	1.407	1.945	0.689	1.350	5.030	3.680	0.678	-1.435	0.498	1.753
4 ng/ml	8	4.184	1.524	3.835	1.401	2.520	6.410	3.890	0.433	-1.513	0.539	1.643
8 ng/ml	8	5.226	1.765	4.885	1.890	2.970	8.110	5.140	0.278	-1.409	0.624	1.815

	Wilcoxon-signed-Rank-Test, correction method: Holm
0.5-8 ng/ml	p.value = 0.0117186855997686; r= 0.8911328
0.5-4 ng/ml	p.value = 0.0117186855997686; r= 0.8911328
0.5-2 ng/ml	p.value = 0.0117186855997686; r= 0.8911328
0.5-1 ng/ml	p.value = 0.0117186855997686; r= 0.8911328
1- 8 ng/ml	p.value = 0.0117186855997686; r= 0.8911328
1-4 ng/ml	p.value = 0.0117186855997686; r= 0.8911328
1-2 ng/ml	p.value = 0.0117186855997686; r= 0.8911328
2-8 ng/ml	p.value = 0.0117186855997686; r= 0.8911328
2-4 ng/ml	p.value = 0.0117186855997686; r= 0.8911328
4-8 ng/ml	p.value = 0.0117186855997686; r= 0.8911328

IgG1+ frequency among B cells

Friedman test: p-value = 2.659×10^{-6}

Descriptive statistics												
	n	mean	sd	median	mad	min	max	range	skew	kurtosis	se	IQR
0.5 ng/ml	8	9.749	3.540	8.920	1.846	6.130	17.700	11.570	1.228	0.364	1.251	1.675
1 ng/ml	8	19.712	6.540	17.450	5.411	13.400	30.400	17	0.588	-1.499	2.312	8.800
2 ng/ml	8	30.625	6.625	27.750	3.262	25.500	41.800	16.300	0.798	-1.314	2.342	7.100
4 ng/ml	8	35.300	4.327	33.950	4.596	30.700	41.800	11.100	0.361	-1.745	1.530	6.750
8 ng/ml	8	37.888	4.937	39	6.005	31.500	43.100	11.600	-0.233	-1.896	1.745	9.075

	Wilcoxon-signed-Rank-Test, correction method: Holm
0.5-8 ng/ml	p.value = 0.0117186855997686; r= 0.8911328
0.5-4 ng/ml	p.value = 0.0117186855997686; r= 0.8911328
0.5-2 ng/ml	p.value = 0.0117186855997686; r= 0.8911328
0.5-1 ng/ml	p.value = 0.0117186855997686; r= 0.8911328
1- 8 ng/ml	p.value = 0.0116160448992625; r= 0.8922269
1-4 ng/ml	p.value = 0.0117186855997686; r= 0.8911328
1-2 ng/ml	p.value = 0.0117186855997686; r= 0.8911328
2-8 ng/ml	p.value = 0.0117186855997686; r= 0.8911328
2-4 ng/ml	p.value = 0.0172902805929063; r= 0.8416254
4-8 ng/ml	p.value = 0.0117186855997686; r= 0.8911328

IgE/IgG1 among B cells

Friedman test: p-value = 2.659×10^{-6}

Descriptive statistics												
	n	mean	sd	median	mad	min	max	range	skew	kurtosis	se	IQR
0.5 ng/ml	8	0.039	0.011	0.039	0.013	0.027	0.056	0.030	0.322	-1.595	0.004	0.015
1 ng/ml	8	0.051	0.014	0.053	0.010	0.028	0.074	0.045	-0.145	-1.228	0.005	0.013
2 ng/ml	8	0.082	0.026	0.073	0.022	0.053	0.125	0.072	0.439	-1.593	0.009	0.040
4 ng/ml	8	0.116	0.030	0.107	0.037	0.082	0.158	0.076	0.236	-1.753	0.011	0.043
8 ng/ml	8	0.135	0.031	0.133	0.031	0.094	0.189	0.095	0.332	-1.271	0.011	0.031

	Wilcoxon-signed-Rank-Test, correction method: Holm
0.5-8 ng/ml	p.value = 0.0117186855997686; r= 0.8911328
0.5-4 ng/ml	p.value = 0.0117186855997686; r= 0.8911328
0.5-2 ng/ml	p.value = 0.0117186855997686; r= 0.8911328
0.5-1 ng/ml	p.value = 0.0499499764547464; r= 0.6931033
1- 8 ng/ml	p.value = 0.0117186855997686; r= 0.8911328
1-4 ng/ml	p.value = 0.0117186855997686; r= 0.8911328
1-2 ng/ml	p.value = 0.0117186855997686; r= 0.8911328
2-8 ng/ml	p.value = 0.0117186855997686; r= 0.8911328
2-4 ng/ml	p.value = 0.0117186855997686; r= 0.8911328
4-8 ng/ml	p.value = 0.0117186855997686; r= 0.8911328

IgE+ frequency among plasmablasts

Friedman test: p-value = 6.114×10^{-5}

Descriptive statistics												
	n	mean	sd	median	mad	min	max	range	skew	kurtosis	se	IQR
0.5 ng/ml	8	4.331	1.519	4.790	1.757	2.470	6.500	4.030	-0.098	-1.785	0.537	2.515
1 ng/ml	8	5.608	2.520	4.415	1.935	3.080	9.390	6.310	0.434	-1.744	0.891	3.635
2 ng/ml	8	6.737	2.983	6.265	3.529	3.160	11.500	8.340	0.272	-1.535	1.055	3.868
4 ng/ml	8	7.722	3.390	7.150	4.047	3.960	13	9.040	0.284	-1.726	1.199	5.440
8 ng/ml	8	7.790	2.709	6.795	2.254	4.260	12	7.740	0.394	-1.507	0.958	3.147

	Wilcoxon-signed-Rank-Test, correction method: Holm
0.5-8 ng/ml	p.value = 0.0117186855997686; r= 0.8911328
0.5-4 ng/ml	p.value = 0.0172902805929063; r= 0.8416254
0.5-2 ng/ml	p.value = 0.0117186855997686; r= 0.8911328
0.5-1 ng/ml	p.value = 0.0687035743228782; r= 0.6435959
1- 8 ng/ml	p.value = 0.0117186855997686; r= 0.8911328
1-4 ng/ml	p.value = 0.0117186855997686; r= 0.8911328
1-2 ng/ml	p.value = 0.0117186855997686; r= 0.8911328
2-8 ng/ml	p.value = 0.0909689479753577; r= 0.5976143
2-4 ng/ml	p.value = 0.0499499764547464; r= 0.6931033
4-8 ng/ml	p.value = 0.888637860895008; r= 0.04950738

IgG1+ frequency among plasmablasts

Friedman test: p-value = 0.009651

Descriptive statistics												
	n	mean	sd	median	mad	min	max	range	skew	kurtosis	se	IQR
0.5 ng/ml	8	10.004	2.437	9.300	1.245	7.790	15.300	7.510	1.140	-0.037	0.861	1.325
1 ng/ml	8	12.137	3.275	10.750	2.150	8.300	17.400	9.100	0.557	-1.454	1.158	3.725
2 ng/ml	8	13.287	2.382	13.200	2.817	10.600	17.600	7	0.542	-1.195	0.842	2.575
4 ng/ml	8	11.775	1.304	11.900	1.705	10.200	13.900	3.700	0.208	-1.578	0.461	1.875
8 ng/ml	8	11.389	1.520	11.600	1.705	9.010	13.500	4.490	-0.160	-1.550	0.538	2

	Wilcoxon-signed-Rank-Test, correction method: Holm
0.5-8 ng/ml	p.value = 0.161429462367083; r= 0.4950738
0.5-4 ng/ml	p.value = 0.0420627333567661; r= 0.7187383
0.5-2 ng/ml	p.value = 0.0117186855997686; r= 0.8911328
0.5-1 ng/ml	p.value = 0.0250618443438836; r= 0.792118
1- 8 ng/ml	p.value = 0.575403022912754; r= 0.1980295
1-4 ng/ml	p.value = 0.779434528427275; r= 0.09901475
1-2 ng/ml	p.value = 0.262618290442521; r= 0.396059
2-8 ng/ml	p.value = 0.0687035743228782; r= 0.6435959

2-4 ng/ml	p.value = 0.0629790512144552; r= 0.6573757
4-8 ng/ml	p.value = 0.326989349598015; r= 0.3465516

IgE/IgG1 among plasmablasts

Friedman test: p-value = 0.001477

Descriptive statistics												
	n	mean	sd	median	mad	min	max	range	skew	kurtosis	se	IQR
0.5 ng/ml	8	0.428	0.106	0.439	0.142	0.310	0.599	0.289	0.162	-1.615	0.038	0.172
1 ng/ml	8	0.450	0.111	0.483	0.086	0.283	0.559	0.276	-0.474	-1.650	0.039	0.145
2 ng/ml	8	0.497	0.170	0.531	0.188	0.252	0.746	0.494	-0.095	-1.551	0.060	0.213
4 ng/ml	8	0.639	0.219	0.634	0.305	0.374	0.935	0.562	0.048	-1.829	0.077	0.374
8 ng/ml	8	0.687	0.212	0.698	0.173	0.333	1.009	0.676	-0.141	-1.154	0.075	0.154

	Wilcoxon-signed-Rank-Test, correction method: Holm
0.5-8 ng/ml	p.value = 0.0117186855997686; r= 0.8911328
0.5-4 ng/ml	p.value = 0.0356919001168044; r= 0.7426107
0.5-2 ng/ml	p.value = 0.0928919408837053; r= 0.5940885
0.5-1 ng/ml	p.value = 0.483839851393568; r= 0.2475369
1- 8 ng/ml	p.value = 0.0117186855997686; r= 0.8911328
1-4 ng/ml	p.value = 0.0172902805929063; r= 0.8416254
1-2 ng/ml	p.value = 0.400814169382934; r= 0.2970443
2-8 ng/ml	p.value = 0.0172902805929063; r= 0.8416254
2-4 ng/ml	p.value = 0.0250618443438836; r= 0.792118
4-8 ng/ml	p.value = 0.326989349598015; r= 0.3465516

9.2.9 Statistics fig. 18: Different glucose concentrations influence the generation of IgE+ and IgG1+ cells

IgE frequency among B cells (non- anti-BCR stimulated cells)

Friedman test: p-value = 0.0002265

Descriptive statistics												
	n	mean	sd	median	mad	min	max	range	skew	kurtosis	se	IQR
50 mg/dL	6	1.265	0.323	1.245	0.133	0.810	1.810	1	0.327	-0.998	0.132	0.143
100 mg/dL	6	2.677	0.499	2.700	0.460	1.820	3.160	1.340	-0.552	-1.262	0.204	0.525
150 mg/dL	6	5.273	1.386	5.085	1.853	3.710	7.050	3.340	0.170	-1.930	0.566	2.150
200 mg/dL	6	4.565	1.493	3.975	1.001	3.180	6.530	3.350	0.390	-1.976	0.609	2.365
300 mg/dL	6	5.723	0.767	5.800	0.986	4.570	6.560	1.990	-0.270	-1.706	0.313	1.008

	Wilcoxon-signed-Rank-Test, correction method: Holm
50-300 mg/dL	p.value = 0.0277078493580799; r= 0.898717
50-200 mg/dL	p.value = 0.0277078493580799; r= 0.898717
50-150 mg/dL	p.value = 0.0277078493580799; r= 0.898717
50-100 mg/dL	p.value = 0.0277078493580799; r= 0.898717
100-300 mg/dL	p.value = 0.0277078493580799; r= 0.898717
100-200 mg/dL	p.value = 0.0277078493580799; r= 0.898717
100-150 mg/dL	p.value = 0.0277078493580799; r= 0.898717
150-300 mg/dL	p.value = 0.600179487140554; r= 0.2139802
150-200 mg/dL	p.value = 0.0277078493580799; r= 0.898717
200-300 mg/dL	p.value = 0.0747354983058825; r= 0.7275328

IgE frequency among B cells (anti-BCR stimulated cells)

Friedman test: p-value = 0.0003469

Descriptive statistics												
	n	mean	sd	median	mad	min	max	range	skew	kurtosis	se	IQR
50 mg/dL	6	0.272	0.063	0.250	0.052	0.210	0.360	0.150	0.395	-1.912	0.026	0.095
100 mg/dL	6	0.898	0.224	0.915	0.237	0.550	1.170	0.620	-0.275	-1.579	0.092	0.262
150 mg/dL	6	1.362	0.388	1.410	0.489	0.770	1.780	1.010	-0.308	-1.688	0.159	0.515

200 mg/dL	6	1.257	0.633	1.015	0.430	0.670	2.260	1.590	0.542	-1.667	0.258	0.803
300 mg/dL	6	2.425	0.618	2.435	0.474	1.620	3.440	1.820	0.317	-1.269	0.252	0.498

	Wilcoxon-signed-Rank-Test, correction method: Holm
50-300 mg/dL	p.value = 0.0277078493580799; r= 0.898717
50-200 mg/dL	p.value = 0.0277078493580799; r= 0.898717
50-150 mg/dL	p.value = 0.0277078493580799; r= 0.898717
50-100 mg/dL	p.value = 0.0277078493580799; r= 0.898717
100-300 mg/dL	p.value = 0.027281171477618; r= 0.9011963
100-200 mg/dL	p.value = 0.248863874937922; r= 0.4707565
100-150 mg/dL	p.value = 0.0277078493580799; r= 0.898717
150-300 mg/dL	p.value = 0.0277078493580799; r= 0.898717
150-200 mg/dL	p.value = 0.916511907863894; r= 0.04279605
200-300 mg/dL	p.value = 0.0277078493580799; r= 0.898717

IgG1 frequency among B cells (non- anti-BCR stimulated cells)

Friedman test: p-value = 0.0003918

Descriptive statistics												
	n	mean	sd	median	mad	min	max	range	skew	kurtosis	se	IQR
50 mg/dL	6	20.733	5.429	21.350	2.595	11.400	28	16.600	-0.438	-1.005	2.217	2.800
100 mg/dL	6	29.600	4.528	31.700	1.112	20.900	32.500	11.600	-1.065	-0.657	1.849	3.200
150 mg/dL	6	33.850	3.767	34.850	3.855	29.100	37.900	8.800	-0.296	-1.947	1.538	5.875
200 mg/dL	6	30.183	3.298	30.500	4.225	25.200	33.600	8.400	-0.279	-1.721	1.346	4.625
300 mg/dL	6	19.667	2.161	18.650	0.964	17.800	23.100	5.300	0.587	-1.681	0.882	2.675

	Wilcoxon-signed-Rank-Test, correction method: Holm
50-300 mg/dL	p.value = 0.753152364765915; r= 0.1283881
50-200 mg/dL	p.value = 0.0277078493580799; r= 0.898717
50-150 mg/dL	p.value = 0.0277078493580799; r= 0.898717
50-100 mg/dL	p.value = 0.0277078493580799; r= 0.898717
100-300 mg/dL	p.value = 0.0277078493580799; r= 0.898717
100-200 mg/dL	p.value = 0.345447530469226; r= 0.3851644
100-150 mg/dL	p.value = 0.0463994618709046; r= 0.8131249
150-300 mg/dL	p.value = 0.0277078493580799; r= 0.898717
150-200 mg/dL	p.value = 0.0277078493580799; r= 0.898717
200-300 mg/dL	p.value = 0.0277078493580799; r= 0.898717

IgG1 frequency among B cells (anti-BCR stimulated cells)

Friedman test: p-value = 0.01547

Descriptive statistics												
	n	mean	sd	median	mad	min	max	range	skew	kurtosis	se	IQR
50 mg/dL	6	5.818	2.977	5.740	2.343	1.390	10.200	8.810	-0.008	-1.375	1.215	2.615
100 mg/dL	6	16.217	3.259	15.950	2.743	10.900	20.200	9.300	-0.320	-1.358	1.331	2.950
150 mg/dL	6	16.918	3.838	17.900	0.964	9.510	20.700	11.190	-1.021	-0.523	1.567	1.175
200 mg/dL	6	14.532	4.703	14.800	4.448	8.190	21.400	13.210	0.070	-1.621	1.920	5.250
300 mg/dL	6	12.862	2.617	13.650	1.557	7.970	15.400	7.430	-0.899	-0.798	1.068	1.700

	Wilcoxon-signed-Rank-Test, correction method: Holm
50-300 mg/dL	p.value = 0.0463994618709046; r= 0.8131249
50-200 mg/dL	p.value = 0.0463994618709046; r= 0.8131249
50-150 mg/dL	p.value = 0.0277078493580799; r= 0.898717
50-100 mg/dL	p.value = 0.0277078493580799; r= 0.898717
100-300 mg/dL	p.value = 0.0747354983058825; r= 0.7275328
100-200 mg/dL	p.value = 0.916511907863894; r= 0.04279605
100-150 mg/dL	p.value = 0.600179487140554; r= 0.2139802
150-300 mg/dL	p.value = 0.0747354983058825; r= 0.7275328
150-200 mg/dL	p.value = 0.248863874937922; r= 0.4707565
200-300 mg/dL	p.value = 0.207160448911461; r= 0.5149693

IgE/IgG1 among B cells (non-anti-BCR stimulated cells)

Friedman test: p-value = 0.0001388

Descriptive statistics												
	n	mean	sd	median	mad	min	max	range	skew	kurtosis	se	IQR
50 mg/dL	6	0.062	0.006	0.061	0.006	0.055	0.071	0.016	0.345	-1.570	0.002	0.007
100 mg/dL	6	0.090	0.009	0.092	0.010	0.079	0.099	0.020	-0.150	-2.131	0.004	0.016
150 mg/dL	6	0.156	0.035	0.157	0.044	0.112	0.196	0.083	-0.037	-2.131	0.014	0.056
200 mg/dL	6	0.149	0.034	0.133	0.017	0.120	0.195	0.075	0.458	-1.948	0.014	0.052
300 mg/dL	6	0.292	0.040	0.283	0.030	0.248	0.363	0.115	0.683	-1.066	0.016	0.031

	Wilcoxon-signed-Rank-Test, correction method: Holm
50-300 mg/dL	p.value = 0.0277078493580799; r= 0.898717
50-200 mg/dL	p.value = 0.0277078493580799; r= 0.898717
50-150 mg/dL	p.value = 0.0277078493580799; r= 0.898717
50-100 mg/dL	p.value = 0.0277078493580799; r= 0.898717
100-300 mg/dL	p.value = 0.0277078493580799; r= 0.898717
100-200 mg/dL	p.value = 0.0277078493580799; r= 0.898717
100-150 mg/dL	p.value = 0.0277078493580799; r= 0.898717
150-300 mg/dL	p.value = 0.0277078493580799; r= 0.898717
150-200 mg/dL	p.value = 0.916511907863894; r= 0.04279605
200-300 mg/dL	p.value = 0.0277078493580799; r= 0.898717

IgE/IgG1 among B cells (anti-BCR stimulated cells)

Friedman test: p-value = 0.001391

Descriptive statistics												
	n	mean	sd	median	mad	min	max	range	skew	kurtosis	se	IQR
50 mg/dL	6	0.064	0.047	0.042	0.014	0.032	0.151	0.119	0.966	-0.877	0.019	0.037
100 mg/dL	6	0.055	0.005	0.055	0.006	0.049	0.063	0.014	0.174	-1.698	0.002	0.006
150 mg/dL	6	0.080	0.013	0.080	0.007	0.063	0.102	0.039	0.301	-1.085	0.005	0.007
200 mg/dL	6	0.084	0.020	0.076	0.013	0.064	0.110	0.046	0.367	-1.945	0.008	0.029
300 mg/dL	6	0.189	0.022	0.187	0.026	0.163	0.223	0.060	0.297	-1.611	0.009	0.028

	Wilcoxon-signed-Rank-Test, correction method: Holm
50-300 mg/dL	p.value = 0.0277078493580799; r= 0.898717
50-200 mg/dL	p.value = 0.345447530469226; r= 0.385164
50-150 mg/dL	p.value = 0.345447530469226; r= 0.385164
50-100 mg/dL	p.value = 0.916511907863894; r= 0.04279605
100-300 mg/dL	p.value = 0.0277078493580799; r= 0.898717
100-200 mg/dL	p.value = 0.0277078493580799 ; r= 0.898717
100-150 mg/dL	p.value = 0.0463994618709046; r= 0.8131249
150-300 mg/dL	p.value = 0.0277078493580799; r= 0.898717
150-200 mg/dL	p.value = 0.753152364765915; r= 0.1283881
200-300 mg/dL	p.value = 0.0277078493580799; r= 0.898717

IgE frequency among plasmablasts (non-anti-BCR stimulated cells)

Friedman test: p-value = 0.0003469

Descriptive statistics												
	n	mean	sd	median	mad	min	max	range	skew	kurtosis	se	IQR
50 mg/dL	6	1.337	0.545	1.155	0.460	0.780	2.080	1.300	0.375	-1.918	0.222	0.805
100 mg/dL	6	3.328	1.044	3.685	0.815	1.700	4.430	2.730	-0.474	-1.674	0.426	1.255
150 mg/dL	6	5.588	0.584	5.745	0.571	4.880	6.220	1.340	-0.246	-2.006	0.238	0.953
200 mg/dL	6	5.425	0.288	5.355	0.297	5.090	5.860	0.770	0.351	-1.688	0.117	0.340
300 mg/dL	6	9.517	4.310	8.235	3.514	5.260	16.900	11.640	0.629	-1.336	1.760	4.585

	Wilcoxon-signed-Rank-Test, correction method: Holm
50-300 mg/dL	p.value = 0.0277078493580799; r= 0.898717
50-200 mg/dL	p.value = 0.0277078493580799; r= 0.898717

50-150 mg/dL	p.value = 0.0277078493580799; r= 0.898717
50-100 mg/dL	p.value = 0.0277078493580799; r= 0.898717
100-300 mg/dL	p.value = 0.0277078493580799; r= 0.898717
100-200 mg/dL	p.value = 0.027281171477618; r= 0.9011963
100-150 mg/dL	p.value = 0.0277078493580799; r= 0.898717
150-300 mg/dL	p.value = 0.0463994618709046; r= 0.8131249
150-200 mg/dL	p.value = 0.600179487140554; r= 0.2139802
200-300 mg/dL	p.value = 0.0463994618709046; r= 0.8131249

IgG1 frequency among plasmablasts (non-anti-BCR stimulated cells)

Friedman test: p-value = 0.005135

Descriptive statistics												
	n	mean	sd	median	mad	min	max	range	skew	kurtosis	se	IQR
50 mg/dL	6	5.435	1.133	5.400	1.290	4.240	7.230	2.990	0.323	-1.563	0.463	1.425
100 mg/dL	6	8.478	1.603	8.630	0.563	5.550	10.400	4.850	-0.713	-0.793	0.654	0.580
150 mg/dL	6	10.605	1.821	10.250	0.845	8.270	13.800	5.530	0.542	-0.966	0.743	0.880
200 mg/dL	6	10.440	1.176	10.650	1.408	8.730	11.700	2.970	-0.288	-1.821	0.480	1.692
300 mg/dL	6	9.252	3.142	9.340	2.676	5.040	13.800	8.760	0.083	-1.673	1.283	3.438

	Wilcoxon-signed-Rank-Test, correction method: Holm
50-300 mg/dL	p.value = 0.0277078493580799; r= 0.898717
50-200 mg/dL	p.value = 0.0277078493580799; r= 0.898717
50-150 mg/dL	p.value = 0.0277078493580799; r= 0.898717
50-100 mg/dL	p.value = 0.0277078493580799; r= 0.898717
100-300 mg/dL	p.value = 0.600179487140554; r= 0.2139802
100-200 mg/dL	p.value = 0.0277078493580799; r= 0.898717
100-150 mg/dL	p.value = 0.0463994618709046; r= 0.8131249
150-300 mg/dL	p.value = 0.600179487140554; r= 0.2139802
150-200 mg/dL	p.value = 0.916511907863894; r= 0.04279605
200-300 mg/dL	p.value = 0.463071015014588; r= 0.2995723

IgE/IgG1 among plasmablasts (non-anti-BCR stimulated cells)

Friedman test: p-value = 0.0004163

Descriptive statistics												
	n	mean	sd	median	mad	min	max	range	skew	kurtosis	se	IQR
50 mg/dL	6	0.241	0.061	0.247	0.079	0.161	0.321	0.160	-0.063	-1.831	0.025	0.085
100 mg/dL	6	0.396	0.110	0.426	0.056	0.197	0.524	0.327	-0.697	-0.936	0.045	0.062
150 mg/dL	6	0.537	0.084	0.563	0.068	0.402	0.624	0.222	-0.462	-1.615	0.034	0.101
200 mg/dL	6	0.525	0.067	0.501	0.051	0.443	0.613	0.170	0.268	-1.849	0.028	0.083
300 mg/dL	6	1.170	0.683	1.060	0.767	0.487	2.145	1.658	0.228	-1.959	0.279	1.002

	Wilcoxon-signed-Rank-Test, correction method: Holm
50-300 mg/dL	p.value = 0.0277078493580799; r= 0.898717
50-200 mg/dL	p.value = 0.0277078493580799; r= 0.898717
50-150 mg/dL	p.value = 0.0277078493580799; r= 0.898717
50-100 mg/dL	p.value = 0.0277078493580799; r= 0.898717
100-300 mg/dL	p.value = 0.0277078493580799; r= 0.898717
100-200 mg/dL	p.value = 0.0277078493580799; r= 0.898717
100-150 mg/dL	p.value = 0.0277078493580799; r= 0.898717
150-300 mg/dL	p.value = 0.11585149752593; r= 0.6419407
150-200 mg/dL	p.value = 0.916511907863894; r= 0.04279605
200-300 mg/dL	p.value = 0.11585149752593; r= 0.6419407

Frequency of B cells (non-anti-BCR stimulated cells)

Friedman rank sum test: Friedman chi-squared = 16.706, df = 4, p-value = 0.002205

Descriptive statistics												
	n	mean	sd	median	mad	min	max	range	skew	kurtosis	se	IQR
50 mg/dL	6	92.250	3.088	92.600	1.334	86.400	95.300	8.900	-0.930	-0.668	1.261	1.450

100 mg/dL	6	91.117	1.702	91.200	2.372	89	93.300	4.300	-0.029	-1.882	0.695	2.500
150 mg/dL	6	89.567	0.933	89.550	1.186	88.600	90.700	2.100	0.052	-2.179	0.381	1.525
200 mg/dL	6	89.317	1.143	89.650	0.964	87.500	90.300	2.800	-0.465	-1.672	0.466	1.575
300 mg/dL	6	93.650	1.221	93.800	1.334	91.900	95.200	3.300	-0.158	-1.757	0.498	1.550

	Wilcoxon-Rank-Test
50-300 mg/dL	p.value = 0.599174265940189, r= 0.2145705
50-200 mg/dL	p.value = 0.0747354983058825, r= 0.7275328
50-150 mg/dL	p.value = 0.0747354983058825, r= 0.7275328
50-100 mg/dL	p.value = 0.463071015014588, r= 0.2995723
100-300 mg/dL	p.value = 0.0277078493580799, r= 0.898717
100-200 mg/dL	p.value = 0.0277078493580799, r= 0.898717
100-150 mg/dL	p.value = 0.0277078493580799, r= 0.898717
150-300 mg/dL	p.value = 0.0277078493580799, r= 0.898717
150-200 mg/dL	p.value = 0.416365677908165, r= 0.3318008
200-300 mg/dL	p.value = 0.0277078493580799, r= 0.898717

Frequency of plasmablasts (non-anti-BCR stimulated cells)

Friedman test: p-value = 0.0001885

Descriptive statistics												
	n	mean	sd	median	mad	min	max	range	skew	kurtosis	se	IQR
50 mg/dL	6	1.608	0.820	1.505	0.823	0.570	2.820	2.250	0.192	-1.694	0.335	0.980
100 mg/dL	6	2.937	1.319	2.805	1.460	1.400	4.920	3.520	0.252	-1.725	0.539	1.705
150 mg/dL	6	3.638	0.998	3.450	0.852	2.680	5.420	2.740	0.714	-1.094	0.408	0.948
200 mg/dL	6	2.932	0.940	2.620	0.704	1.940	4.520	2.580	0.602	-1.374	0.384	0.917
300 mg/dL	6	0.515	0.131	0.475	0.052	0.420	0.770	0.350	1.112	-0.499	0.053	0.070

	Wilcoxon-Rank-Test
50-300 mg/dL	p.value = 0.0463994618709046, r= 0.8131249
50-200 mg/dL	p.value = 0.0277078493580799, r= 0.898717
50-150 mg/dL	p.value = 0.0277078493580799, r= 0.898717
50-100 mg/dL	p.value = 0.0277078493580799, r= 0.898717
100-300 mg/dL	p.value = 0.0277078493580799, r= 0.898717
100-200 mg/dL	p.value = 0.916511907863894, r= 0.04279605
100-150 mg/dL	p.value = 0.0277078493580799, r= 0.898717
f150-300 mg/dL	p.value = 0.0277078493580799, r= 0.898717
150-200 mg/dL	p.value = 0.0277078493580799, r= 0.898717
200-300 mg/dL	p.value = 0.0277078493580799, r= 0.898717

Counted Living cells (non-anti-BCR stimulated cells)

Friedman test: p-value = 0.008197

Descriptive statistics												
	n	mean	sd	median	mad	min	max	range	skew	kurtosis	se	IQR
50 mg/dL	6	380,405	182,863.400	390,280	246,007.800	145,690	610,560	464,870	-0.051	-1.899	74,653.670	270,565
100 mg/dL	6	836,551.700	522,359.100	732,045	579,437.100	317,460	1,455,820	1,138,360	0.170	-2.105	213,252.200	916,582.500
150 mg/dL	6	680,143.400	198,674.300	626,070	119,467.900	508,200	1,050,560.000	542,360.300	0.898	-0.846	81,108.460	151,835
200 mg/dL	6	889,677.900	536,984.200	822,983.600	684,974.000	308,950	1,515,060	1,206,110	0.096	-2.124	219,222.900	921,925.700
300 mg/dL	6	436,954.600	135,905.600	424,510	120,374.000	235,980	630,239.700	394,259.700	-0.018	-1.468	55,483.230	130,281.700

	Wilcoxon-Rank-Test
50-300 mg/dL	p.value = 0.345447530469226

50-200 mg/dL	p.value = 0.0277078493580799
50-150 mg/dL	p.value = 0.0277078493580799
50-100 mg/dL	p.value = 0.0277078493580799
100-300 mg/dL	p.value = 0.11585149752593
100-200 mg/dL	p.value = 0.600179487140554,
100-150 mg/dL	p.value = 0.345447530469226, "
150-300 mg/dL	p.value = 0.0277078493580799
150-200 mg/dL	p.value = 0.345447530469226
200-300 mg/dL	p.value = 0.0463994618709046

Frequency of living cells (non-anti-BCR stimulated cells)

Friedman rank sum test: p-value = 0.01837

Descriptive statistics												
	n	mean	sd	median	mad	min	max	range	skew	kurtosis	se	IQR
50 mg/dL	6	83.683	5.980	85.250	4.374	73.800	91.300	17.500	-0.418	-1.293	2.441	4.650
100 mg/dL	6	86.683	0.624	86.650	0.371	85.800	87.700	1.900	0.239	-1.149	0.255	0.400
150 mg/dL	6	83.283	2.340	84.100	1.853	80.400	86	5.600	-0.311	-1.900	0.955	3.275
200 mg/dL	6	84.783	2.276	84.200	2.076	82.600	88.600	6	0.561	-1.443	0.929	2.675
300 mg/dL	6	87.600	1.968	87.300	1.038	84.900	90.900	6	0.354	-1.085	0.803	1.100

	Wilcoxon-Rank-Test
50-300 mg/dL	p.value = 0.248863874937922; r = 0.4707565
50-200 mg/dL	p.value = 0.916282441329102; r = 0.04291411
50-150 mg/dL	p.value = 0.916511907863894; r = 0.04279605
50-100 mg/dL	p.value = 0.172954917988421r = 0.5563486
100-300 mg/dL	p.value = 0.40038080315208; r = 0.3433129
100-200 mg/dL	p.value = 0.0739374358521521; r = 0.7295398
100-150 mg/dL	p.value = 0.0277078493580799; r = 0.898717
150-300 mg/dL	p.value = 0.0277078493580799; r = 0.898717
150-200 mg/dL	p.value = 0.345447530469226; r = 0.3851644
200-300 mg/dL	p.value = 0.0277078493580799; r = 0.898717

9.2.10 Statistics fig. 23: A higher glucose concentration is associated with a lower frequency of apoptotic cells

Frequency of early apoptotic cells (non-anti-BCR stimulated cells)

Descriptive statistics												
	n	mean	sd	median	mad	min	max	range	skew	kurtosis	se	IQR
100 mg/dL	6	2.713	0.775	2.560	0.823	1.800	3.870	2.070	0.272	-1.746	0.317	0.977
200 mg/dL	6	1.617	0.537	1.415	0.193	1.230	2.680	1.450	1.188	-0.374	0.219	0.232

Wilcoxon signed rank test: p-value = 0.02771; r= 0.898717

Frequency of early apoptotic cells (anti-BCR stimulated cells)

Descriptive statistics												
	n	mean	sd	median	mad	min	max	range	skew	kurtosis	se	IQR
100 mg/dL	6	2.783	0.459	2.670	0.482	2.330	3.410	1.080	0.300	-1.941	0.187	0.730
200 mg/dL	6	1.877	0.383	2.085	0.082	1.230	2.180	0.950	-0.708	-1.478	0.157	0.393

Wilcoxon signed rank test: p-value =0.02771; r= 0.898717

Frequency of late apoptotic cells (non-anti-BCR stimulated cells)

Descriptive statistics												
	n	mean	sd	median	mad	min	max	range	skew	kurtosis	se	IQR
100 mg/dL	6	9.133	4.754	8.500	5.856	4.370	15.100	10.730	0.124	-2.120	1.941	8.002
200 mg/dL	6	5.513	2.591	5.320	3.781	2.210	8.450	6.240	0.037	-1.924	1.058	4.105

Wilcoxon signed rank test: p-value 0.02771; r= 0.898717

Frequency of late apoptotic cells (anti-BCR stimulated cells)

Descriptive statistics												
	n	mean	sd	median	mad	min	max	range	skew	kurtosis	se	IQR

100 mg/dL	6	6.513	3.183	6.220	4.062	3.340	10.100	6.760	0.053	-2.223	1.299	5.575
200 mg/dL	6	4.712	2.139	4.045	1.742	2.720	7.800	5.080	0.332	-1.917	0.873	3.202

Wilcoxon signed rank test: p-value =0.02771; r= 0.898717

9.2.11 Statistics fig. 20: The median fluorescence intensity (MFI) of the glucose uptake

2-NBDG among IgE+ cells

Friedman test: p-value = 0.002527

Descriptive statistics												
	n	mean	sd	median	mad	min	max	range	skew	kurtosis	se	IQR
0µg/ml	6	28.729	30.203	18.983	24.773	0	69.457	69.457	0.308	-1.996	12.330	48.006
1µg/ml	6	9.266	26.615	1.321	23.197	-16.788	41.240	58.029	0.243	-2.067	10.866	45.302
2 µg/ml	6	16.618	25.911	22.266	29.127	-17.883	46.873	64.757	-0.237	-1.893	10.578	37.523
4 µg/ml	6	36.729	27.292	38.807	40.040	4.197	70.129	65.932	-0.067	-1.939	11.142	43.174
6 µg/ml	6	77.488	14.051	74.675	15.074	63.321	100	36.679	0.437	-1.605	5.736	17.953

2-NBDG among IgG1+ cells

Friedman test: p-value = 0.002015

Descriptive statistics												
	n	mean	sd	median	mad	min	max	range	skew	kurtosis	se	IQR
0µg/ml	6	40.351	31.706	33.001	32.830	0	87.409	87.409	0.260	-1.649	12.944	35.511
1µg/ml	6	8.031	14.447	1.190	7.040	-3.832	26.977	30.809	0.484	-1.956	5.898	22.334
2µg/ml	6	15.472	15.017	17.188	17.230	-3.832	36.124	39.956	-0.006	-1.793	6.131	19.696
4µg/ml	6	35.203	14.983	36.434	17.856	15.876	52.403	36.527	-0.083	-2.063	6.117	22.536
6µg/ml	6	71.967	15.919	70.008	10.957	53.285	100	46.715	0.602	-1.052	6.499	11.327

2 NBDG: comparison IgE and IgG1

	Wilcoxon-signed-Rank-Test, correction method: Holm
0 µg/ml, MFI for IgE vs MFI for IgG1	p.value = 0.3454; r= 0.3851644
1 µg/ml, MFI for IgE vs MFI for IgG1	p.value = 0.6002; r= 0.2139802
2 µg/ml, MFI for IgE vs MFI for IgG1	p.value = p-value = 0.9165; r= 0.04279605
4 µg/ml, MFI for IgE vs MFI for IgG1	p.value = 0.7532; r= 0.1283881
6 µg/ml, MFI for IgE vs MFI for IgG1	p.value = 0.3454; r= 0.3851644

10. References

Acharya, M., Borland, G., Edkins, A. L., MacLellan, L. M., Matheson, J., Ozanne, B. W., & Cushley, W. (2010). CD23/FcεRII: Molecular multi-tasking. *Clinical and Experimental Immunology*, *162*(1), 12–23. https://doi.org/10.1111/j.1365-2249.2010.04210.x

Amboss. (2021). *Diabetes mellitus*. https://www.amboss.com/de/wissen/Diabetes_mellitus [date of last access: 12.07.2021]

Antolin, A. A., Sanfelice, D., Crisp, A., Villasclaras Fernandez, E., Mica, I. L., Chen, Y., Collins, I., Edwards, A., Müller, S., Al-Lazikani, B., & Workman, P. (2023). The Chemical Probes Portal: an expert review-based public resource to empower chemical probe assessment, selection and use. *Nucleic Acids Research*, *51*(1 D), D1492–D1502. https://doi.org/10.1093/nar/gkac909. URL: http://www.chemicalprobes.org/

Anvari, S., Miller, J., Yeh, C. Y., & Davis, C. M. (2019). IgE-Mediated Food Allergy. *Clinical Reviews in Allergy and Immunology*, *57*(2), 244–260. https://doi.org/10.1007/s12016-018-8710-3

Aouinti, S., Giudicelli, V., Duroux, P., Malouche, D., Kossida, S., & Lefranc, M. P. (2016). IMGT/statclonotype for pairwise evaluation and visualization of NGS IG and TR IMGT clonotype (AA) diversity or expression from IMGT/HighV-QUEST. *Frontiers in Immunology*, *7*(SEP), 1–14. https://doi.org/10.3389/fimmu.2016.00339

Aouinti, S., Malouche, D., Giudicelli, V., Kossida, S., & Lefranc, M. P. (2015). IMGT/HighV-QUEST statistical significance of IMGT clonotype (AA) diversity per gene for standardized comparisons of next generation sequencing immunoprofiles of immunoglobulins and T cell receptors. *PLoS ONE*, *10*(11), 1–22. https://doi.org/10.1371/journal.pone.0142353

Arrowsmith, C. H., Audia, J. E., Austin, C., Baell, J., Bennett, J., Young, R. N., & Zuercher, W. J. (2015). The promise and peril of chemical probes. *Nat Chem Biol.*, *11*(8), 536–541. https://doi.org/doi:10.1038/nchembio.1867.

Ashraf Uzzaman, S. H. C. (2012). Classification of hypersensitivity reactions. *Allergy Astma Proc.*, *33*, S96–S99. https://doi.org/10.2500/aap.2012.33.3561.

Aufheimer, M. (2021). DSUR.noof: Collection of Additional Functions Used in Andy Field's "Discovering Statistics Using R." In *R package version 0.1.1.* http://github.com/Frostarella/DSUR.noof

Bajnok, A., Serény-Litvai, T., Temesfoi, V., Nörenberg, J., Herczeg, R., Kaposi, A., Berki, T., & Mezosi, E. (2023). An Optimized Flow Cytometric Method to Demonstrate the Differentiation Stage-Dependent Ca 2 + Flux Responses of Peripheral Human B Cells. *International Journal of Molecular Sciences*, *24*(9107). https://doi.org/https://doi.org/10.3390/ijms24109107

Banfalvi, G. (2017). Methods to detect apoptotic cell death. *Apoptosis*, *22*(2), 306–323. https://doi.org/10.1007/s10495-016-1333-3

Berry, C. T., Liu, X., Myles, A., Nandi, S., Chen, Y. H., Hershberg, U., Brodsky, I. E., Cancro, M. P., Lengner, C. J., May, M. J., & Freedman, B. D. (2020). BCR-Induced Ca2+ Signals Dynamically Tune Survival, Metabolic Reprogramming, and Proliferation of Naive B Cells. *Cell Reports*, *31*(2), 107474. https://doi.org/10.1016/j.celrep.2020.03.038

Boughter, C. T., Borowska, M. T., Guthmiller, J. J., Bendelac, A., Wilson, P. C., Roux, B., & Adams, E. J. (2020). Biochemical patterns of antibody polyreactivity revealed through a bioinformatics-based analysis of cdr loops. *ELife*, *9*, 1–47. https://doi.org/10.7554/eLife.61393

Boyce, J., Assa'ad, A., AW, B., Jones, S., Sampson, H., Wood, R., Plaut, M., Cooper, S., Fenton, M., Arshad, S., Bahna, S., Beck, L., Byrd-Bredbenner, C., Camargo Jr., C., Eichenfield, L., Furuta, G., Hanifin, J., Jones, C., Kraft, M., … Schwaninger, J. (2010). Guidelines for the diagnosis and management of food allergy in the United States: report of the NIAID-sponsored expert panel. *J Allergy Clin Immunol*, *126(6 Supp*. https://doi.org/doi: 10.1016/j.jaci.2010.10.007.

Brochet X, Lefranc MP, G. V. (2008). IMGT/V-QUEST: the highly customized and integrated system for IG and TR standardized V-J and V-D-J sequence analysis. *Nucleic Acids Res.*, *1*(36), W503-8. https://doi.org/10.1093/nar/gkn316

Cantrell, W., Huang, Y., Menchaca, A. A., Kulik, G., & Welker, M. E. (2018). Synthesis and PI3 kinase inhibition activity of a Wortmannin-Leucine derivative. *Molecules*, *23*(7), 1–7. https://doi.org/10.3390/molecules23071791

Chandrasekhar, J. L., Cox, K. M., & Erickson, L. D. (2020). B Cell Responses in the Development of Mammalian Meat Allergy. *Frontiers in Immunology*, *11*(July), 1–16. https://doi.org/10.3389/fimmu.2020.01532

Chen, Zhangguo; Getahun, Andrew; Chen, Xiaomi; Dollin, Yonatan; Cambier, John C.; Wang, J. H. (2015). Imbalanced PTEN and Phosphoinositide 3-kinase signaling impairs class switch recombination. *J Immunol.*, *195*(11), 5461–5471. https://doi.org/10.4049/jimmunol.1501375

Chen, J., Trounstine, M., Kurahara, C., Young, F., Kuo, C. C., Xu, Y., Loring, J. F., Alt, F. W., & Huszar, D. (1993). B cell development in mice that lack one or both immunoglobulin κ light chain genes. *EMBO Journal*, *12*(3), 821–830. https://doi.org/10.1002/j.1460-2075.1993.tb05722.x

Chen, Q., Liu, H., Luling, N., Reinke, J., & Dent, A. L. (2023). Evidence that High-Affinity IgE Can Develop in the Germinal Center in the Absence of an IgG1-Switched Intermediate. *The Journal of Immunology*, *210*(7), 905–915. https://doi.org/10.4049/jimmunol.2200521

Chen, Z., & Wang, J. H. (2019). Signaling control of antibody isotype switching. *Advances in Immunology*, *141*, 105–164. https://doi.org/10.1016/bs.ai.2019.01.001

Corrado, A., Ramonell, R. P., Woodruff, M. C., Tipton, C., Wise, S., Levy, J., DelGaudio, J., Kuruvilla, M. E., Magliocca, K. R., Tomar, D., Garimalla, S., Scharer, C. D., Boss, J. M., Wu, H., Gumber, S., Fucile, C., Gibson, G., Rosenberg, A., Sanz, I., & Lee, F. E. H. (2021). Extrafollicular IgD+ B cells generate IgE antibody secreting cells in the nasal mucosa. *Mucosal Immunology*, *14*(5), 1144–1159. https://doi.org/10.1038/s41385-021-00410-w

Datema, M. R., Eller, E., Zwinderman, A. H., Poulsen, L. K., Versteeg, S. A., van Ree, R., & Bindslev-Jensen, C. (2019). Ratios of specific IgG4 over IgE antibodies do not improve prediction of peanut allergy nor of its severity compared to specific IgE alone. *Clinical and Experimental Allergy*, *49*(2), 216–226. https://doi.org/10.1111/cea.13286

Davis, M. M., Jay Boniface, J., Reich, Z., Lyons, D., Hampl, J., Arden, B., & Chien, Y. H. (1998). Ligand recognition by αβ T cell receptors. *Annual Review of Immunology*, *16*, 523–544. https://doi.org/10.1146/annurev.immunol.16.1.523

Depoil, D., Fleire, S., Treanor, B. L., Weber, M., Harwood, N. E., Marchbank, K. L., Tybulewicz, V. L. J., & Batista, F. D. (2008). CD19 is essential for B cell activation by promoting B cell receptor-antigen microcluster formation in response to membrane-bound ligand. *Nature Immunology*, *9*(1), 63–72. https://doi.org/10.1038/ni1547

Diegel, M. L., Rankini, B. M., Bolen, J. B., Dubois, P. M., & Kiener, P. A. (1994). Cross-linking of Fcγ receptor to surface immunoglobulin on B cells provides an inhibitory

signal that closes the plasma membrane calcium channel. *Journal of Biological Chemistry*, *269*(15), 11409–11416. https://doi.org/10.1016/s0021-9258(19)78139-3

Doughty, C. A., Bleiman, B. F., Wagner, D. J., Dufort, F. J., Mataraza, J. M., Roberts, M. F., & Chiles, T. C. (2006). Antigen receptor-mediated changes in glucose metabolism in B lymphocytes: Role of phosphatidylinositol 3-kinase signaling in the glycolytic control of growth. *Blood*, *107*(11), 4458–4465. https://doi.org/10.1182/blood-2005-12-4788

Engeroff, P., Caviezel, F., Mueller, D., Thoms, F., Bachmann, M. F., & Vogel, M. (2020). CD23 provides a noninflammatory pathway for IgE-allergen complexes. *Journal of Allergy and Clinical Immunology*, *145*(1), 301-311.e4. https://doi.org/10.1016/j.jaci.2019.07.045

Engeroff, P., & Vogel, M. (2021). The role of CD23 in the regulation of allergic responses. *Allergy: European Journal of Allergy and Clinical Immunology*, *76*(7), 1981–1989. https://doi.org/10.1111/all.14724

Erazo, A., Kutchukhidze, N., Leung, M., Christ, A. P. G., Urban, J. F., Curotto de Lafaille, M. A., & Lafaille, J. J. (2007). Unique Maturation Program of the IgE Response In Vivo. *Immunity*, *26*(2), 191–203. https://doi.org/10.1016/j.immuni.2006.12.006

Feng, Y., Wang, Y., Zhang, S., Haneef, K., & Liu, W. (2020). Structural and immunogenomic insights into B-cell receptor activation. *Journal of Genetics and Genomics*, *47*(1), 27–35. https://doi.org/10.1016/j.jgg.2019.12.003

Fong, A. T., Ahlstedt, S., Golding, M. A., & Protudjer, J. L. P. (2022). The Economic Burden of Food Allergy: What We Know and What We Need to Learn. *Current Treatment Options in Allergy*, *9*(3), 169–186. https://doi.org/10.1007/s40521-022-00306-5

Galibert, L., Burdin, N., Barthélémy, C., Meffre, G., Durand, I., Garcia, E., Garrone, P., Rousset, F., Banchereau, J., & Liu, Y. J. (1996). Negative selection of human germinal center B cells by prolonged BCR cross-linking. *Journal of Experimental Medicine*, *183*(5), 2075–2085. https://doi.org/10.1084/jem.183.5.2075

Giudicelli V, Brochet X, L. M. (2011). IMGT/V-QUEST: IMGT standardized analysis of the immunoglobulin (IG) and T cell receptor (TR) nucleotide sequences. *Cold Spring Harb Protoc.*, *6*, 695–715. https://doi.org/10.1101/pdb.prot5633

Haase, P., & Voehringer, D. (2021). Regulation of the humoral type 2 immune response against allergens and helminths. *European Journal of Immunology*, *51*(2), 273–279. https://doi.org/10.1002/eji.202048864

Haniuda, K., Fukao, S., Kodama, T., Hasegawa, H., & Kitamura, D. (2016). Autonomous membrane IgE signaling prevents IgE-memory formation. *Nature Immunology*, *17*(9), 1109–1117. https://doi.org/10.1038/ni.3508

Haniuda, K., & Kitamura, D. (2019). Induced Germinal Center B Cell Culture System. *Bio-Protocol*, *9*(4), 1–10. https://doi.org/10.21769/bioprotoc.3163

Haniuda, K., & Kitamura, D. (2021). Multi-faceted regulation of IgE production and humoral memory formation. *Allergology International*, *70*(2), 163–168. https://doi.org/10.1016/j.alit.2020.11.002

He, J. S., Subramaniam, S., Narang, V., Srinivasan, K., Saunders, S. P., Carbajo, D., Wen-Shan, T., Hidayah Hamadee, N., Lum, J., Lee, A., Chen, J., Poidinger, M., Zolezzi, F., Lafaille, J. J., & Curotto De Lafaille, M. A. (2017). IgG1 memory B cells keep the memory of IgE responses. *Nature Communications*, *8*(1), 0–11. https://doi.org/10.1038/s41467-017-00723-0

Hlavac, M. (2018). *stargazer: Well-Formatted Regression and Summary Statistics Tables.*

(R package version 5.2.1.). https://cran.r-project.org/package=stargazer

Hlavac, M. (2022). *stargazer: Well-Formatted Regression and Summary Statistics Tables* (R package version 5.2.3). https://cran.r-project.org/package=stargazer

Hoh, R. A., Joshi, S. A., Lee, J. Y., Martin, B. A., Varma, S., Kwok, S., Nielsen, S. C. A., Nejad, P., Haraguchi, E., Dixit, P. S., Shutthanandan, S. V., Roskin, K. M., Zhang, W., Tupa, D., Bunning, B. J., Manohar, M., Tibshirani, R., Fernandez-Becker, N. Q., Kambham, N., … Boyd, S. D. (2020). Origins and clonal convergence of gastrointestinal IgE+ B cells in human peanut allergy. *Science Immunology*, *5*(45), 1–26. https://doi.org/10.1126/sciimmunol.aay4209

Hoof, Ilka; Schulten, V. et al. (2020). Allergen-specific IgG+ memory B cells are temporally linked to IgE memory responses. *J Allergy Clin Immunol*, *146*(1), 180–191. https://doi.org/10.1016/j.jaci.2019.11.046.

Hou, P., Araujo, E., Zhao, T., Zhang, M., Massenburg, D., Veselits, M., Doyle, C., Dinner, A. R., & Clark, M. R. (2006). B cell antigen receptor signaling and internalization are mutually exclusive events. *PLoS Biology*, *4*(7), 1147–1158. https://doi.org/10.1371/journal.pbio.0040200

Huang, C. (2020a). Germinal Center Reaction. In J.-Y. Wang (Ed.), *B cells in Immunity and Tolerance* (pp. 47–52). Springer Singapore. https://doi.org/https://doi.org/10.1007/978-981-15-3532-1

Huang, C. (2020b). SHM and CSR. In J.-Y. Wang (Ed.), *B cells in Immunity and Tolerance* (p. 49). Springer Singapore. https://doi.org/10.1007/978-981-15-3532-1

Ise, W., & Kurosaki, T. (2020). Regulation of Plasma Cell Differentiation. In J.-Y. Wang (Ed.), *B cells in Immunity and Tolerance* (pp. 63–74). Springer Singapore. https://doi.org/https://doi.org/10.1007/978-981-15-3532-1

Ise, Wataru, & Kurosaki, T. (2019). Plasma cell differentiation during the germinal center reaction. *Immunological Reviews*, *288*(1), 64–74. https://doi.org/10.1111/imr.12751

Jabara, H. H., Chaudhuri, J., Dutt, S., Dedeoglu, F., Weng, Y., Murphy, M. M., Franco, S., Alt, F. W., Manis, J., & Geha, R. S. (2008). B-cell receptor cross-linking delays activation-induced cytidine deaminase induction and inhibits class-switch recombination to IgE. *Journal of Allergy and Clinical Immunology*, *121*(1). https://doi.org/10.1016/j.jaci.2007.08.008

James, L. K. (2022). B cells defined by immunoglobulin isotypes. *Clinical and Experimental Immunology*, *210*(3), 230–239. https://doi.org/10.1093/cei/uxac091

Jiménez-Saiz, R., Bruton, K., Koenig, J. F. E., Waserman, S., & Jordana, M. (2018). The IgE memory reservoir in food allergy. *Journal of Allergy and Clinical Immunology*, *142*(5), 1441–1443. https://doi.org/10.1016/j.jaci.2018.08.029

Jiménez-Saiz, R., Chu, D. K., Mandur, T. S., Walker, T. D., Gordon, M. E., Chaudhary, R., Koenig, J., Saliba, S., Galipeau, H. J., Utley, A., King, I. L., Lee, K., Ettinger, R., Waserman, S., Kolbeck, R., & Jordana, M. (2017). Lifelong memory responses perpetuate humoral T H 2 immunity and anaphylaxis in food allergy. *Journal of Allergy and Clinical Immunology*, *140*(6), 1604-1615.e5. https://doi.org/10.1016/j.jaci.2017.01.018

Kaji, T., Ishige, A., Hikida, M., Taka, J., Hijikata, A., Kubo, M., Nagashima, T., Takahashi, Y., Kurosaki, T., Okada, M., Ohara, O., Rajewsky, K., & Takemori, T. (2012). Distinct cellular pathways select germlineencoded and somatically mutated antibodies into immunological memory. *Journal of Experimental Medicine*, *209*(11), 2079–2097. https://doi.org/10.1084/jem.20120127

Klamt, S., Vogel, M., Kapellen, T. M., Hiemisch, A., Prenzel, F., Zachariae, S., Ceglarek,

U., Thiery, O., & Kiess, W. (2015). Association between IgE-mediated allergies and diabetes mellitus type 1 in children and adolescents. *Pediatr Diabetes*, *16*(7), 493–503. https://doi.org/10.1111/pedi.12298

Kläsener, K., Maity, P. C., Hobeika, E., Yang, J., & Reth, M. (2014). B cell activation involves nanoscale receptor reorganizations and inside-out signaling by Syk. *ELife*, *3*, 1–17. https://doi.org/10.7554/elife.02069

Kucuk, Z. Y., Strait, R., Khodoun, M. V., Mahler, A., Hogan, S., & Finkelman, F. D. (2012). Induction and suppression of allergic diarrhea and systemic anaphylaxis in a mouse model of food allergy. *J Allergy Clin Immunol*, *129*(5), 343–1348.

Lefranc, M.-P., Giudicelli, V., Ginestoux, C., Jabado-Michaloud, J., Folch, G., Bellahcene, F., Wu, Y. et al. (2009). *IMGT®, the international ImMunoGeneTics information system®*. Nucl. Acids Res., 37:D1006-D1012. https://doi.org/10.1093/nar/gkn838

Lilienthal, G. M., Rahmöller, J., Petry, J., Bartsch, Y. C., Leliavski, A., & Ehlers, M. (2018). Potential of murine IgG1 and Human IgG4 to inhibit the classical complement and Fcγ receptor activation pathways. Frontiers in Immunology, 9(MAY). https://doi.org/10.3389/fimmu.2018.00958

Lobo EO, Zhang Z, S. J. . (2009). Pivotal advance: CEACAM1 is a negative coreceptor for the B cell receptor and promotes CD19-mediated adhesion of B cells in a PI3K-dependent manner. *J Leukoc Biol.*, *86*(2), 205–218. https://doi.org/doi: 10.1189/jlb.0109037

Lu, L. L., Suscovich, T. J., Fortune, S. M., & Alter, G. (2018). Beyond binding: Antibody effector functions in infectious diseases. *Nature Reviews Immunology*, *18*(1), 46–61. https://doi.org/10.1038/nri.2017.106

Ma, R. X., Hu, J. Q., Fu, W., Zhong, J., Cao, C., Wang, C. C., Qi, S. Q., Zhang, X. L., Liu, G. H., & Gao, Y. D. (2023). Intermittent fasting protects against food allergy in a murine model via regulating gut microbiota. *Frontiers in Immunology*, *14*(May), 1–15. https://doi.org/10.3389/fimmu.2023.1167562

Macdougall, J. D., Thomas, K. O., & Iweala, O. I. (2022). The Meat of the Matter: Understanding and Managing Alpha-Gal Syndrome. *ImmunoTargets and Therapy*, *11*(September), 37–54. https://doi.org/10.2147/ITT.S276872

Maity, P. C., Blount, A., Jumaa, H., Ronneberger, O., Lillemeier, B. F., & Reth, M. (2015). B cell antigen receptors of the IgM and IgD classes are clustered in different protein islands that are altered during B cell activation. *Science Signaling*, *8*(394). https://doi.org/10.1126/scisignal.2005887

Maker, J. H., Stroup, C. M., Huang, V., & James, S. F. (2019). Antibiotic Hypersensitivity Mechanisms. *Pharmacy*, *7*(3), 122. https://doi.org/10.3390/pharmacy7030122

Mandler, R., Finkelman, F., Levine, A., & Snapper, C. (1993). IL-4 induction of IgE class switching by lipopolysaccharide-activated murine B cells occurs predominantly through sequential switching. *J Immunol.*, *150*(2), 407–418.

MERCK. (2023). *Goat Anti-Mouse Ig kappa chain Antibody, F(ab')2 SDS*. https://www.merckmillipore.com/DE/de/product/msds/MM_NF-AQ500?Origin=PDP [date of last access: 12.06.2024]

MERCK. (2024). *LY 294002 - CAS 154447-36-6 - Calbiochem*. https://www.merckmillipore.com/DE/de/product/LY-294002-CAS-154447-36-6-Calbiochem,EMD_BIO-440202 [date of last access: 02.07.2024]

Mike Kulis, Benjamin L. Wright, S. M. J. and A. W. B. (2015). Diagnosis, Management, and Investigational Therapies for Food Allergies. *Gastrooenterology*, *148*(6), 1132–1142. https://doi.org/10.1053/j.gastro.2015.01.034.

Mix, E., Goertsches, R., & Zett, U. K. (2006). Immunoglobulins - Basic considerations. *Journal of Neurology*, *253*(SUPPL. 5), 9–17. https://doi.org/10.1007/s00415-006-5002-2

Moriyama, S., Adachi, Y., Tonouchi, K., & Takahashi, Y. (2020). Memory B Cells in Local and Systemic Sites. In J.-Y. Wang (Ed.), *B cells in Immunity and Tolerance* (pp. 55–62). Springer Singapore. https://doi.org/https://doi.org/10.1007/978-981-15-3532-1

Murphy, K., & Weaver, C. (2018a). Antigenerkennung durch B-Zell und T-Zell-Rezeptoren. In *Janeway Immunologie* (9. edition, pp. 179–186). Springer Spektrum. https://doi.org/10.1007/978-3-662-56004-4

Murphy, K., & Weaver, C. (2018b). Die Entstehung von Antigenrezeptoren in Lymphocyten. In *Janeway Immunologie* (9. edition, p. 237). Springer Spektrum. https://doi.org/10.1007/978-3-662-56004-4

Murphy, K., & Weaver, C. (2018c). IgE ist größtenteils an Zellen gebunden und bewirkt auf anderen Wegen als die übrigen Antikörperisotypen Effektormechanismen des Immunsystems. In *Janeway Immunologie* (9. edition, p. 798). Springer Spektrum. https://doi.org/10.1007/978-3-662-56004-4

Nelms, K., Keegan, A., Zamorano, J., Ryan, J., & Paul, W. (1999). The IL-4 receptor: signaling mechanisms and biologic functions. *Annu Rev Immunol*, *17*, 701–738. https://doi.org/10.1146/annurev.immunol.17.1.701

Nojima, T., Haniuda, K., Moutai, T., Matsudaira, M., Mizokawa, S., Shiratori, I., Azuma, T., & Kitamura, D. (2011). In-vitro derived germinal centre B cells differentially generate memory B or plasma cells in vivo. *Nature Communications*, *2*(1), 411–465. https://doi.org/10.1038/ncomms1475

Nowak-Węgrzyn, A., Katz, Y., Mehr, S. S., & Koletzko, S. (2015). Non-IgE-mediated gastrointestinal food allergy. *Journal of Allergy and Clinical Immunology*, *135*(5), 1114–1124. https://doi.org/10.1016/j.jaci.2015.03.025

Okamoto, S., Taniuchi, S., Sudo, K., Hatano, Y., Nakano, K., Shimo, T., & Kaneko, K. (2012). Predictive value of IgE/IgG4 antibody ratio in children with egg allergy. *Allergy, Asthma and Clinical Immunology*, *8*(1), 1. https://doi.org/10.1186/1710-1492-8-9

Osborne, N. J., Koplin, J. J., Martin, P. E., Gurrin, L. C., Lowe, A. J., Matheson, M. C., Ponsonby, A. L., Wake, M., Tang, M. L. K., Dharmage, S. C., & Allen, K. J. (2011). Prevalence of challenge-proven IgE-mediated food allergy using population-based sampling and predetermined challenge criteria in infants. *Journal of Allergy and Clinical Immunology*, *127*(3), 668-676.e2. https://doi.org/10.1016/j.jaci.2011.01.039

Osorio, D., Rondon-Villarreal, P. & Torres, R. (2015). Peptides: A package for data mining of antimicrobial peptides. *The R Journal*, *7*(1), 4–14.

Park, S. R., Seo, G. Y., Choi, A. J., Stavnezer, J., & Kim, P. H. (2005). Analysis of transforming growth factor-β1-induced Ig germ-line γ2b transcription and its implication for IgA isotype switching. *European Journal of Immunology*, *35*(3), 946-956. https://doi.org/https://doi.org/10.1002/eji.200425848

Peters, R. L., Koplin, J. J., Gurrin, L. C., Dharmage, S. C., Wake, M., Ponsonby, A. L., Tang, M. L. K., Lowe, A. J., Matheson, M., Dwyer, T., & Allen, K. J. (2017). The prevalence of food allergy and other allergic diseases in early childhood in a population-based study: HealthNuts age 4-year follow-up. *Journal of Allergy and Clinical Immunology*, *140*(1), 145-153.e8. https://doi.org/10.1016/j.jaci.2017.02.019

Peters, R. L., Krawiec, M., Koplin, J. J., & Santos, A. F. (2021). Update on food allergy. *Pediatric Allergy and Immunology*, *32*(4), 647–657. https://doi.org/10.1111/pai.13443

Pincetic, A., Bournazos, S., Dilillo, D. J., Maamary, J., Wang, T. T., Dahan, R., Fiebiger, B., & Ravetch, J. V. (2014). Type-I and Type-II Fc receptors regulate innate and adaptive immunity. *Nat Immunol.*, *15*(8), 707–716. https://doi.org/10.1038/ni.2939

Poulsen, L. K., & Hummelshoj, L. (2007). Triggers of IgE class switching and allergy development. *Annals of Medicine*, *39*(6), 440–456. https://doi.org/10.1080/07853890701449354

Putney, J. W., & Bird, G. S. J. (1993). The signal for capacitative calcium entry. *Cell*, *75*(2), 199–201. https://doi.org/10.1016/0092-8674(93)80061-I

Rabia, L. A., Zhang, Y., Ludwig, S. D., Julian, M. C., Tessier, P. M., & Arbor, A. (2019). *Net charge of antibody complementarity- determining regions is a key predictor of speci fi city*. *31*(11), 409–418. https://doi.org/10.1093/protein/gzz002

Revelle, W. (2020). *psych: Procedures for Personality and Psychological Research*. Northwestern University, Evanston, Illinois, USA.

Ring, J., Beyer, K., Biedermann, T., Bircher, A., Fischer, M., Fuchs, T., Heller, A., Hoffmann, F., Huttegger, I., Jakob, T., Klimek, L., Kopp, M. V., Kugler, C., Lange, L., Pfaar, O., Rietschel, E., Ruëff, F., Schnadt, S., Seifert, R., … Brockow, K. (2021). Leitlinie zu Akuttherapie und Management der Anaphylaxie – Update 2021. *Allergologie*, *44*(5), 356–388. https://doi.org/10.5414/ALX02232

Roco, J. A., Mesin, L., Binder, S. C., Nefzger, C., Gonzalez-Figueroa, P., Canete, P. F., Ellyard, J., Shen, Q., Robert, P. A., Cappello, J., Vohra, H., Zhang, Y., Nowosad, C. R., Schiepers, A., Corcora, L. M., & Vinuesa, C. G. (2019). Class Switch Recombination Occurs Infrequently in Germinal Centers. *Immunity*, *51*(2), 337–350. https://doi.org/10.1016/j.immuni.2019.07.001.

Sampson, H. A., Berin, M. C., Plaut, M., Sicherer, S. H., Jones, S., Burks, A. W., Lindblad, R., Leung, D. Y. M., & Wood, R. A. (2019). The Consortium for Food Allergy Research (CoFAR): The first generation. *Journal of Allergy and Clinical Immunology*, *143*(2), 486–493. https://doi.org/10.1016/j.jaci.2018.12.989

Santos, A. F., James, L. K., Bahnson, H. T., Shamji, M. H., Couto-Francisco, N. C., Islam, S., Houghton, S., Clark, A. T., Stephens, A., Turcanu, V., Durham, S. R., Gould, H. J., & Lack, G. (2015). IgG4 inhibits peanut-induced basophil and mast cell activation in peanut-tolerant children sensitized to peanut major allergens. *Journal of Allergy and Clinical Immunology*, *135*(5), 1249–1256. https://doi.org/10.1016/j.jaci.2015.01.012

Satitsuksanoa, P., van de Veen, W., & Akdis, M. (2021). B cells in food allergy. *Journal of Allergy and Clinical Immunology*, *147*(1), 49–51. https://doi.org/10.1016/j.jaci.2020.11.014

Schrader, J. S. and C. E. (2014). Ig heavy chain class switch recombination: mechanism and regulation. *J. Immunol.*, *193*(11), 5370–5378. https://doi.org/10.4049/jimmunol.1401849.

Shade, K.-T., Conroy, M. E., & Anthony, R. M. (2019). IgE Glycosylation in Health and Disease. *Curr Top Microbiol Immunol.*, *423*, 77–93. https://doi.org/10.1007/82_2019_151

Shulman, Z., Gitlin, A. D., Weinstein, J. S., Lainez, B., Esplugues, E., Flavell, R. A., Craft, J. E., & Nussenzweig, M. C. (2014). Dynamic signaling by T follicular helper cells during germinal center B cell selection. *Science*, *345*(6200), 1058–1062. https://doi.org/10.1126/science.1257861

Sicherer, S. H., & Sampson, H. A. (2014). Food allergy: Epidemiology, pathogenesis, diagnosis, and treatment. *Journal of Allergy and Clinical Immunology*, *133*(2), 291-

307.e5. https://doi.org/10.1016/j.jaci.2013.11.020

Sicherer, S. H., & Sampson, H. A. (2018). Food allergy: A review and update on epidemiology, pathogenesis, diagnosis, prevention, and management. *Journal of Allergy and Clinical Immunology*, *141*(1), 41–58. https://doi.org/10.1016/j.jaci.2017.11.003

Snapper CM, Finkelman FD, P. W. (1988). Regulation of IgG1 and IgE production by interleukin 4. *Immunol Rev*, *102*, 51–75. https://doi.org/10.1111/j.1600-065x.1988.tb00741.x

Stone, K. D., Prussin, C., & Metcalfe, D. D. (2010). IgE, Mast Cells, Basophils, and Eosinophils. *J Allergy Clin Immunol*, *125*(2 Suppl 2), 73–80. https://doi.org/10.1016/j.jaci.2009.11.017.

Suan, D., Sundling, C., & Brink, R. (2017). Plasma cell and memory B cell differentiation from the germinal center. *Current Opinion in Immunology*, *45*, 97–102. https://doi.org/10.1016/j.coi.2017.03.006

Tanaka, S., & Baba, Y. (2020). B Cell Receptor Signaling. In J.-Y. Wang (Ed.), *B cells in Immunity and Tolerance* (pp. 23–36). Springer Singapore. https://doi.org/https://doi.org/10.1007/978-981-15-3532-1

Taylor, J. J., Pape, K. A., & Jenkins, M. K. (2012). A germinal center-independent pathway generates unswitched memory B cells early in the primary response. *Journal of Experimental Medicine*, *209*(3), 597–606. https://doi.org/10.1084/jem.20111696

Team, R. C. (2021). *R: A language and environment for statistical computing*. R Foundation for Statistical Computing, Vienna, Austria. https://www.r-project.org/

Tolomeo, M., & Cascio, A. (2024). STAT4 and STAT6, their role in cellular and humoral immunity and in diverse human diseases. *International Reviews of Immunology*, 1–25. https://doi.org/https://doi.org/10.1080/08830185.2024.2395274

Turner, P., Gowland, M., Sharma, V., Ierodiakonou, D., Harper, N., Garcez, T., Pumphrey, R., & Boyle, R. (2015). Increase in anaphylaxis-related hospitalizations but no increase in fatalities: an analysis of United Kingdom national anaphylaxis data, 1992-2012. *J Allergy Clin Immunol*, *135*(4), 956-963.e1. https://doi.org/10.1016/j.jaci.2014.10.021

Turqueti-Neves, A., Otte, M., Schwartz, C., Schmitt, M. E. R., Lindner, C., Pabst, O., Yu, P., & Voehringer, D. (2015). The Extracellular Domains of IgG1 and T Cell-Derived IL-4/IL-13 Are Critical for the Polyclonal Memory IgE Response In Vivo. *PLoS Biology*, *13*(11), 1–24. https://doi.org/10.1371/journal.pbio.1002290

Udoye, C. C., Ehlers, M., & Manz, R. A. (2023). The B Cell Response and Formation of Allergenic and Anti-Allergenic Antibodies in Food Allergy. *Biology*, *12*(12), 1–16. https://doi.org/10.3390/biology12121501

Udoye, C. C., Rau, C. N., Freye, S. M., Almeida, L. N., Vera-Cruz, S., Othmer, K., Korkmaz, R., Clauder, A. K., Lindemann, T., Niebuhr, M., Ott, F., Kalies, K., Recke, A., Busch, H., Fähnrich, A., Finkelman, F. D., & Manz, R. A. (2022). B-cell receptor physical properties affect relative IgG1 and IgE responses in mouse egg allergy. *Mucosal Immunology*, *15*(6), 1375–1388. https://doi.org/10.1038/s41385-022-00567-y

Vazquez-Ortiz, M., Pascal, M., Jiménez-Feijoo, R., Lozano, J., Giner, M. T., Alsina, L., Martín-Mateos, M. A., & Plaza, A. M. (2014). Ovalbumin-specific IgE/IgG4 ratio might improve the prediction of cooked and uncooked egg tolerance development in egg-allergic children. *Clinical and Experimental Allergy*, *44*(4), 579–588.

https://doi.org/10.1111/cea.12273

Venkataramana, D., Erlewyn-Lajeunessea, M., Kurukulaaratchya, R., Potter, S., Roberts, G., Matthews, S., & Arshada, S. H. (2018). Prevalence and longitudinal trends of food allergy during childhood and adolescence: results of the Isle of Wight Birth Cohort study. *Clin Exp Allergy*, *48*(4), 394–402. https://doi.org/doi:10.1111/cea.13088

Victora, G. D., & Nussenzweig, M. C. (2012). Germinal centers. *Annual Review of Immunology*, *30*, 429–457. https://doi.org/10.1146/annurev-immunol-020711-075032

Victora, G. D., & Nussenzweig, M. C. (2022). Germinal Centers. *Annual Review of Immunology*, *40*, 413–442. https://doi.org/10.1146/annurev-immunol-120419-022408

Vieira, P., & Rajewsky, K. (1988). The half-lives of serum immunoglobulins in adult mice. *European Journal of Immunology*, *18*(2), 313–316. https://doi.org/https://doi.org/10.1002/eji.1830180221

Vivas-García, Y., & Efeyan, A. (2022). The metabolic plasticity of B cells. *Frontiers in Molecular Biosciences*, *9*(September), 1–7. https://doi.org/10.3389/fmolb.2022.991188

Vlahos, C. J., Matter, W. F., Hui, K. Y., & Brown, R. F. (1994). A specific inhibitor of phosphatidylinositol 3-kinase, 2-(4-morpholinyl)-8-phenyl-4H-1-benzopyran-4-one (LY294002). *Journal of Biological Chemistry*, *269*(7), 5241–5248. https://doi.org/10.1016/s0021-9258(17)37680-9

Volkmann, C., Brings, N., Becker, M., Hobeika, E., Yang, J., & Reth, M. (2016). Molecular requirements of the B-cell antigen receptor for sensing monovalent antigens. *The EMBO Journal*, *35*(21), 2371–2381. https://doi.org/10.15252/embj.201694177

Wade-Vallance, A. K., & Allen, C. D. C. (2021). Intrinsic and extrinsic regulation of IgE B cell responses. *Current Opinion in Immunology*, *72*, 221–229. https://doi.org/10.1016/j.coi.2021.06.005

Wang, Z., Zhang, H., Shen, X.-H., Jin, K.-L., Ye, G., Qiu, W., Qian, L., BoLi, Zhang, Y.-H., & Shi, G.-P. (2013). Immunoglobulin E and mast cell proteases are potential risk factors of impaired fasting glucose and impaired glucose tolerance in humans. *Annals of Medicine*, *45*(3), 220–229. https://doi.org/10.3109/07853890.2012.732234.

Wang, Z., Zhang, H., Shen, X. H., Jin, K. L., Ye, G. fen, Qian, L., Li, B., Zhang, Y. H., & Shi, G. P. (2011). Immunoglobulin E and mast cell proteases are potential risk factors of human pre-diabetes and diabetes mellitus. *PLoS ONE*, *6*(12), 4–12. https://doi.org/10.1371/journal.pone.0028962

Warren, C. M., Jiang, J. J., & Gupta, R. S. (2020). Epidemiology and Burden of Food Allergy. *Curr Allergy Asthma Rep*, *20*(2), 6. https://doi.org/doi:10.1007/s11882-020-0898-7

Wesemann, D. R., Magee, J. M., Boboila, C., Calado, D. P., Gallagher, M. P., Portuguese, A. J., Manis, J. P., Zhou, X., Recher, M., Rajewsky, K., Notarangelo, L. D., & Alt, F. W. (2011). Immature B cells preferentially switch to IgE with increased direct Sμ to Sε recombination. *Journal of Experimental Medicine*, *208*(13), 2733–2746. https://doi.org/10.1084/jem.20111155

Wickham, H., & Bryan, J. (2019). *readxl: Read Excel Files* (R package version 1.3.1.). https://cran.r-project.org/package=readxl

Workman, P., Clarke, P. A., Raynaud, F. I., & Van Montfort, R. L. M. (2010). Drugging the PI3 kinome: From chemical tools to drugs in the clinic. *Cancer Research*, *70*(6), 2146–2157. https://doi.org/10.1158/0008-5472.CAN-09-4355

Worsley, C. M., Veale, R. B., & Mayne, E. S. (2022). Inducing apoptosis using chemical

treatment and acidic pH, and detecting it using the Annexin V flow cytometric assay. *PLoS ONE*, *17*(6 June), 1–7. https://doi.org/10.1371/journal.pone.0270599

Xiong, H., Dolpady, J., Wabl, M., de Lafaille, M. A. C., & Lafaille, J. J. (2012). Sequential class switching is required for the generation of high affinity IgE antibodies. *Journal of Experimental Medicine*, *209*(2), 353–364. https://doi.org/10.1084/jem.20111941

Xu, J. L., & Davis, M. M. (2000). Diversity in the CDR3 region of V(H) is sufficient for most antibody specificities. *Immunity*, *13*(1), 37–45. https://doi.org/10.1016/S1074-7613(00)00006-6

Yang, J., & Reth, M. (2010). The dissociation activation model of B cell antigen receptor triggering. *FEBS Letters*, *584*(24), 4872–4877. https://doi.org/10.1016/j.febslet.2010.09.045

Yang, Z., Robinson, M. J., Chen, X., Smith, G. A., Taunton, J., Liu, W., & Allen, C. D. C. (2016). Regulation of B cell fate by chronic activity of the IgE B cell receptor. *ELife*, *5*, 1–31. https://doi.org/10.7554/elife.21238

Yang, Z., Sullivan, B. M., & Allen, C. D. C. (2012). Fluorescent In Vivo Detection Reveals that IgE+ B Cells Are Restrained by an Intrinsic Cell Fate Predisposition. *Immunity*, *36*(5), 857–872. https://doi.org/10.1016/j.immuni.2012.02.009

Yang, Z., Wu, C. A. M., Targ, S., & Allen, C. D. C. (2020). IL-21 is a broad negative regulator of IgE class switch recombination in mouse and human B cells. *Yang, Z., Wu, C. A. M., Targ, S., & Allen, C. D. C. (2020). IL-21 Is a Broad Negative Regulator of IgE Class Switch Recombination in Mouse and Human B Cells. Journal of Experimental Medicine, 217(5). Https://Doi.Org/10.1084/Jem.20190472Journal of Experime*, *217*(5). https://doi.org/10.1084/jem.20190472

Yu, W., Freeland, D. M. H., & Nadeau, K. C. (2017). *Food allergy: immune mechanisms, diagnosis and immunotherapy*. *16*(12), 751–765. https://doi.org/10.1038/nri.2016.111.Food

References of figures

- **Figure 1:**

Modified after: Jiménez-Saiz, R., Bruton, K., Koenig, J. F. E., Waserman, S., & Jordana, M. (2018). The IgE memory reservoir in food allergy. Journal of Allergy and Clinical Immunology, 142(5), 1441–1443. https://doi.org/10.1016/j.jaci.2018.08.029

- **Figure 2:**

Modified after: O'Kennedy, R., Murphy, C., & Devine, T. (2016). Technology advancements in antibody purification. Antibody Technology Journal, Volume 6, 17–32. https://doi.org/10.2147/anti.s64762

- **Figure 3:**

Modified after: Victora, G. D., & Nussenzweig, M. C. (2012). Germinal centers. Annual Review of Immunology, 30, 446. https://doi.org/10.1146/annurev-immunol-020711-075032

- **Figure 4:**

Modified after: Schrader, J. S. and C. E. (2014). Ig heavy chain class switch recombination: mechanism and regulation. J. Immunol., 193(11), 5370–5378. https://doi.org/10.4049/jimmunol.1401849.

- **Figure 5:**

Modified after: Haniuda, K., & Kitamura, D. (2019). Induced Germinal Center B Cell Culture System. *Bio-Protocol*, *9*(4), 1–10. https://doi.org/10.21769/bioprotoc.316

Publication and presentations

Udoye CC, Rau CN, **Freye SM**, Almeida LN, Vera-Cruz S, Othmer K, Korkmaz RÜ, Clauder AK, Lindemann T, Niebuhr M, Ott F, Kalies K, Recke A, Busch H, Fähnrich A, Finkelman FD, Manz RA. B-cell receptor physical properties affect relative IgG1 and IgE responses in mouse egg allergy. Mucosal Immunol. 2022 Jun;15(6):1375-1388. doi: 10.1038/s41385-022-00567-y.

Udoye CC, **Freye SM**, Othmer K: Othmer K: From NGS to a cell culture model- The role of B cell receptor crosslinking on class switch to IgE and IgG1.
Oral presentation, 01.07.2021
ISEF seminar: Institute for Systemic Inflammation Research, University of Lübeck, Lübeck, Germany

Freye SM: The role of B cell receptor signalling on class switch to IgE and IgG1.
Progress Report, 13.07.2021
IRTG seminar: International Research Training Group 1911, University of Lübeck, Lübeck, Germany

Acknowledgements

“Im normalen Leben wird einem oft gar nicht bewußt, daß der Mensch überhaupt unendlich mehr viel mehr empfängt, als er gibt, und daß Dankbarkeit das Leben erst reich macht.“[1]

„In normal life, one often does not even realize that the human receives infinitely more than he gives, and that gratitude is what makes life rich."

Dietrich Bonhoeffer

First and foremost, I would like to express my deepest gratitude to my supervisor Prof. Dr. Rudolf Manz who enabled me to realize this thesis. I am grateful for the discussions, his advice and feedback, answering my questions at any time during my laboratory work and during the analysis and writing process. I would like to extend my appreciation to my second supervisor, Prof. MD Fred D Finkelman, especially for his detailed feedback.
I could not have undertaken this journey without the research group Manz, the “AG Manz”, notably Dr. Chinweike Christopher Udoye who introduced me to NGS analysis and supported my experiments by providing murine spleens. Equally, I would like to thank Kathleen K. for her support and advice in the laboratory. Thanks should also go to Sarah R. for her generous help when I broke my arm. I do not want to miss to thank Timo L. for sharing learnings from his laboratory experiences and for providing protocols for ELISA and glucose uptake experiments. In general, I appreciate the support of all members of the group, including professional and personal discussions.

Next, I want to express my sincerest gratitude to the International Research Training Group 1911 for the scientific qualification program, the networking possibilities and the financial support. I would like to extend these acknowledgements for the financial support to the “Stiftung der deutschen Wirtschaft”, providing me a grant during my medical studies including the semester when I analyzed the results and wrote this thesis.

Furthermore, I am very thankful for the administrative and academic support of all members of the ISEF (Institut für Systemische Entzündungsforschung). I would like to recognize T. V. who introduced me to flow cytometry measurement.

Finally, I would like to highlight A.N.’s support and patience, providing me with the best advice I could have wished for on language issues. I do not want to miss to thank my family and my boyfriend for their encouragement and faith in me as well as my friends for their moral support, co-working possibilities and inspiration.

[1] https://beruhmte-zitate.de/zitate/126486-dietrich-bonhoeffer-im-normalen-leben-wird-einem-oft-gar-nicht-bewusst/ (date of last access: 03.10.2024)